

# **Exploring Siderophore-Mineral Interaction Using Force Microscopy and Computational Chemistry**

**Treavor A. Kendall**

*Dissertation submitted to the faculty of the Virginia Polytechnic Institute  
and State University in partial fulfillment of the requirements for the degree  
of*

**Doctor of Philosophy in Geological Sciences**

## ***Committee***

Michael F. Hochella, Jr., Chair  
Larry Hersman  
Malcolm Potts  
J. Donald Rimstidt  
Christopher Tadanier

April 11, 2003  
Blacksburg, Virginia

Keywords: azotobactin, goethite, diaspore, ligand, AFM, force microscopy, molecular modeling, quantum mechanical calculations

Copyright © 2003, Treavor A. Kendall

# Exploring Siderophore-Mineral Interaction Using Force Microscopy and Computational Chemistry

Treavor A. Kendall

## Abstract

The forces of interaction were measured between the siderophore azotobactin and the minerals goethite (FeOOH) and diaspore (AlOOH) in solution using force microscopy. Azotobactin was covalently linked to a hydrazide terminated atomic force microscope tip using a standard protein coupling technique. Upon contact with each mineral surface, the adhesion force between azotobactin and goethite was two to three times the value observed for the isostructural Al-equivalent diaspore. The affinity for the solid iron oxide surface reflected in the force measurements correlates with the specificity of azotobactin for aqueous ferric iron. Further, the adhesion force between azotobactin and goethite significantly decreases when small amounts of soluble iron are added to the system suggesting a significant specific interaction between the azotobactin and the mineral surface. Changes in the force signature with pH and ionic strength were fairly predictable when considering mineral solubility, the charge character of the mineral surfaces, the molecular structure of azotobactin, and the intervening solution.

Molecular and quantum mechanical calculations which were completed to further investigate the interaction between azotobactin and iron/aluminum oxide surfaces, and to more fully understand the force measurements, also showed an increased force affinity for Fe over Al. *Ab initio* calculations on siderophore fragment analogs suggest the iron affinity can be attributed to increased electron density associated with the Fe-O bond compared to the Al-O bond; an observation that correlates with iron's larger electronegativity compared to aluminum. Attachment of the ligand to each surface was directed by steric forces within the molecule and coulombic interactions between the siderophore oxygens and the metals in the mineral. Chelating ligand pairs coordinated with neighboring metal atoms in a bidentate, binuclear geometry. Upon simulated retraction of azotobactin from each surface, the Fe-O(siderophore) bonds persisted into a higher force regime than Al-O(siderophore) bonds, and surface metals were removed from both minerals. Extrapolation of the model to more realistic hydrated conditions using a PCM model in the quantum mechanical calculations and water clusters in the molecular mechanical model demonstrated that the presence of water energetically favors and enhances metal extraction, making this a real possibility in a natural system.

## Acknowledgements

Rarely is the value of a mentor or teacher realized in real time. The obvious example is the lag in appreciation our parents must endure until we emerge from our four to five year-long, self absorbed, teenage reality. And although my friends and wife may argue this transition has yet to occur for me, I see with clarity the positive and significant impact my advisor Michael Hochella has had on shaping my talents as a scientist. His skills as an innovative and accomplished researcher are known to many, but his students know him also as an exemplary advocate, psychologist, editor, motivator and friend, all in one. His efforts and guidance are greatly appreciated.

The work, support and direction provided by my committee was invaluable. Each member provided a unique perspective that diversified my approach to the project, and for this I thank Larry Hersman, Malcolm Potts, Don Rimstidt and Chris Tadanier. I also thank my collaborators Udo Becker (U. of Michigan) who introduced me to the fascinating and all-consuming realm of computational chemistry while supplying the requisite expertise, equipment, software and caffeine; and Steven Lower (U. of Maryland) who, in addition to being an inspiring officemate and colleague, gave me the opportunity to co-author the review article contained in the Appendix of my dissertation.

“I get by with a little help from my friends” – A gross understatement by Lennon and McCartney. The rich personalities, unique humor, and amazing ideas of the people in our research group make our lab a great place to work. Much gratitude is extended to current group members Saumya Bose, Tracy Cail, Brian Lower and Andy Madden, and past members, Barry Bickmore, Erin O'Reilly, Eric Rufe and Rob Weaver. Also acknowledged are the many friends I've made in the past four years who provided support at the lab bench, over a beer, or on the trail, including Greg Bank, Jeane Jerz, Megan Elwood-Madden, Jason Pope, Jason Reed, Jim Spotila and many others. Non-Virginians deserving of thanks include my lifelong friends Stephen Cronin, Jimmy Breihan and Rick Ngo.

The success this Department enjoys is attributable to the outstanding leadership provided by Department Chair Dr. Cahit Coruh, the high quality of the faculty, and the dedicated work of the support staff including Linda Bland, Mary McMurray, Connie Lowe, Carolyn Williams and Ellen Mathena. Thank you all.

And to my wife Katy, I share this accomplishment with you. Thank you for being my foundation and voice of reason. Your patient, kind and giving heart is a model for me and all those around you. I love you, I thank you and I can't wait to share our next adventure with you.

My parents Joyce and Bill, Conrad and Angela and my brother Kevin are the reason I am at this juncture in my life. Their love, guidance and life lessons were essential to this achievement. I am also fortunate to have a wonderful immediate and extended family, all of whom I love dearly. Thank you Maw-maw, Granny, my late grandfathers James A. Kendall and T.O. Syper, Uncle John, Aunt Jo, Susanne, McKenzie and Cole, Jessica, Justin, Tommy, Uncle Allen, Aunt Paula, Gabe and Marlena, Louann and Pete Pearson, Chuck, Kathryn, James and Charlie Campbell.

This work was funded by a fellowship awarded under the Department of Education's GAAN Program, NSF and the Department of Energy.

In closing, this work was made possible by many people I haven't met: Sophie Germain, Doug Martsch, Jeff Mangum, Andrew Wiles, Edgar Degas, Robert Wolke, Ron Tiner, Charles Bukowski, Nikki Giovanni, Kathe Kollwitz, Derek Hess and the Nerf Corporation.

## Table of Contents

<b>Abstract.....</b>	<b>ii</b>
<b>Acknowledgements .....</b>	<b>iii</b>
<b>Table of Contents .....</b>	<b>iv</b>
<b>List of Tables .....</b>	<b>vi</b>
<b>List of Figures.....</b>	<b>vii</b>
<b>Chapter 1 – Introduction .....</b>	<b>1</b>
<i>Siderophore-Mineral Reactivity.....</i>	<i>1</i>
<i>Significance of This Work.....</i>	<i>3</i>
<i>Structure of Dissertation.....</i>	<i>4</i>
<b>Chapter 2 – The Measurement and Interpretation of Molecular Level Forces of Interaction Between the Siderophore Azotobactin and Mineral Surfaces.....</b>	<b>5</b>
<i>Abstract.....</i>	<i>5</i>
<i>Introduction.....</i>	<i>6</i>
<i>Experimental.....</i>	<i>8</i>
Azotobactin production and isolation .....	8
Tip activation .....	9
Solution conditions and mineral specimens.....	10
AFM operation and data processing .....	11
<i>Results and Discussion .....</i>	<i>13</i>
Forces of siderophore interaction with an iron versus aluminum oxide.....	13
Effect of added soluble iron on forces between azotobactin and goethite.....	14
Assessment of the azotobactin-goethite/diaspore interaction .....	14
Details of force curve features .....	17
Ionic strength and pH effects on the forces of interaction .....	19
<i>Summary and Conclusions.....</i>	<i>21</i>
Outlook and Possibilities .....	22
<i>Tables.....</i>	<i>25</i>
<i>Figures .....</i>	<i>27</i>
<i>References.....</i>	<i>36</i>
<b>Chapter 3 – Computational Modeling of Azotobactin-Goethite/Diaspore Interactions: Applications to Siderophore-Mineral Reactivity and Molecular Force Measurements .....</b>	<b>40</b>
<i>Abstract.....</i>	<i>40</i>
<i>Introduction.....</i>	<i>41</i>
<i>Methods.....</i>	<i>42</i>
Molecular mechanics .....	42
Quantum mechanical/ab initio calculations .....	45
<i>Results and Discussion .....</i>	<i>46</i>
Simulated approach force trace - Azotobactin and goethite/diaspore .....	46
Simulated azotobactin and free Fe <sup>3+</sup> interaction .....	49
Simulated retraction force trace - Azotobactin and goethite/diaspore.....	50
Goethite.....	50

Diaspore .....	51
Quantum mechanical calculations and discussion of metal removal.....	52
Siderophore affinity for Fe <sup>3+</sup> over Al <sup>3+</sup> .....	55
<i>Summary and Conclusions</i> .....	56
<i>Tables</i> .....	57
<i>Figures</i> .....	60
<i>References</i> .....	70
<b>APPENDIX - Intermolecular Forces at the Interface of Biological and Mineralogical Particles</b> .....	<b>72</b>
<b>Curriculum Vitae</b> .....	<b>139</b>

## List of Tables

Table 2.1 Comparison of average force parameters collected while probing azotobactin on diasporite and goethite. ....	25
Table 2.2 Comparison of Fe(III) and Al(III) overall (1:1) formation constants (K <sub>f</sub> ) for selected siderophores and their component/analog ligands. ....	25
Table 2.3 Ratios of average adhesion force for goethite and diasporite (F <sub>adh</sub> goethite/F <sub>adh</sub> diasporite) under various solution conditions. ....	26
Table 3.1 Comparison of GULP and experimental lattice energies. ....	57
Table 3.2 Comparison of jump to contact distances (j <sub>tcd</sub> ) and forces (j <sub>tcf</sub> ) associated with extending azotobactin towards goethite surface with simulated values (see text). Experimental values are shown for various pH and ionic strength (I). ....	58
Table 3.3 Differentiated energy peak values (dE/dx) associated with simulated siderophore release from the surface. Pullout energies represent energy required to position metal atom to an infinite distance from the lattice (in the absence of a siderophore). ....	58
Table 3.4 Quantum mechanical calculations of fully deprotonated siderophore fragments (analogs) binding Fe <sup>3+</sup> and Al <sup>3+</sup> . ....	59

## List of Figures

Figure 2.1	Annotated azotobactin $\delta$ structure (adapted from Palanche, 1999).....	27
Figure 2.2	Confocal Scanning Laser Image of an a) unactivated AFM tip with no fluorescent signal evident, and b) a tip activated with the inherently fluorescent azotobactin molecule. Images are a composite of two channels (Ch 1,2) collected under a C-Apochromat 40X/1.2 water immersion objective. Ch 1 consists of transmitted light which provides a dark silhouette of the cantilever; Ch 2 uses a 505 nm long pass filter to collect fluorescence generated when the cantilever and tip are exposed to a UV laser (364nm). .....	28
Figure 2.3	Representative force-distance plots showing the interaction between the CFM tip and two minerals, diaspore (empty and filled triangles) and goethite (empty and filled circles). Figure a) shows data collected using an azotobactin-activated tip, and b) shows data collected with a control hydrazide terminated tip. Both force signatures were collected at pH 7; I=10-1M. Insets represent the same force plot, but with the x axis range increased to show the region of no contact. ....	29
Figure 2.4	Histogram showing variability in adhesion forces ( $F_{adh}$ ) with mineral sample location. Sample locations were randomly selected. ....	30
Figure 2.5	Average adhesion force ( $F_{adh}$ ) between azotobactin and goethite versus added ferric iron (as $FeCl_3 \cdot 6H_2O$ ). The tip was immersed in each Fe concentration for a minimum 15 minutes and then rinsed thoroughly with Millipore water before collecting force measurements. Note the small rebound in adhesion values upon the addition of a small amount of EDTA. Fe(III) solids precipitation is not predicted at the selected pH (3.5) and maximum Fe concentrations (0.1 mM).....	31
Figure 2.6	Retraction curve showing plateau that is commonly observed in force signatures collected with azotobactin activated tips. It is suggested that this feature may represent the extension of the azotobactin and linker molecule during separation from the mineral surface.....	32
Figure 2.7	Schematic showing extension of the azotobactin molecule during retraction from the mineral surface. Note the geometry and nature of the peptide linkage that joins the molecule to the AFM tip. Not to scale. ....	33
Figure 2.8	Average adhesion forces ( $F_{adh}$ ) for goethite and diaspore collected with azotobactin-activated tip under various solution conditions. Control values collected with only a hydrazide terminated tip are added for reference. ....	34
Figure 2.9	Effect of pH and ionic strength on the azotobactin-goethite force signature. See text for details.....	35
Figure 3.1	Starting point of extension simulation with linearized azotobactin molecule, approaching the goethite cluster. ....	60
Figure 3.2	Annotated azotobactin $\delta$ structure (Palanche, 1999) with oxygens numbered in series; those highlighted in red coordinated with metals on the mineral surface during the simulation. ....	61
Figure 3.3	Simulated energy profile showing the successive attachment of azotobactin groups upon extension (approach) to the goethite and diaspore. Inset is a screen shot from the simulation showing the extension of the molecule onto the surface.	

Oxygen numbers (O1,O2,O4, etc.) refer to numbering system shown in Figure 3.2. .....	62
Figure 3.4 Molecular models of azotobactin interacting with a goethite surface. Arrows point to terminal hydroxamate group oxygens coordinating with irons in the lattice in a binuclear fashion. Note the spacing of the siderophore oxygens allow for “bonds” (i.e., Fe-O(siderophore) distances ~2 Å) with neighboring irons. With this coordination, the distance between a siderophore oxygen and an iron diagonally across is over 3Å.....	63
Figure 3.5 Arrow indicates extension of the Au atom/molecule towards the mineral surface with a) no lateral component and b) an arbitrary and varied lateral component The dot at the beginning of the arrow indicates the starting position of the Au atom.....	64
Figure 3.6 Fe displacements from the goethite lattice upon retraction of the siderophore from the surface. Y-axis shows bond distances between the metal and a lattice oxygen directly beneath it. Note the large displacement associated with the β-hydroxyacid group and total removal of an Fe by the Hse (lactone). .....	65
Figure 3.7 Simulated energy profile of siderophore retraction from goethite and diaspoire. .....	66
Figure 3.8 Al displacements from the diaspoire lattice upon retraction of the siderophore from the surface. Y-axis shows bond distances between the metal and a lattice oxygen directly beneath it. ....	67
Figure 3.9 Molecular conformation and Mulliken charges predicted for a) hydroxycarboxylic acid and its associated b) Fe and c) Al complexes. ....	68
Figure 3.10 Molecular conformation and Mulliken charges predicted for a) acetohydroxamic acid and its associated b) Fe and c) Al complexes. ....	69



## **Chapter 1 – Introduction**

### **SIDEROPHORE-MINERAL REACTIVITY**

Biologically produced ligands in near surface environments (e.g., soils) may represent a metabolic by-product, serving no specific physiological function, or they may be essential to a microorganism's very survival, acting as an electron shuttle or playing a vital role in nutrient acquisition. In both cases these ligands have the potential to significantly impact the geochemistry of near surface systems by altering pH and redox conditions, thereby increasing or decreasing mineral solubilities. Further, ligands enter into sorption or desorption reactions with minerals, altering their charge character and surface chemistry. Ultimately dissolution, passivation, or activation of a mineral surface can occur, making ligands a key factor in nutrient cycling and possibly contaminant mobility.

This study focuses on an intriguing class of ligands called siderophores and their interaction with iron and aluminum oxide surfaces. Produced by microorganisms to acquire the essential nutrient iron, siderophores' unique chelating ability and formation of an ultra stable Fe(III) complex results from their optimal structure and design. This, coupled with their presence in a variety of systems, have made siderophores the subject of research in fields ranging from geochemistry to medical science. Siderophore coordination chemistry with aqueous metal ions is well defined; however, in near surface systems (e.g. soils) the main sources of ferric iron are minerals such as hematite, goethite, and ferrihydrite. Extracting an iron atom from these solid forms presents many challenges that are thermodynamic, kinetic and mechanistically steric in nature. The extreme insolubility of iron containing minerals limits aqueous iron concentrations to a level that is up to 6 orders of magnitude below what is required for growth, yet siderophores are able to overcome this; dissolving minerals to provide the requisite amount of iron for growth. The mechanism by which this is done is not known. The minute amount of aqueous iron in equilibrium with the mineral surface may be chelated by the siderophore causing a shift in the reaction towards dissolution. Or, surface contact may be involved where the siderophore sorbs to the mineral, destabilizes the coordination

of the iron in the solid structure and releases it into solution. This study addresses the latter possibility.

Thermal motion and coulombic considerations (e.g., the negative charge of the siderophore and the neutral to positive character of many oxides at circumneutral pH), suggest that the siderophore will invariably come into contact with the surface, presenting an opportunity for it to react with the surface possibly leading to iron extraction. Here steric considerations come into play and depending on the micro- to nanotopography of the mineral surface group (e.g. on an atomically flat growth face, an edge or step) the siderophore encounters varying reductions in the degrees of freedom with which it can coordinate the iron. In all instances the normal hexadentate geometry characteristic of the aqueous complex is unlikely, raising the question of how this affects the ligand's affinity and reactivity with iron.

Using a unique force microscopy approach coupled with molecular and quantum mechanical calculations, this study demonstrates that indeed a certain amount of activity is retained when the siderophore azotobactin encounters iron in a mineral surface. Moreover, these observations present iron removal from the lattice via direct contact as a distinct possibility.

Specifically, molecular level forces recorded after covalently linking an azotobactin molecule to an AFM tip and bringing it into contact with isostructural iron and aluminum oxides produce force signatures that are unique to each mineral. A larger adhesion for the iron oxide surface is recorded, a phenomenon that parallels the siderophore's increased affinity for aqueous iron versus aluminum. Variation in the force signatures with changes in solution conditions reveal a balance of interactions with electrostatic forces dominating the approach to the surface and more specific interactions directing surface adhesion. Molecular simulations confirm the distinction in the interaction between the siderophore and the two minerals ( $\alpha$ -FeOOH and  $\alpha$ -AlOOH), again indicating an increased affinity for the iron oxide. The simulations emphasized the importance of steric considerations as the various oxygens associated with both the

peptide backbone and amino acid sidechains were integral in interacting with the surface. Interesting simulated surface geometries included, 1) chelating pairs of oxygen atoms (e.g., the hydroxyl and carbonyl of the  $\delta$  N OH ornithine hydroxamate group) each coordinating with single, neighboring iron atoms, and 2) the coupled extraction of an iron atom by a peptide backbone carbonyl oxygen and a sidechain hydroxyl that are separated by a nanometer in contour length. The simulations even suggest that metals may be removed from the structure by single coordinating oxygen atoms (e.g. in the  $\beta$ -hydroxycarboxylic acid).

## **SIGNIFICANCE OF THIS WORK**

Emphasized herein is the value of understanding and quantifying the molecular level forces that direct ligand interaction with a mineral surface. To make these measurements, we developed a unique chemical force microscopy method that allowed linkage of a siderophore to an AFM tip to ultimately be probed on mineral surfaces under aqueous and environmentally relevant conditions. This technique can be used with other siderophores or modified for use with various ligand-mineral systems, and represents an entirely new way to investigate sorption and desorption reactions, as well as ligand-mediated dissolution, passivation or alteration of mineral surfaces.

As applied here, in broad terms, we were able to demonstrate a unique specificity of a biomolecule for an inorganic surface. Moreover, we demonstrated that direct surface contact and reactivity could play a role in siderophore extraction of iron from minerals. This is especially significant for the model ligand we selected – azotobactin, which, because of its size, has often been relegated to a scavenger ligand that steals iron from smaller, lower affinity ligands.

While demonstrating the benefit of directly coupling computational chemistry with experimental results, model simulations also afforded a better picture of what these ligands may look like at the surface, gave further insight into the source of their affinity for the metals in the surface, and provided evidence of siderophore removal of iron from

the surface. Also, generated in this work is a novel, customized algorithm for processing AFM force data that identifies and detects prominent features in force signatures; a computational force field with potential sets specifically parameterized for goethite and diasporite; and an effective technique for isolating and purifying pyoverdine siderophores that represents a modification of an existing protocol but is more detailed and is designed for higher throughput.

## STRUCTURE OF DISSERTATION

This dissertation consists of three manuscripts divided into two chapters and an Appendix<sup>\*</sup>. Chapter 2 is a paper currently in press with *Geochimica Cosmochimica et Acta* entitled, “The measurement and interpretation of molecular level forces of interaction between the siderophore azotobactin and mineral surfaces”. It describes the force microscopy method and details how the siderophore was isolated and attached to the AFM tip. Force signatures documenting the interaction between azotobactin and diasporite as well as azotobactin and goethite at various pH, ionic strengths and soluble Fe concentrations are included. Chapter 3 is a paper in preparation with Udo Becker (University of Michigan) and contains the results from the molecular mechanics calculations simulating the interaction of azotobactin with the mineral surfaces and with a free Fe<sup>3+</sup>. Also included are results from quantum mechanical calculations on fragments representative of azotobactin’s chelating groups interacting with Fe<sup>3+</sup> and Al<sup>3+</sup>. The Appendix is a review article on using biological and chemical force microscopy in biogeochemistry and soil science. I am the first author with Steven Lower (University of Maryland) as a co-author. Entitled “Intermolecular forces at the interface of biological and mineralogical particles”, the article is currently in review with *Advances in Agronomy*.

---

<sup>\*</sup> Technical Note: In the \*.pdf and MS Word \*.doc electronic versions of this dissertation, the table of contents entries, and the figure and table references within the text are hyperlinked to the appropriate location, figure or table in the document.

## Chapter 2 – The Measurement and Interpretation of Molecular Level Forces of Interaction Between the Siderophore Azotobactin and Mineral Surfaces

Treavor A. Kendall\* and Michael F. Hochella, Jr.  
NanoGeoscience and Technology Laboratory, Department of Geological Sciences,  
Virginia Tech, Blacksburg, VA 24061 USA

\*Corresponding author: [tkendall@vt.edu](mailto:tkendall@vt.edu), 540.231.8575

IN PRESS

*Geochimica et Cosmochimica Acta*

Copyright © 2003, Elsevier Science, Ltd.

### ABSTRACT

The forces of interaction were measured between the siderophore azotobactin and the minerals goethite ( $\alpha$ -FeOOH) and diaspore ( $\alpha$ -AlOOH) in aqueous solution using chemical force microscopy. Azotobactin, a pyoverdine-type siderophore, was covalently linked to a hydrazide terminated atomic force microscope tip using a standard active ester protein coupling technique. Upon contact with each mineral surface, the adhesion force between azotobactin and goethite was two to three times the value observed for the isostructural Al-equivalent diaspore. The affinity for the solid iron oxide surface reflected in the force measurements correlates with the specificity of azotobactin for aqueous ferric iron. Further, the adhesion force between azotobactin and goethite significantly decreases (4 nN to 2 nN) when small amounts of soluble iron (0.1  $\mu$ M FeCl<sub>3</sub>·6H<sub>2</sub>O) are added to the system at pH 3.5 suggesting a significant specific interaction between the chelating reactive center of azotobactin and the mineral surface. Changes in the force signature with pH and ionic strength were fairly predictable when considering mineral solubility, the charge character of the mineral surfaces, the molecular structure of azotobactin, and the intervening solution. For example, azotobactin-goethite adhesion values were consistently smaller at pH 3.5 relative to the forces at pH 7. At the lower pH, the large number of protons and the increase in the mineral solubility provides additional electron acceptors (e.g., H<sup>+</sup> and Fe<sup>3+</sup>(aq)) that are free to compete for the basic oxygen chelating sites in the azotobactin structure. It is believed that this competition disrupts siderophore affinity for the surface resulting in decreased adhesion values.

## INTRODUCTION

Siderophores are being recognized for their potential to influence geochemical processes in near surface systems. Given a widespread distribution, and the small, but relatively significant siderophore concentration in soils (Bossier et al., 1988; Hersman, 2000), the implications of siderophore-mineral interactions are far reaching. The influence of these interactions on mineral weathering and nutrient cycling, and the release of toxic constituents from mineral surfaces must be considered.

Siderophores are soluble, organic ligands released by microorganisms to chelate iron. The exceptional affinity ( $K_f = 10^{20}$ - $10^{50}$ ) siderophores exhibit for aqueous ferric iron allows many organisms to assimilate this essential nutrient in spite of the extremely low solubility of the solid iron forms that are dominant in oxidizing environments. Indeed, Page and Hoyer (1984) document siderophore-producing bacteria successfully extracting ferric iron from minerals for growth and many studies have demonstrated dissolution of common iron oxides and silicates in the presence of siderophores (Hersman et al., 1995a; Hersman et al., 1995b; Holmen and Casey, 1996; Liermann et al., 2000; Maurice et al., 2000; Seaman et al., 1992; Watteau and Berthelin, 1994). Recent studies emphasize the role siderophores may have in contaminant fate and transport by providing quantitative evidence of their ability to affect the sorption of toxic metals and radionuclides on soil minerals (Kraemer et al., 1999; Kraemer et al., 2002; Neubauer et al., 2000).

Key to siderophore-influenced mineral dissolution and sorption/desorption reactions are the forces that bring the ligand into and out of contact with the mineral surface. It is well known that ligand-mineral interaction consists of a complex interplay between electrostatic, van der Waals, hydrophobic and steric forces that are dependent on the charge character and structure of the ligand and mineral surface, as well as the chemistry of the interstitial solution (Dzombak and Morel, 1990; Israelachvili, 1992; Stumm, 1992). Our objective is to extend the investigation of siderophore-mineral

interaction to an extremely small dimensional scale by quantifying electrostatic and bonding forces. We utilize a novel force measuring technique called chemical force microscopy (CFM) (Noy et al., 1997). For the first time, we have directly measured the forces of interaction between a siderophore ligand and a mineral, in solution at the nano- to picoNewton force sensitivity level. This information is used to determine if a siderophore can “differentiate” between a ferric iron-containing mineral and the aluminum-bearing isostructural equivalent; detect, quantify and characterize specific and non-specific siderophore-mineral interactions under various solution conditions; predict surface association geometries based on the magnitude and pattern of the force data; and evaluate the possibility and nature of a siderophore-surface complex. In doing so, we hope to further define the role siderophores play in mineral dissolution and iron acquisition while opening up a new area of research that explores the forces of interaction between metal-specific ligands/biomolecules, and inorganic/mineral surfaces.

The siderophore azotobactin was selected as the model ligand to be attached to an atomic force microscope (AFM) tip in these force measurement experiments. Azotobactin is a relatively large (1.3 kDa), pyoverdine-type siderophore (Figure 2.1) produced under iron limiting conditions by the nitrogen-fixing bacteria *Azotobacter vinelandii*. Other *A. vinelandii* siderophores include the catecholates aminochelin, azotochelin and protochelin; however, all exhibit an affinity for ferric iron that is below azotobactin (Cornish and Page, 1998; Palanche et al., 1999). Azotobactin was targeted for these experiments because it is a natural product from an environmentally relevant bacterium; its structure and size facilitated covalent linkage to an AFM tip; the fluorescent quinoline chromophore at the base of its polypeptide backbone allows small concentrations of the molecule to easily be detected and quantified; and several studies on the coordination chemistry and kinetics of iron complexation exist (Albrecht-Gary and Crumbliss, 1998; Albrecht-Gary et al., 1995; Demange et al., 1988; Hider, 1984; Schaffner et al., 1996; Winkelmann, 1991). Finally, we were able to obtain an *A. vinelandii* mutant (F196; courtesy Dr. William Page, Univ. of Alberta) that produces/hyper-produces azotobactin as its sole known siderophore, facilitating production and isolation (Sevinc and Page, 1992).

Goethite was selected for these experiments because it is the most abundant soil ferric iron oxide and is estimated to represent up to 70% of the total surface area available in a soil (Rakovan et al., 1999). Diaspore is a less common soil mineral, but was chosen because it is the isostructural Al-equivalent to goethite. Additionally, both mineral species were ideal for force measurements because single crystals with recognizable crystallographic faces presenting an optically flat surface could be obtained.

## **EXPERIMENTAL**

### **Azotobactin production and isolation**

Azotobactin was isolated from relatively large volumes of *A. vinelandii* F196 supernatant using a reverse phase chromatography procedure adapted from Demange et al. (1988). Briefly, multiple batches of 100 mL Fe-limited Burk media, pH 7.1, were inoculated with *A. vinelandii* F196 and incubated at 25°C with shaking at 200 rpm for 3-6 days. All glassware used during F196 growth and siderophore isolation was soaked overnight in 4N HCl, then 50 mM EDTA and rinsed with Millipore water in order to minimize Fe contamination (Page, 1993). F196 cultures were removed from incubation when azotobactin concentrations reached ~150 mg/L ( $\epsilon = 23500 \text{ M}^{-1}\text{cm}^{-1}$ ) as determined with A380 measurements (pH 1.8) on a Beckman-Coulter DU 640 UV-vis spectrophotometer. Two and a half (2.5) liters total culture were pooled and centrifuged at 36,400g for 15 minutes. In 0.5L batches, the supernatant containing the soluble azotobactin fraction was filtered (0.1  $\mu\text{m}$ ), adjusted to pH 4 using HCl and loaded on to a 19 cm x 2 cm reverse phase octadecyl silane (RP-18) preparative chromatography column using 0.05M pyridine-acetic acid buffer, pH 5.0 (Demange et al., 1988). The column was flushed with 200 mL of 0.05M buffer and azotobactin was then eluted with acetonitrile and buffer (1:1) at an average flow rate of 1 mL/min. The various fractions were scanned at A380 and those containing >15 mg/L azotobactin were pooled and loaded onto a 24 cm x 3.5 cm diethylaminoethyl (DEAE) cellulose column with 0.05M



pyridine-acetic acid buffer. The column was flushed with 200-250 mL of 0.05M buffer and the azotobactin eluted with a linear gradient of 0.05M-1M pyridine-acetic acid buffer. Fractions containing >20mg/L azotobactin were pooled, dried under N<sub>2</sub>, resuspended in doubly deionized Millipore water (18 MΩ cm<sup>-1</sup> Millipore water A10 system; Millipore Corp.), lyophilized and stored at -20°C. The purity of each separation fraction was monitored with reverse phase high performance liquid chromatography (HPLC) and UV-vis spectrophotometry. In contrast to the filtered supernatant and RP-18 fractions, the HPLC spectra (380 nm) of the final azotobactin fraction consisted of a single, narrow peak with no shoulders at ~1.7 minutes (data not shown). Chrome Azurol-S (CAS) assays (Schwyn and Neilands, 1987), indicated consistent, robust siderophore activity in all fractions.

### **Tip activation**

Azotobactin molecules were linked to the AFM tip using an active ester crosslinking technique commonly used to couple two proteins (Grabarek and Gergely, 1990; Lahiri et al., 1999; Staros et al., 1986). In our scheme the azotobactin Asp carboxyl (see Figure 2.1) was targeted for linkage with the amino group associated with a hydrazide terminated (-NH-NH<sub>2</sub>) AFM tip (BioForce Labs). One (1) mg of lyophilized azotobactin was dissolved in 1 mL activation buffer (0.1M MES; 0.5M NaCl; pH 5). Taking advantage of the fact that pyoverdine siderophores complex Al<sup>3+</sup> in the same octahedral coordination as it does with Fe<sup>3+</sup>, but with a much lower affinity for Al (Hider, 1984; Mertz et al., 1991), azotobactin's oxygen ligands thought to participate in chelation (specifically those associated with the β-OH Asp) were protected prior to the linkage reaction by adding 110 μL of 1M AlCl<sub>3</sub> (1:100 Azb:Al) to the solution and reacting for 20 min. Ten (10) μL each of 280 mM 1-Ethyl-3-(3-Dimethylaminopropyl) carbodiimide (EDC; Pierce) and 560 mM N-hydroxysuccinimide (NHS; Pierce) was added and reacted for an additional 15 min. Exposure of the azotobactin's targeted carboxyl group to EDC in combination with NHS results in a stable, hydrolysis resistant, active succinimidyl ester that readily forms a peptide bond in the presence of an amino group. Here the amino group is supplied by the hydrazide terminated AFM tip which was submerged and mixed

with the EDC-NHS solution. After 2 hours at room temperature the tip was then removed and sequentially rinsed with 0.04M EDTA (to remove the Al and regenerate the reactive groups), 10mM NH<sub>2</sub>OH, and Millipore water. The tip was allowed to incubate in each rinse solution for a minimum of 20 minutes. When not in use, activated tips were stored at 4°C in MES activation buffer at pH 5. Each activated tip was used within 24 hours of preparation. Fluorescent images used to confirm the presence of azotobactin to the tip were collected on a Zeiss 510 Confocal Scanning Laser Microscope (CSLM) before and after the CFM experiments (Figure 2.2).

### **Solution conditions and mineral specimens**

Force measurements were made in a Digital Instrument fluid cell filled with Millipore water adjusted to various pHs using HCl and NaOH, and ionic strengths using NaCl. The effect of soluble iron on the forces of interaction was also assessed. Baseline adhesion values between azotobactin and goethite were first collected with no iron added to the system. Successively increasing concentrations (0.001, 0.01, 0.1 µM) of FeCl<sub>3</sub>·6H<sub>2</sub>O were then introduced while monitoring the change in the force signatures. A final measurement was collected after an attempt to remove the added Fe<sup>3+</sup>(aq) from the azotobactin chelating groups with a high concentration of a competing ligand (1 mM EDTA). Available data on the iron exchange kinetics between EDTA and azotobactin (Albrecht-Gary et al., 1995) were considered when selecting the competing ligand concentration and tip immersion time. Specifically, the following equation was used to calculate a pseudo-first order rate constant ( $k_{obs}$ ) at pH 3.5:

$$k_{obs} = \frac{K_1 K_2 k_3 [H^+]_0 [EDTA]_0}{1 + K_1 [H^+]_0 + K_1 K_2 [H^+]_0 [EDTA]_0}$$

This relationship is derived from experimental data collected at pH 3.6-5.2 and EDTA concentrations ranging from 0.42 – 45 mM and assumes a three step ligand exchange mechanism where  $K_1$  (1080 mol<sup>-1</sup> L) and  $K_2$  (0.008 mol<sup>-1</sup> L) are equilibrium constants corresponding to the first two reactions: 1) protonation of the iron-azotobactin

complex, and 2) the formation of an azotobactin-iron-EDTA complex.  $k_3$  ( $500 \text{ s}^{-1}$ ) is the first order rate constant of the final, rate limiting iron exchange reaction between azotobactin and EDTA. At pH 3.5, and an initial EDTA concentration of 1 mM ( $k_{\text{obs}} = 1.0 \times 10^{-3} \text{ s}^{-1}$ ), the half-life of the pseudo first order exchange reaction equals 11.5 min. Based on this we selected a minimum immersion period of 15 minutes to minimize the EDTA concentration in the system and to insure an effect could be observed within a reasonable time.

All solutions were exchanged after flushing the cell with 5-10 cell volumes of the new solution and the system was allowed to thermally stabilize (as monitored by drift in the photodiode signal) for a minimum of 15 min. The pH of the solutions was measured after the force measurements to monitor any changes in solution conditions during the experiments. Small (600-800  $\mu\text{m}$ ) single crystals of goethite ( $\alpha\text{-FeOOH}$ ) and diasporite ( $\alpha\text{-AlOOH}$ ) containing recognizable (010) faces with optically flat step terraces were carefully selected and cleaned using a series of acetone, methanol and Millipore water rinses immediately prior to force measurements (Stipp and Hochella, 1991).

### **AFM operation and data processing**

Force data were collected at room temperature on a NanoScope IIIa MultiMode SPM (Digital Instrument) at a cycle rate of 2 Hz over a 300 nm ramp with translation rates not exceeding  $3 \mu\text{m s}^{-1}$ . Diode voltages were converted into cantilever deflection (nm) using the slope of the constant compliance region of the force curve. Cantilevers used in the experiments were triangular, 200  $\mu\text{m}$  long, narrow legged and fixed with a pyramid shaped tip. Spring constants were determined by measuring the change in resonant frequency with added masses as described by (Cleveland et al., 1993). Deflection values were then converted into force using Hooke's Law. Force plots were generated by plotting force versus relative piezo movement or force versus tip-sample separation. A comprehensive description and discussion of AFM force plots is provided by (Cappella and Dietler, 1999).

A single force plot at a particular sample location does not always fully describe the force regime of a given interaction. As a result, force landscapes are often summarized by averaging single-point parameters identified in both the approach and retraction curve in a force plot. For example, once the tip and sample are in contact, the level of affinity that the molecules on the end of the AFM tip show for the surface is characterized by an average rupture or adhesion force, defined as a change in slope and/or minimum in the retraction force data. Likewise, a lack of affinity can be described by repulsion force values, often defined as local maxima in the approach data. Force curve processing and automated determination of these parameters, plus statistical calculations, whole force curve averaging, energy calculations and histogram generation was completed using a customized routine written by T. Kendall and H. Skulason for Igor Pro 4.04 (WaveMetrics, Inc.). The parameter extraction module quickly selects the values based on a set of given criteria such as maxima thresholds in the differentiated force data and tolerance limits for specific changes in slope.

A large number of force curves can be processed rapidly with the customized Igor routine, and, as a result, 120-150 curves were commonly collected at a single sample location. After examining histograms of the main parameters of interest (e.g., adhesion force, jump to contact distance), we found the data to be Gaussian with a relatively low standard error. Experience showed that in most cases, a sample size of 60-70 force curves adequately described parameter distributions and means for our system. Most of the data collected were included in the averages and statistical analysis herein, with less than 3% of the curves from each sample location being excluded. Most of the eliminated curves contained a significant slope or periodic oscillation present in the region of no contact. This was believed to reflect a drift in the sample position due to a relaxation or shift of the fluid cell gasket and optical interference from stray laser light reflecting off of the mineral surface, respectively.

## RESULTS AND DISCUSSION

### Forces of siderophore interaction with an iron versus aluminum oxide

Significant differences exist in the forces of interaction between azotobactin and goethite, and azotobactin and diaspore. Most notable is the disparity in the attractive force associated with the approach; and the considerable difference in the force of adhesion upon retraction (Figure 2.3a). The force associated with the jump to contact, an indicator of tip affinity for the surface, is on average 0.7 nN higher for goethite versus diaspore. Also during approach the jump to contact distance at which the tip began to “feel” the surface is larger for goethite (~13 nm) than for diaspore (~6 nm). Upon retraction the average maximum force of adhesion between azotobactin and the iron oxide surface was consistently 2-3 times the value associated with the diaspore surface (Table 2.1). In contrast, control experiments with a hydrazide terminated tip lacking the azotobactin molecule produced similar force signatures for each mineral (Figure 2.3b), indicating the large distinction between the diaspore and goethite forces are due to the presence of azotobactin and interference from the linker molecule is minimal.

Disparate populations in adhesion force values corresponding to different locations on a single mineral were observed. Figure 2.4 shows histograms of adhesion forces collected with the same tip at different sample locations on a goethite and diaspore surface. Changes in force with sample location reflect, in part, the influence of mineral microtopography on the force measurements. Single (010) growth faces were probed, but it is likely that force measurements reflect to some degree the interaction between the azotobactin and surface features such as step edges and defects. Given the pN to nN sensitivity of this method it may be possible to capture the variation in surface reactivity associated with these features in the force signatures; however, definitive confirmation will require better constraint of the topography at each sample location. The observed variations due to microtopography, however, did not affect the overall force trends observed between goethite and diaspore.

## **Effect of added soluble iron on forces between azotobactin and goethite**

The large adhesion force associated with goethite significantly decreased upon the successive addition of small concentrations of soluble iron ( $\text{FeCl}_3 \cdot 6\text{H}_2\text{O}$ ) (Figure 2.5). The lowered adhesion values then partially rebounded after the tip was immersed in 1 mM EDTA.

Albeit a qualitative observation, it should be noted that the  $0.001 \mu\text{M}$  Fe(III) concentration detected in these force measurements is an order of magnitude below the detection limit reported when azotobactin is used as a spectrophotometric chemosensor for iron (Palanche et al., 1999). This speaks to the extreme sensitivity of this CFM technique, and further emphasizes the importance of minimizing iron contamination in the model system.

## **Assessment of the azotobactin-goethite/diaspore interaction**

Collectively, the observations above suggest that the large adhesion values associated with the goethite surface reflect an affinity between the azotobactin on the tip and the iron associated with the goethite surface. The similarity in the point of zero charge for goethite ( $\text{pzc}=7-9$ ) (Cornell and Schwertmann, 1996; Kosmulski, 2001) and diaspore ( $\text{pzc}=7-8$ ) (Kosmulski, 2001) indicates the charge character of each surface on a large scale is comparable, with both being slightly positive to neutral at pH 7. A net negative charge is predicted on the azotobactin molecule ( $\text{pK}_a$  hydroxycarboxylate = 4-5; see Table 2.2), thus presenting a possible electrostatic or hydrogen bonding component to the interaction. It is possible our model systems deviate from pristine charge conditions causing a significant differential shift in the  $\text{pzc}$  values of the two minerals, such that the diaspore is negatively charged or neutral while goethite remains positively charged. This of course could result in a larger adhesion to the goethite surface. Three observations, however, indicate differences in surface charge alone do not satisfactorily explain the discrepancy in the goethite and diaspore force affinities. First, at pH 3.5, far from each mineral's  $\text{pzc}$  value, and where the azotobactin is predominantly fully protonated and

neutral, we observe the same increase in adhesion for goethite over diaspore (see Section 3.5). Second, this relationship was also consistently observed when comparing data from several different locations on each mineral. This is in spite of changes in microtopography (discussed previously), or possible localized or anomalous charge distribution associated with each sample site. Finally, goethite force signatures collected at pH 7 often show a long range, electrostatic repulsion on approach that was equal to or significantly lower in the diaspore signatures collected under the same conditions and with the same tip (Experiment 2; data not shown); yet, the goethite adhesion force averaged 3.81 nN compared to 1.38 nN for diaspore.

The observed force relationship likely reflects differences in the electronic character of each metal (e.g., Fe(III) versus Al(III)) contained in the mineral structure. The smaller ionic radius and electronegativity value of Al(III) predicts a lower affinity for the negative charges associated with the chelating oxygen groups. In contrast, the larger, more electronegative Fe(III) will behave as a harder acid with a higher affinity for the oxygens, presumably resulting in larger adhesion forces. A similar argument is used to explain the increased thermodynamic stability of the Fe(III)-siderophore complex (aq) compared to the Al(III)-complex (aq) (i.e., see DFAM Table 2.2) (Albrecht-Gary and Crumbliss, 1998; Hider, 1984). However, here the difference in formation constants between iron and aluminum is orders of magnitude (Table 2.2) which is in contrast to the 2-3 fold change observed in the adhesion to each surface (Table 2.1). This discrepancy is difficult to explain, and one that can not be reconciled by the certain reduction in denticity associated with a siderophore-Fe(III) surface complex (Cocozza et al., 2002; Holmen and Casey, 1996) compared to the cognate hexadentate aqueous form. Assuming the adhesion force primarily reflects a monodentate interaction of the azotobactin hydroxamate group with each surface, there still exists a three order of magnitude increase in the stability of the acetohydroxamic acid(aH)-Fe(III) complex over the aH-Al(III) (Table 2.2). Schmitt et al. (2000), however, report a similar relationship between force measurements and thermodynamic constants. The average adhesion force associated with a nitriloacetic acid (NTA)-histidine (His) complex containing  $\text{Cu}^{2+}$  was

2.6 times the value associated with the NTA-His/Co<sup>2+</sup> complex, yet the thermodynamic stability constant of the copper complex is over 3 orders of magnitude higher.

The addition of ferric chloride at pH 3.5 presents an available source of aqueous ferric iron primarily as Fe<sup>3+</sup> and Fe(OH)<sup>2+</sup> ions that readily interact with the hydroxyl moieties believed to be involved in iron chelation (Figure 2.1). With these reactive groups previously available for interaction with the surface now occupied by the iron, the force of attraction to the surface is decreased. This trend is reversed when EDTA is added, presumably removing the iron associated with the azotobactin. It is also possible that the rebound in adhesion values reflects the interaction between a ternary azotobactin-Fe(III)-EDTA complex with the surface. Albrecht-Gary et al. (1995) include the formation of a negatively charged ternary complex (LH<sub>3</sub>FeEDTA<sup>-</sup>) as an intermediate step in the exchange of iron from azotobactin to EDTA in solution which, if associated with the tip, could exhibit an attractive electrostatic force towards the positively charged goethite surface. The stability of this ternary complex, however, is relatively low. It is formed during an intermediate, fast (e.g., not rate limiting) reaction with an equilibrium constant (8.0x10<sup>1</sup> M) that is three orders of magnitude below the value of ferrioxamine B (2.4x10<sup>4</sup> M). The instability of the azotobactin-Fe-EDTA ternary complex is cited as one reason for azotobactin's fast exchange kinetics.

The effect of added soluble iron on adhesion values further demonstrates that an interaction between the azotobactin and the surface is being captured by this technique, but it also provides evidence that the siderophore is retaining a level of chelation activity when attached to the tip. The residual adhesion that exists once the iron is added, however, raises interesting questions. Assuming complete coverage and a 1:1 linkage ratio (e.g., one azotobactin molecule linked to a single hydrazide group), the number of azotobactin molecules on the substrate including the tip and cantilever is on the order of 2.5x10<sup>11</sup>. With a fluid cell volume of ca. 150 µL, this gives a maximum effective azotobactin concentration of 3 nM. At the higher iron concentrations of 0.01 and 0.1 µM the azotobactin concentration is exceeded by several orders of magnitude, suggesting that there is enough iron available to fully satisfy all of the azotobactin molecules. The flow



through nature of the fluid cell also makes it unlikely that transport to the molecules on the tip could be limiting. The residual adhesion, however, may reflect interaction with some of the azotobactin groups that remain uncomplexed due to kinetic limitations. Or,

if initial chelation of the soluble iron by a single oxygen ligand pair does occur, steric hindrances and changes in molecule conformation imposed by the linkage may prevent complete, octahedral coordination leaving additional ligand pairs free to interact with the surface. A final component of the residual adhesion could be attributed to non-specific interactions between the surface and amino acid side chains or functional groups not involved in chelation, or between the surface and the chelated metal (i.e., as a ternary complex).

### **Details of force curve features**

Typical force curves display a single, discrete rupture event (Figure 2.3a), in the force regime of 3-5 nN at a loading rate of  $120 \text{ nN sec}^{-1}$  upon retracting from the goethite surface (in the absence of added iron). This feature was consistently observed across disparate experiments using different tips indicating that a similar interaction was reproducibly captured. Using a tip surface interaction geometry described by Derjaguin, Muller and Topov (DMT) theory, which assumes no deformation and a zero contact area upon bond rupture, and a nominal tip curvature radius of 40 nm, the estimated contact area for these experiments is  $0.003 \mu\text{m}^2$  (Noy et al., 1997; Stout, 2001). Spacing between the individual self-assembled monolayer (SAM) groups that anchor each azotobactin molecule to the tip is estimated to be 5-10 angstroms (Kondoh et al., 2001; Lahiri et al., 1999). At a linkage reaction yield of 100% (Grabarek and Gergely, 1990), this puts the number of molecules in contact with the surface on the order of a few thousand. With no way of determining how many of these potential interactions contribute to the observed forces in a single force curve, it is difficult to comment on the type of interaction that is being disrupted upon retraction (i.e., covalent, ionic, non-covalent, etc.). Grandbois et al. (1999) report similar force values for the rupture of a covalent bond, however, their loading rate was an order of magnitude lower ( $10 \text{ nN sec}^{-1}$ ) and, unlike this study, their experiment was specifically designed to capture single molecule interactions.

Hundreds of force curves were collected at a single sample location over sampling periods ranging from 10 to 50 minutes. During this time adhesion force values for both diaspore and goethite fluctuated in a random fashion about the mean ( $2\sigma=10\%$ ) with no discernible time dependence. The consistency of the values suggests that the interacting groups associated with the molecule and the surface remained relatively unchanged after each measurement, and that the bonds that were being disrupted during retraction did not systematically affect subsequent measurements. In contrast to disrupting pre-existing structural bonds associated with the siderophore molecule or mineral surface, the data suggest that each rupture event recorded in sequence represents the breakage of bonds/interactions that were formed and broken during a single approach and retraction cycle.

A clue as to which siderophore functional group is interacting with the surface can be found in a distinctive plateau that is present in many of the retraction curves near the jump from contact. Here, the force slope remains constant over the initial 6-7 nm of retraction (Figure 2.6 and Figure 2.7) and then plateaus as energy is being absorbed. This is interpreted as the extension of the siderophore and linker molecules attached to the mineral surface in parallel. Given the linkage geometry shown in Figure 2.7, the dimensions of the plateau require that the azotobactin molecule be associated with the surface via groups at the C-terminus of the molecule, specifically the homoserine lactone or the hydroxamate group associated with the  $\delta$  N OH-ornithine residue. This is based on calculations that assume an extended length of 0.38 nm for each amino acid (Garrett and Grisham, 1999) and an additional 3 nm added for the 11 carbon hydrazide terminated linker molecule. Reports that the azotobactin hydroxamate group initiates chelation in aqueous systems (Albrecht-Gary and Crumbliss, 1998; Telford and Raymond, 1996) coupled with its terminal position on the molecule, further strengthens the idea that this group is a dominant component during surface interaction.

## **Ionic strength and pH effects on the forces of interaction**

Observed force relationships, specifically the enhanced rupture forces between azotobactin and goethite, were reproducible in both duplicate experiments, and under various solution conditions (Figure 2.8; Table 2.3). However, a closer examination of changes in the forces with pH and ionic strength provides additional information on the nature of the siderophore-mineral interaction and its dependence on electrostatics, mineral surface charge and solubility, and proton equilibria.

First, general trends with pH and ionic strength are identified by comparing results from all data sets independently generated during this study. A more controlled experiment where a single activated tip was probed on goethite while multiple solutions were exchanged from the fluid cell then allowed us to study, in detail, the dependence of these forces on the charge character of the biomolecule mineral interface.

In the separate experiments run up to several months apart, the adhesion force ratio between goethite and diaspore ranged from 2.1 to 3.6 under various pH and ionic strengths (Table 2.3). A notable increase in the goethite/diaspore adhesion ratio is evident with decreasing pH and appears to be driven by a larger drop in the diaspore adhesion values. Going from pH 7 to 3.5 diaspore values decrease on average by 43% compared to 20% for goethite. A disparity also exists when comparing the solubilities of each mineral with pH (3-7) where the change in diaspore solubility is ~3 orders of magnitude higher than the change in goethite solubility. This dictates that as the pH is lowered, more Al(aq) relative to Fe(aq) will become available to satisfy azotobactin's reactive groups and thereby disproportionately disrupt its affinity for the diaspore surface. Similar to the results when soluble iron was added, this technique again demonstrates its ability to capture subtle changes in solution composition at the biomolecule-mineral interface. However, caution must be taken when making absolute comparisons of data sets collected with different tips and mineral samples. Differences in force magnitudes can be produced by relative disorder of the SAM associated with each tip (Ito et al., 1999). And, although many steps were taken to minimize iron contamination, clearly with the extreme

selectivity and sensitivity of azotobactin for Fe(III), even in minute concentrations (this study; Palanche et al., 1999), unforeseen, minimal amounts of iron could alter force values and must be considered.

To further comment on the effect of pH and ionic strength while minimizing the variability associated with data from different tips, an experiment with a single activated tip probed on goethite under various solution conditions was conducted. Representative force curves collected under four different solution conditions (Figure 2.9) show subtle but important effects on the forces of interaction. An increase in ionic strength at constant pH (compare Figure 2.9a and Figure 2.9b) results in a shortened jump to contact distance during approach. A similar decrease in the range of interaction with decreased Debye length has been observed in other force measurements (Lower et al., 2000; Noy et al., 1997) and is attributed to the collapse of the electrical double layer associated with the surface (Israelachvili, 1992; Noy et al., 1997). The small decrease in adhesion shown in Figure 2.9b could reflect the small increase in goethite solubility at higher ionic strengths (Cornell and Schwertmann, 1996; Hsu and Marion, 1985), but is more likely connected with changes in the electrostatic component of the interaction. A decrease in the long-range attractive force on approach (jump to contact; compare Figure 2.9c and 9b) with increasing ionic strength confirms the interaction's susceptibility to changes in the ionic character of the intervening solution. Specifically, the forces drop because the decreased positive surface potential of the goethite at the higher ionic strength (0.1M) (Stumm, 1992) reduces the relative affinity of the negatively charged azotobactin for the surface. Yao and Yeh (1996) invoke a similar argument to explain a drop in the adsorption of smaller ionizable organic ligands (e.g., fumarate and malate) onto  $\delta$ -Al<sub>2</sub>O<sub>3</sub> with higher ionic strengths.

Lower adhesion values were recorded at pH 3.5 (Figure 2.9c) relative to pH 7; an observation that was consistently made throughout this study (e.g., see Figure 2.8, Table 2.3). The additional soluble iron resulting from the 4-5 orders of magnitude increase in goethite solubility at pH 3.5 likely contributes to the decline in adhesion; however, additional lability may also result from proton competition. At lower pH more protons are

available to compete with Fe(III) as a hard acid for the basic, oxygen ligands in the siderophore structure (Crumbliss, 1991). The result is a disruption of azotobactin's affinity for the surface and lowered adhesion values. A change in ionic strength from 0.1M to  $10^{-3.5}$ M at pH 3.5 shows a small rebound in adhesion values (Figure 2.9d). As expected, the change in adhesion values with a change in ionic strength at pH 7 is not present at pH 3.5, where the molecule is predominantly neutral.

## SUMMARY AND CONCLUSIONS

This study has demonstrated the ability of force microscopy to detect the interaction between siderophores and metals contained on mineral surfaces. Specifically, it is believed that the strong adhesion force between azotobactin and goethite is generated by an attraction, both specific and electrostatic (esp. at pH 7) in nature, between chelating groups of azotobactin and the iron contained on the surface of a mineral. This observation alone has implications on the role of azotobactin in mineral dissolution. Page and Huyer (1984) and Page and Grant (1988) have indicated azotobactin works in combination with the smaller ligand dihydroxybenzoic acid (DHBA) to acquire iron from a mineral source. The mechanism they propose begins with DHBA release of  $\text{Fe}^{3+}(\text{s})$  from the mineral via reductive dissolution followed by a transfer of  $\text{Fe}^{3+}(\text{aq})$  to the higher affinity ligand azotobactin and ultimately back to the cell. Studies with other siderophores provide evidence of a possible binary or ternary system for iron transfer from the mineral to the microorganism, including the recent observation of a positive, synergistic effect of desferrioxamine-B with oxalate on goethite dissolution rates (Cervini-Silva and Sposito, 2002). This scenario downplays the siderophore surface interaction of larger ligands, instead relegating the high molecular weight hexadentate chelators (e.g., azotobactin) to a shuttle in solution that uses its superior chelating ability to scavenge iron from bidentate ligands. While dissolution facilitated by this multi-ligand mechanism is feasible, the force evidence demonstrating azotobactin's strong surface affinity presents the distinct possibility of a relatively large siderophore entering into a complex with the mineral surface. Further, steric constraints imposed by ligand size, structure and conformation, together with the limited access to an iron atom contained on

a mineral surface, would certainly preclude hexadentate coordination with the surface (Hersman, 2000). Instead, our force data suggest a coordination formed by oxygen pairs that terminate the azotobactin molecule as one possibility. This observation supports the notion that adsorption and surface complexes are less dependent on ligand structure than aqueous complex formation (Stone, 1997). Evidence of surface complexes involving other siderophores and ligands, albeit much smaller than azotobactin, has also been found with Fourier transform infrared (FT-IR) (Hansen et al., 1995; Holmen and Casey, 1996) and x-ray photoelectron (XPS) (Kalinowski et al., 2000) spectroscopy.

## **Outlook and Possibilities**

This CFM technique allows us to directly monitor ligand-surface interaction under environmentally relevant conditions with pico- to nanoNewton force resolution and a spatial resolution of tens of nanometers down to potentially the atomic level. While investigating the effect of solution conditions on this interaction, it became apparent that the sensitivity of this technique also allows small changes in mineral solubility and associated metal concentrations, pH, and ionic strength to be detected, opening up the possibility of using this technique to detect localized solution micro- or even nanoenvironments associated with a surface.

Force maps that display the spatial distribution of lateral force values which correspond to different levels of tip-sample interaction are also possible with this technique (Noy et al., 1997). Here, a tip activated with a ligand specific for a particular metal (e.g., the siderophore and Fe(III) system) is rastered across a mineral surface. Large adhesion forces associated with areas on the mineral where the complementary metal is found in high concentration, as either a sorbed or structural species, would then provide the contrast necessary to image the metal's spatial distribution. Such images could be useful for identifying contaminant distribution on a surface or pinpointing impurity concentrations on a mineral growth face. Because a near continuum of force values is necessary to generate a complete force map, this technique requires the ligand to remain relatively unaltered upon interaction with the metal or the surface. This appears to be the

case for azotobactin based on the lack of a discernible time dependence of the forces detected over hundreds of measurements.

Parallels may be drawn between predictable trends in forces measured between a ligand and a mineral with trends in ligand adsorption behavior. Briefly, adhesion values between a ligand-activated tip and a mineral could be collected over a given pH range. A plot of these values could then be compared with an adsorption edge for the same ligand over the same pH range in an effort to assess the level of correlation between force measurements and adsorption. For example, a rise in adsorption that is not explained by protonation or deprotonation of the ligand or surface may be explained by a short-range specific interaction recorded as an increase in adhesion force.

The concentration of the siderophore or ligand attached to the tip dictates the number of groups interacting with the surface, and ultimately, the absolute force values of the interaction (Florin et al., 1994; Schmitt et al., 2000). To capture consistent force and energy values at the ligand-mineral interface that can be compared across model systems, the next challenge will be to work towards single molecule force measurements – a task that becomes increasingly difficult with decreasing molecular weight of the molecule of interest. Such measurements have the potential to add to the broad, load-dependent energy landscape (Merkel et al., 1999) that is used to describe the nature of the bonds that are being ruptured upon retraction of the ligand from the mineral.

*Acknowledgements* – We thank S. Lower (U. of Maryland), L. Hersman (Los Alamos Nat'l Lab), C. Tadanier and the remainder of Virginia Tech mineral-microbe/NIRT group including M. Potts, A. Madden, T. Cail, S.E. O'Reilly, C. Airey, A. Doernte for lab assistance, useful discussions, and early reviews of this manuscript. J. Jerz and J.D. Rimstidt also contributed helpful comments and suggestions. F. Rabel and B. Lower provided assistance in modifying the chromatography method, F. Etzkorn and P. Deck assisted in developing the protein linkage scheme and K. DeCourcy provided CSLM support. The manuscript was improved with the comments of two anonymous reviewers. HPLC analysis was completed by E. Smiley (CEE, Virginia Tech). This research was

funded by a GAAN Fellowship (U.S. Dept. of Education) awarded to T. Kendall, NSF's Nanoscale Science and Engineering (NSE) Program (EAR 01-03053), and the Department of Energy's OBES Geosciences Program (DE-FG02-99ER 15002).



## TABLES

Table 2.1 Comparison of average force parameters collected while probing azotobactin on diaspore and goethite.

<b>I=10<sup>-1</sup>M; pH 7</b>	<b>diaspore</b>	<b>goethite</b>
<b>F<sub>adh</sub> (nN)</b>	1.70 ± 0.21	3.58 ± 0.20
<b>Retraction Energy (aJ<sup>1</sup>)</b>	17.2 ± 3.6	69.9 ± 6.8
<b>Jump to contact force (nN)</b>	0.14 ± 0.06	0.81 ± 0.10

<sup>1</sup> aJ = 10<sup>-18</sup> J

Table 2.2 Comparison of Fe(III) and Al(III) overall (1:1) formation constants (K<sub>f</sub>) for selected siderophores and their component/analog ligands.

<b>ligand</b>	<b>log K<sub>f</sub> Fe(III)</b>	<b>log K<sub>f</sub> Al(III)</b>	<b>pK<sub>a1</sub></b>	<b>pK<sub>a2</sub></b>
<b>azotobactin<sup>1</sup></b>	28	n/a	4-5	n/a
<b>deferriferrioxamine B<sup>2</sup></b>	31	22	8.3	9.00
<b>catechol<sup>3</sup></b>	19	17	9.2	13
<b>hydroxycarboxylic acid<sup>4</sup></b>	3.6	0.85	5	>14
<b>acetohydroxamic acid<sup>5</sup></b>	11.5	8	8-10	--

n/a = not available

References: <sup>1</sup> (Palanche et al., 1999; Telford and Raymond, 1996) <sup>2</sup> pK<sub>a3</sub>=9.46, pK<sub>a4</sub>=10.84; (Crumbliss, 1991; Gaspar et al., 1999) <sup>3</sup> (Crumbliss, 1991; Hider, 1984) <sup>4</sup> log K<sub>f</sub> values are for lactic acid; (Perrin, 1979; Telford and Raymond, 1996) <sup>5</sup> (Hider, 1984; Nguyen-Van-Duong et al., 2001)

Table 2.3 Ratios of average adhesion force for goethite and diaspore ( $F_{adh \text{ goethite}}/F_{adh \text{ diaspore}}$ ) under various solution conditions.

Experiment	Ionic strength (M)	pH	$F_{adh \text{ goethite}}/F_{adh \text{ diaspore}}$
1	$10^{-1}$	7	$3.95/1.58 = \mathbf{2.5}$
1 (duplicate)	$10^{-1}$	7	$3.58/1.70 = \mathbf{2.1}$
2	$10^{-3.5}$	7	$3.81/1.38 = \mathbf{2.7}$
3	$10^{-3.5}$	3.5	$3.06/0.86 = \mathbf{3.6}$
4 control (no azotobactin)	$10^{-1}$	7	$0.63/0.87 = \mathbf{0.7}$

## FIGURES

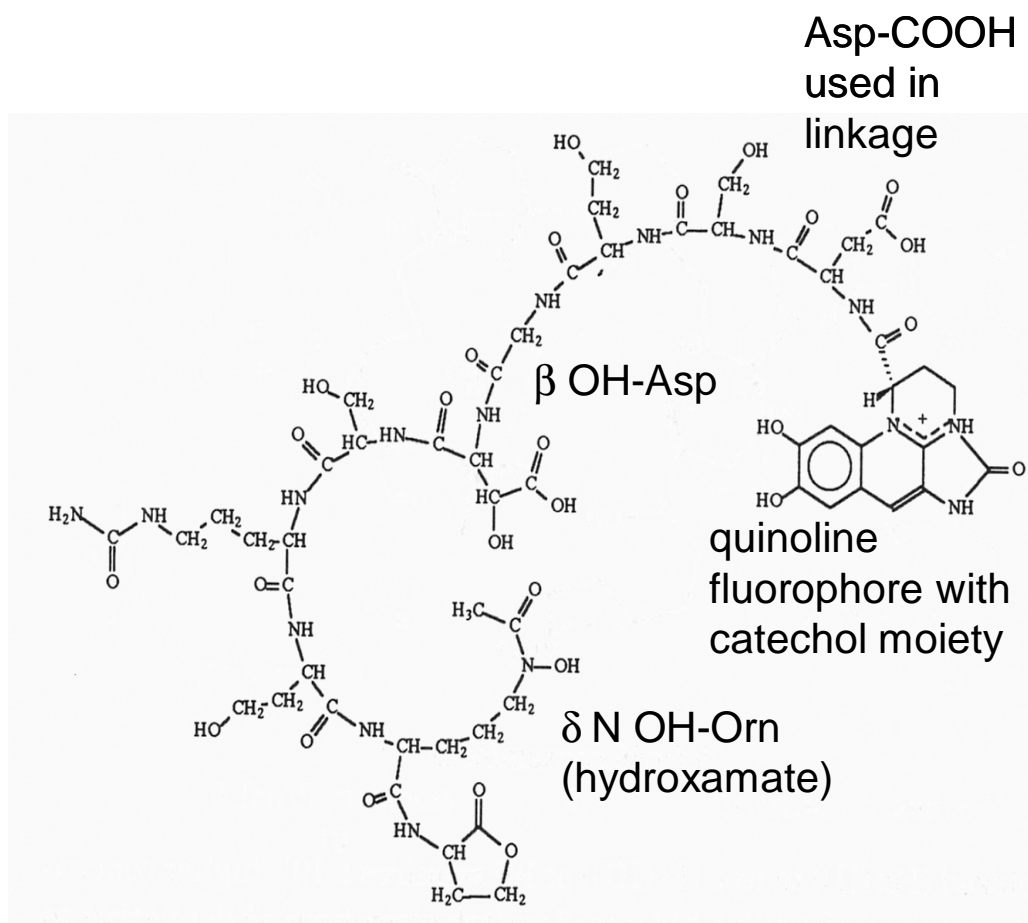


Figure 2.1 Annotated azotobactin  $\delta$  structure (adapted from Palanche, 1999).

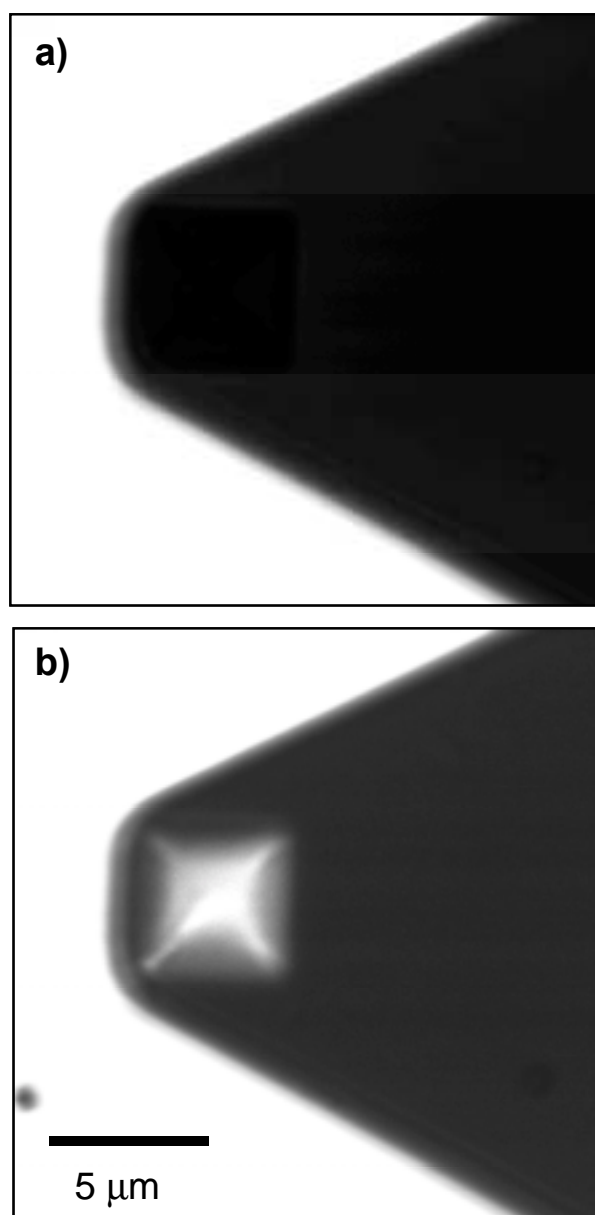


Figure 2.2 Confocal Scanning Laser Image of an a) unactivated AFM tip with no fluorescent signal evident, and b) a tip activated with the inherently fluorescent azotobactin molecule. Images are a composite of two channels (Ch 1,2) collected under a C-Apochromat 40X/1.2 water immersion objective. Ch 1 consists of transmitted light which provides a dark silhouette of the cantilever; Ch 2 uses a 505 nm long pass filter to collect fluorescence generated when the cantilever and tip are exposed to a UV laser (364nm).

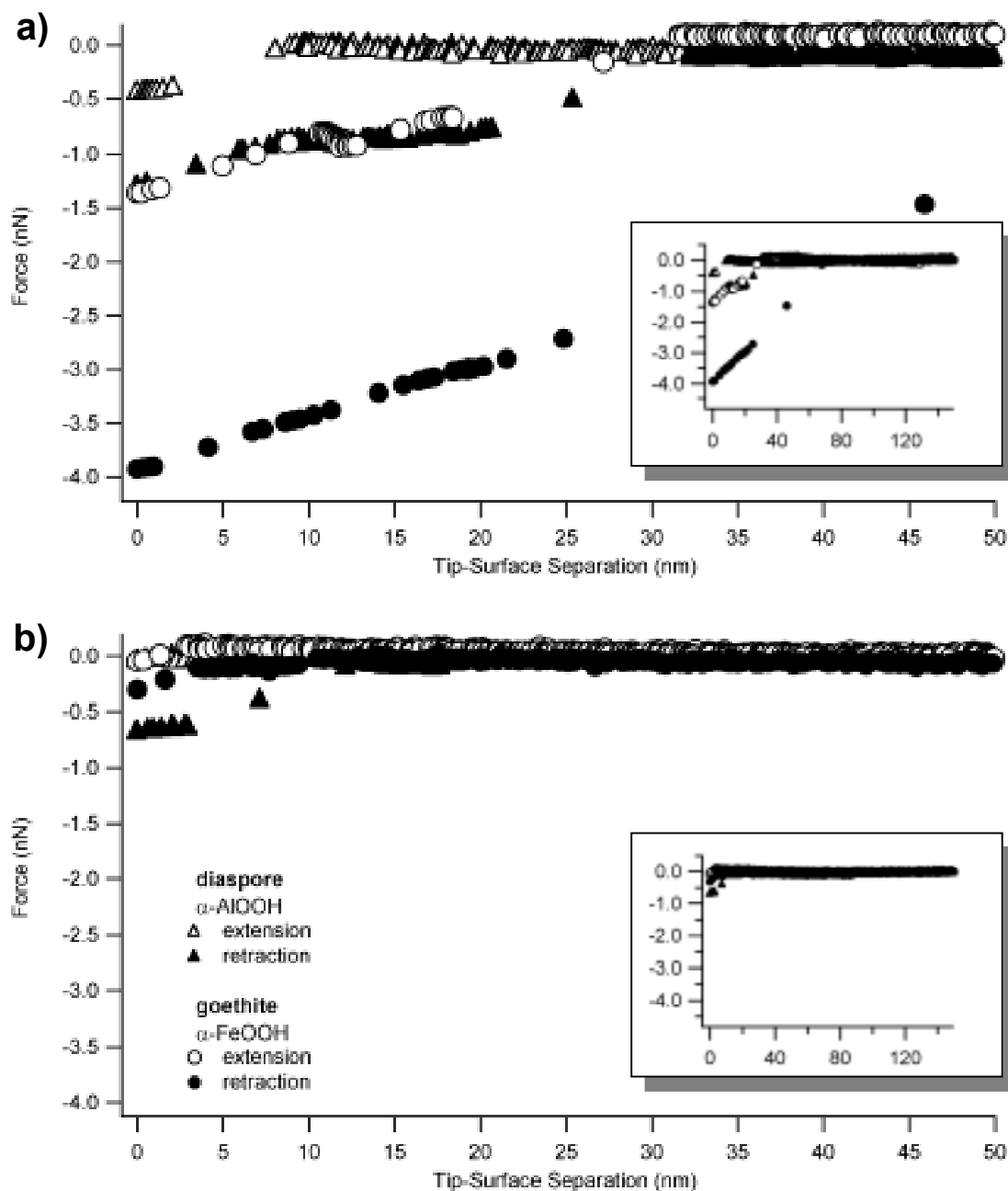


Figure 2.3 Representative force-distance plots showing the interaction between the CFM tip and two minerals, diaspore (empty and filled triangles) and goethite (empty and filled circles). Figure a) shows data collected using an azotobactin-activated tip, and b) shows data collected with a control hydrazide terminated tip. Both force signatures were collected at pH 7;  $I=10$ -1M. Insets represent the same force plot, but with the x axis range increased to show the region of no contact.

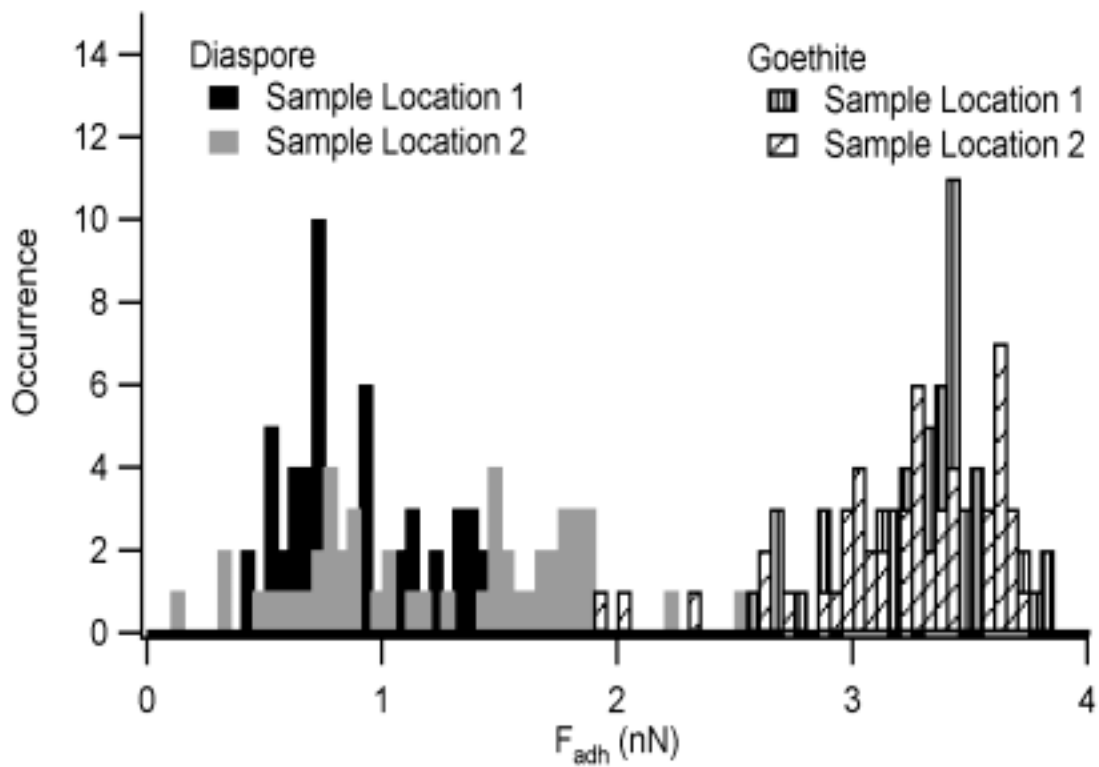


Figure 2.4 Histogram showing variability in adhesion forces ( $F_{adh}$ ) with mineral sample location. Sample locations were randomly selected.

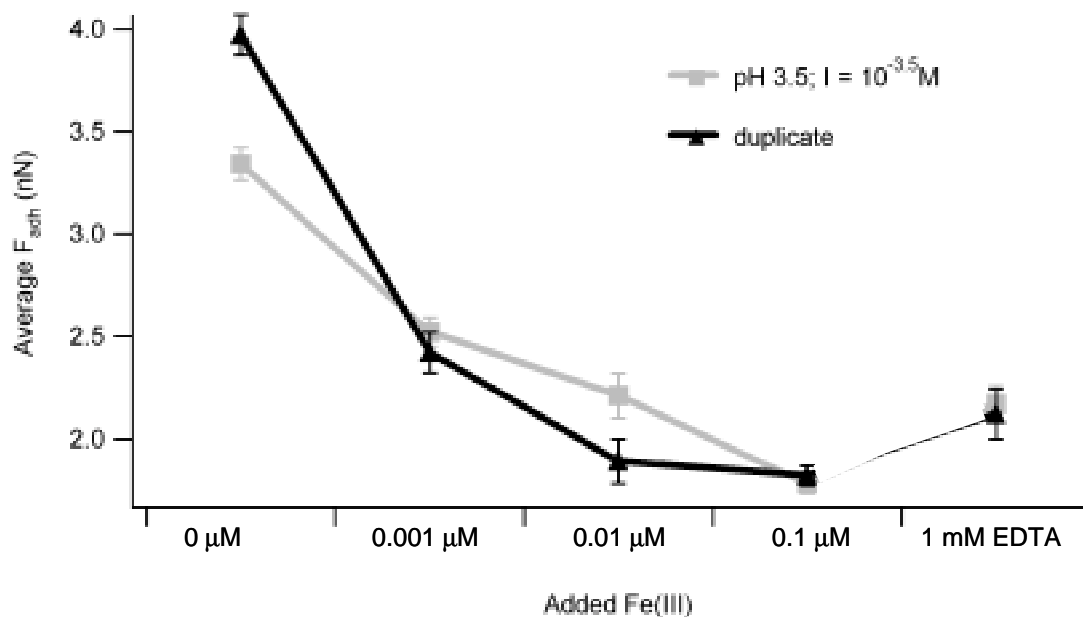


Figure 2.5 Average adhesion force ( $F_{adh}$ ) between azotobactin and goethite versus added ferric iron (as  $FeCl_3 \cdot 6H_2O$ ). The tip was immersed in each Fe concentration for a minimum 15 minutes and then rinsed thoroughly with Millipore water before collecting force measurements. Note the small rebound in adhesion values upon the addition of a small amount of EDTA. Fe(III) solids precipitation is not predicted at the selected pH (3.5) and maximum Fe concentrations (0.1 mM).

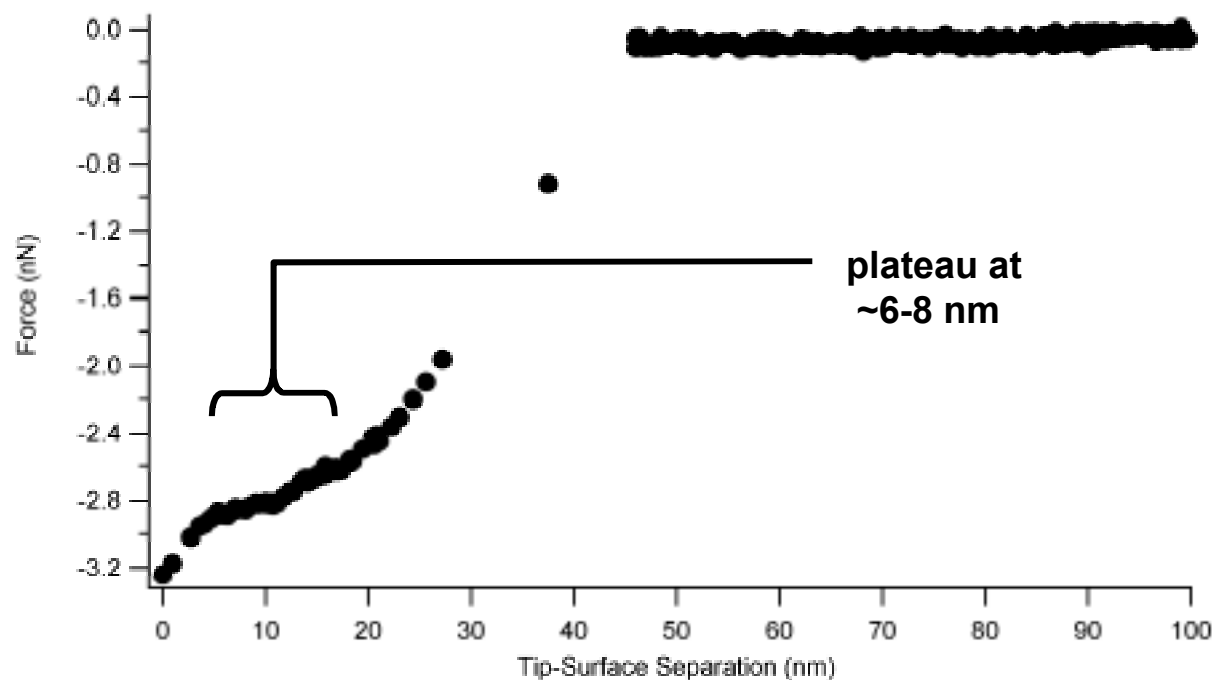


Figure 2.6 Retraction curve showing plateau that is commonly observed in force signatures collected with azotobactin activated tips. It is suggested that this feature may represent the extension of the azotobactin and linker molecule during separation from the mineral surface.



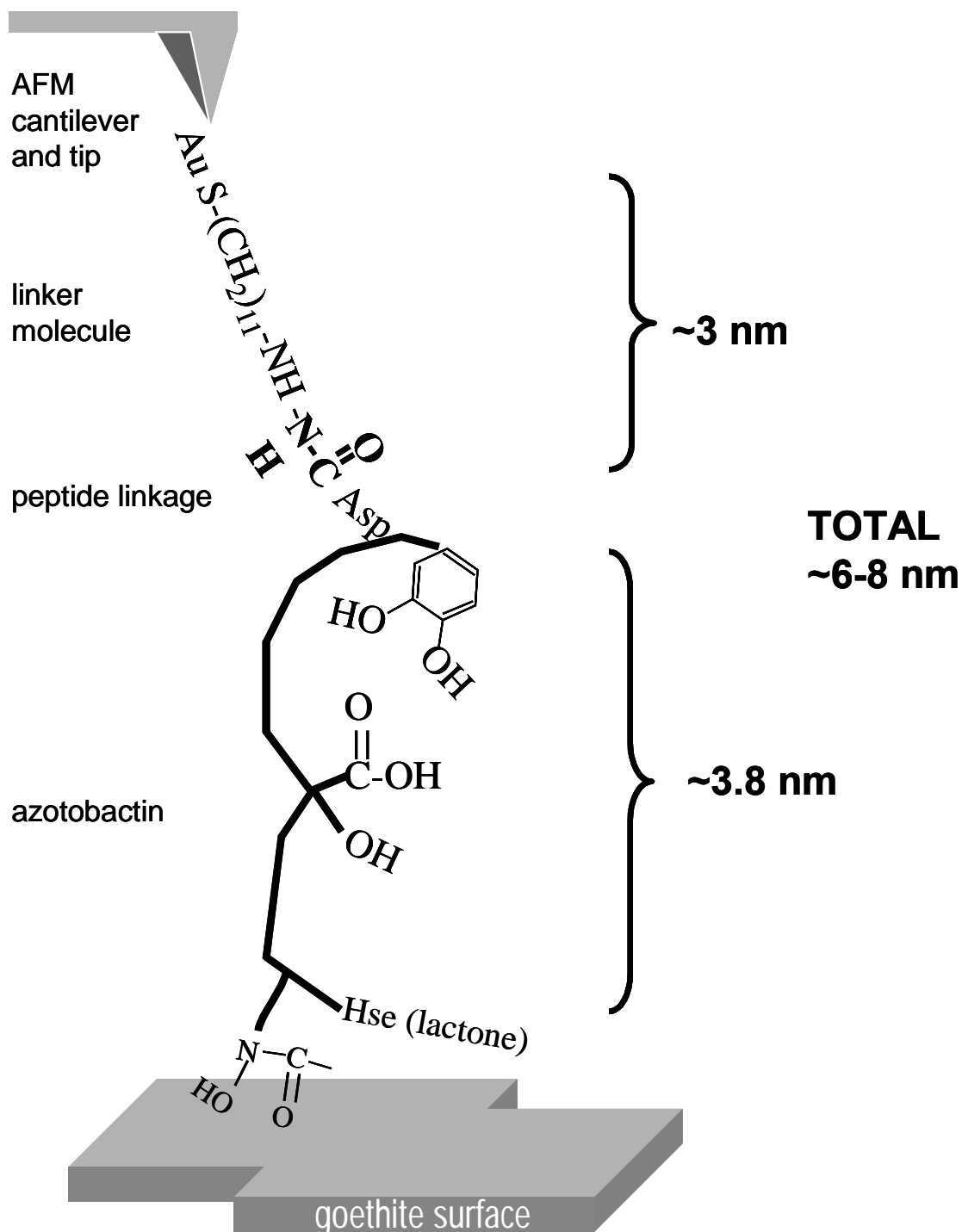


Figure 2.7 Schematic showing extension of the azotobactin molecule during retraction from the mineral surface. Note the geometry and nature of the peptide linkage that joins the molecule to the AFM tip. Not to scale.

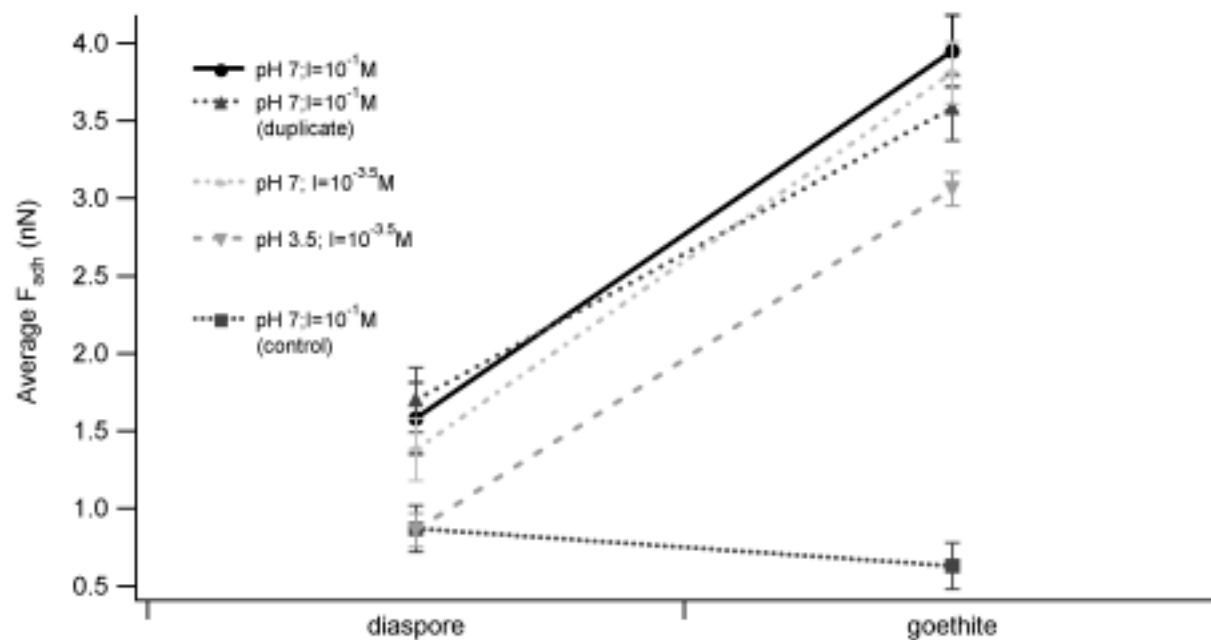


Figure 2.8 Average adhesion forces ( $F_{adh}$ ) for goethite and diaspore collected with azotobactin-activated tip under various solution conditions. Control values collected with only a hydrazide terminated tip are added for reference.

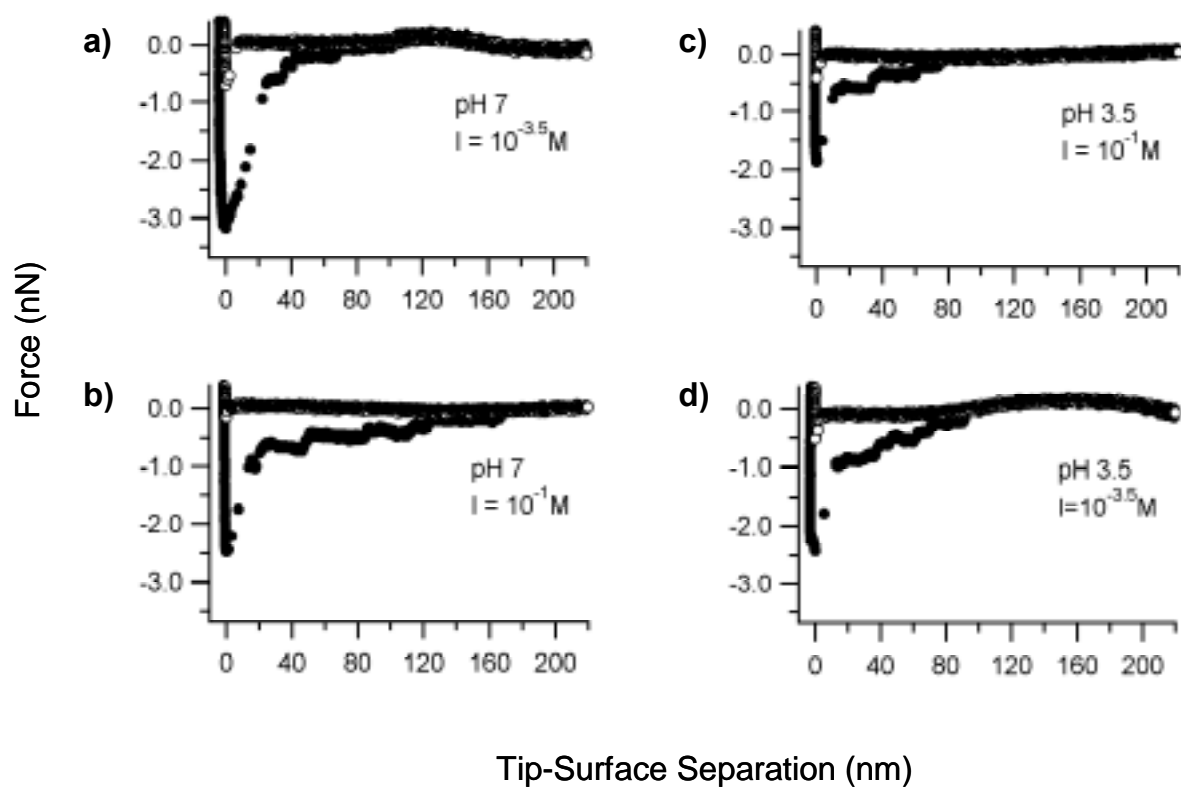


Figure 2.9 Effect of pH and ionic strength on the azotobactin-goethite force signature. See text for details.

## REFERENCES

- Albrecht-Gary A.-M. and Crumbliss A. L. (1998) Coordination chemistry of siderophores: Thermodynamics and kinetics of iron chelation and release. In *Iron transport and storage in microorganisms, plants, and animals*, Vol. 35 (ed. A. Sigel and H. Sigel), pp. 239-327. Marcel Dekker.
- Albrecht-Gary A.-M., Palanche-Passeron T., Rochel N., Hennard C., and Abdallah M. A. (1995) Bacterial siderophores: iron exchange mechanism with ethylenediaminetetraacetic acid. *New J. Chem.* **19**(1), 105-13.
- Bossier P., Hofte M., and Verstraete W. (1988) Ecological Significance of Siderophores in Soil. In *Advances in Microbial Ecology*, Vol. 10 (ed. K. C. Marshall), pp. 385-414. Plenum Press.
- Cappella B. and Dietler G. (1999) Force-distance curves by atomic force microscopy. *Surface Science Reports* **34**, 1-104.
- Cervini-Silva J. and Sposito G. (2002) Steady-state dissolution kinetics of aluminum-goethite in the presence of desferrioxamine-B and oxalate ligands. *Environmental Science & Technology* **36**(3), 337-342.
- Cleveland J. P., Manne S., Bocek D., and Hansma P. K. (1993) A nondestructive method for determining the spring constant of cantilevers for scanning force microscopy. *Review of Scientific Instruments* **64**, 403-405.
- Cocozza C., Tsao C. C. G., Cheah S. F., Kraemer S. M., Raymond K. N., Miano T. M., and Sposito G. (2002) Temperature dependence of goethite dissolution promoted by trihydroxamate siderophores. **66**(3), 431-438.
- Cornell R. M. and Schwertmann U. (1996) *The Iron Oxides: Structure, Properties, Reactions, Occurrence and Uses*. VCH.
- Cornish A. S. and Page W. J. (1998) The catecholate siderophores of *Azotobacter vinelandii*: their affinity for iron and role in oxygen stress management. *Microbiology-Uk* **144**, 1747-1754.
- Crumbliss A. L. (1991) Aqueous solution equilibrium and kinetic studies of iron siderophore and model siderophore complexes. In *CRC Handbook of Microbial Iron Chelates* (ed. G. Winkelmann), pp. 177-235. CRC Press.
- Demange P., Bateman A., Dell A., and Abdallah M. A. (1988) Structure of Azotobactin D, a Siderophore of *Azotobacter- Vinelandii* Strain-D (Ccm-289). *Biochemistry* **27**(8), 2745-2752.
- Dzombak D. A. and Morel F. M. M. (1990) *Surface complexation modeling : hydrous ferric oxide*. Wiley -Interscience.
- Florin E. L., Moy V. T., and Gaub H. E. (1994) Adhesion Forces Between Individual Ligand-Receptor Pairs. *Science* **264**(5157), 415-417.
- Garrett R. H. and Grisham C. M. (1999) *Biochemistry*. Saunders College Publishing.
- Gaspar M., Grazina R., Bodor A., Farkas E., and Santos M. A. (1999) Siderophore analogues: a new macrocyclic tetraamine tris(hydroxamate) ligand; synthesis and solution chemistry of the iron(III), aluminium(III) and copper(II) complexes. *Journal of the Chemical Society-Dalton Transactions*(5), 799-806.
- Grabarek Z. and Gergely J. (1990) Zero-length crosslinking procedure with the use of active esters. *Anal. Biochem.* **185**(1), 131-5.
- Grandbois M., Beyer M., Rief M., Clausen-Schaumann H., and Gaub H. E. (1999) How strong is a covalent bond? *Science* **283**(5408), 1727-1730.

- Hansen D. C., McCafferty E., Lins C. W., and Fitzpatrick J. J. (1995) An FT-IR investigation of parabactin adsorbed onto aluminum. *Appl. Surf. Sci.* **84**(1), 85-90.
- Hersman L., Lloyd T., and Sposito G. (1995a) Siderophore-promoted dissolution of hematite. *Geochimica et Cosmochimica Acta* **59**, 3327-3330.
- Hersman L., Maurice P., and Sposito G. (1995b) Iron Acquisition From Hematite By an Aerobic Pseudomonas Sp. *Abstracts of Papers of the American Chemical Society* **209**, 94-GEOC.
- Hersman L. E. (2000) The role of siderophores in iron oxide dissolution. In *Environmental microbe-metal interactions* (ed. D. R. Lovley), pp. 395. ASM Press.
- Hider R. C. (1984) Siderophore mediated adsorption of iron. In *Structure and Bonding, Vol. 58: Siderophores from Microorganisms and Plants*, Vol. 58, pp. 25-87.
- Holmen B. A. and Casey W. H. (1996) Hydroxamate ligands, surface chemistry, and the mechanism of ligand-promoted dissolution of goethite [ $\alpha$ -FeOOH(s)]. *Geochimica et Cosmochimica Acta* **22**, 4403-4416.
- Hsu P. H. and Marion G. (1985) The solubility product of goethite. *Soil Sci.* **140**(5), 344-51.
- Israelachvili J. N. (1992) *Intermolecular and Surface Forces*. Academic Press.
- Ito T., Citterio D., Buehlmann P., and Umezawa Y. (1999) Observation of Silver and Hydrogen Ion Binding to Self-Assembled Monolayers Using Chemically Modified AFM Tips. *Langmuir* **15**(8), 2788-2793.
- Kalinowski B. E., Liermann L. J., Brantley S. L., Barnes A., and Pantano C. G. (2000) X-ray photoelectron evidence for bacteria-enhanced dissolution of hornblende. *Geochimica Et Cosmochimica Acta* **64**(8), 1331-1343.
- Kondoh H., Saito N., Matsui F., Yokoyama T., Ohta T., and Kuroda H. (2001) Structure of Alkanethiolate Monolayers on Cu(100): Self-Assembly on the Four-Fold-Symmetry Surface. *Journal of Physical Chemistry B* **105**(51), 12870-12878.
- Kosmulski M. (2001) *Chemical properties of material surfaces*. Marcel Dekker.
- Kraemer S. M., Cheah S. F., Zapf R., Xu J. D., Raymond K. N., and Sposito G. (1999) Effect of hydroxamate siderophores on Fe release and Pb(II) adsorption by goethite. *Geochimica Et Cosmochimica Acta* **63**(19-20), 3003-3008.
- Kraemer S. M., Xu J. D., Raymond K. N., and Sposito G. (2002) Adsorption of Pb(II) and Eu(III) by oxide minerals in the presence of natural and synthetic hydroxamate siderophores. *Environmental Science & Technology* **36**(6), 1287-1291.
- Lahiri J., Isaacs L., Tien J., and Whitesides G. M. (1999) A strategy for the generation of surfaces presenting ligands for studies of binding based on an active ester as a common reactive intermediate: A surface plasmon resonance study. *Analytical Chemistry* **71**(4), 777-790.
- Liermann L. J., Kalinowski B. E., Brantley S. L., and Ferry J. G. (2000) Role of bacterial siderophores in dissolution of hornblende. *Geochimica Et Cosmochimica Acta* **64**(4), 587-602.
- Lower S. K., Tadanier C. J., and Hochella M. F. (2000) Measuring interfacial and adhesion forces between bacteria and mineral surfaces with biological force microscopy. *Geochimica Et Cosmochimica Acta* **64**(18), 3133-3139.

- Maurice P. A., Lee Y. J., and Hersman L. E. (2000) Dissolution of Al-substituted goethites by an aerobic *Pseudomonas mendocina* var. bacteria. *Geochimica Et Cosmochimica Acta* **64**(8), 1363-1374.
- Merkel R., Nassoy P., Leung A., Ritchie K., and Evans E. (1999) Energy landscapes of receptor-ligand bonds explored with dynamic force spectroscopy. *Nature* **397**, 50-53.
- Neubauer U., Nowack B., Furrer G., and Schulin R. (2000) Heavy metal sorption on clay minerals affected by the siderophore desferrioxamine B. *Environmental Science & Technology* **34**(13), 2749-2755.
- Nguyen-van-Duong M. K., Guillot V., Nicolas L., Gaudemer A., Lowry L., Spasojevic I., and Crumbliss A. L. (2001) Synthesis, ligand pK(a), and Fe(III) complexation constants for a series of bipodal dihydroxamic acids. *Inorganic Chemistry* **40**(23), 5948-5953.
- Noy A., Vezenov D. V., and Lieber C. M. (1997) Chemical force microscopy. *Annual Review of Materials Science* **27**, 381-421.
- Page W. J. (1993) Growth conditions for the demonstration of siderophores and iron-repressible outer membrane proteins in soil bacteria, with an emphasis on free-living diazotrophs. In *Iron chelation in plants and soil microorganisms* (ed. L. L. Barton and B. C. Hemming), pp. 76-108. Academic Press.
- Page W. J. and Grant G. A. (1988) Partial repression of siderophore-mediated iron transport in *Azotobacter vinelandii* grown with mineral iron. *Can. J. Microbiol.* **34**(5), 675-9.
- Page W. J. and Huyer M. (1984) Derepression of the *Azotobacter vinelandii* siderophore system, using iron-containing minerals to limit iron repletion. *Journal of Bacteriology* **158**, 496-502.
- Palanche T., Marmolle F., Abdallah M. A., Shanzer A., and Albrecht-Gary A. M. (1999) Fluorescent siderophore-based chemosensors: iron(III) quantitative determinations. *Journal of Biological Inorganic Chemistry* **4**(2), 188-198.
- Perrin D. D. (1979) *Stability Constants of Metal-ion Complexes, Part B Organic Ligands*. Pergamon Press.
- Rakovan J., Becker U., and Hochella M. F., Jr. (1999) Aspects of goethite surface microtopography, structure, chemistry, and reactivity. *American Mineralogist* **84**(5-6), 884-894.
- Schaffner E. M., Hartmann R., Taraz K., and Budzikiewicz H. (1996) Structure elucidation of Azotobactin 87, isolated from *Azotobacter vinelandii* ATCC 12837. *Zeitschrift Fur Naturforschung C-a Journal of Biosciences* **51**(3-4), 139-150.
- Schmitt L., Ludwig M., Gaub H. E., and Tampe R. (2000) A metal-chelating microscopy tip as a new toolbox for single-molecule experiments by atomic force microscopy. *Biophysical Journal* **78**(6), 3275-3285.
- Schwyn B. and Neilands J. B. (1987) Universal chemical assay for the detection and determination of siderophores. *Anal. Biochem.* **160**(1), 47-56.
- Seaman J. C., Alexander D. B., Loeppert R. H., and Zuberer D. A. (1992) The Availability of Iron From Various Solid-Phase Iron Sources to a Siderophore Producing *Pseudomonas* Strain. *Journal of Plant Nutrition* **15**(10), 2221-2233.

- Sevinc M. S. and Page W. J. (1992) Generation of *Azotobacter-Vinelandii* Strains Defective in Siderophore Production and Characterization of a Strain Unable to Produce Known Siderophores. *Journal of General Microbiology* **138**, 587-596.
- Staros J. V., Wright R. W., and Swingle D. M. (1986) Enhancement by N-hydroxysulfosuccinimide of water-soluble carbodiimide-mediated coupling reactions. *Anal. Biochem.* **156**(1), 220-2.
- Stipp S. L. and Hochella M. F., Jr. (1991) Structure and bonding environments at the calcite surface as observed with x-ray photoelectron spectroscopy (XPS) and low energy electron diffraction (LEED). *Geochim. Cosmochim. Acta* **55**(6), 1723-36.
- Stone A. T. (1997) Reactions of extracellular organic ligands with dissolved metal ions and mineral surface. In *Geomicrobiology: Interactions Between Microbes and Minerals.*, Vol. 35 (ed. J. F. Banfield and K. H. Nealson), pp. 309-341. Mineralogical Society of America.
- Stout A. L. (2001) Detection and characterization of individual intermolecular bonds using optical tweezers. *Biophysical Journal* **80**(6), 2976-2986.
- Stumm W. (1992) *Chemistry of the Solid-Water Interface: Processes at the Mineral-Water and Particle-Water Interface in Natural Systems*. Wiley-Interscience.
- Telford J. R. and Raymond K. N. (1996) Siderophores. *Comprehensive Supramolecular Chemistry* **1**, 245-266.
- Watteau F. and Berthelin J. (1994) Microbial Dissolution of Iron and Aluminum From Soil Minerals - Efficiency and Specificity of Hydroxamate Siderophores Compared to Aliphatic-Acids. *European Journal of Soil Biology* **30**(1), 1-9.
- Winkelmann G. (1991) CRC Handbook of Microbial Iron Chelates. CRC Press.
- Yao H.-L. and Yeh H.-H. (1996) Fumarate, Maleate, and Succinate Adsorption on Hydrous  $\gamma$ - $\text{Al}_2\text{O}_3$ . 2. Electrophoresis Observations and Ionic-Strength Effects on Adsorption. *Langmuir* **12**(12), 2989-2994.

### **Chapter 3 – Computational Modeling of Azotobactin-Goethite/Diapsore Interactions: Applications to Siderophore-Mineral Reactivity and Molecular Force Measurements**

Treavor A. Kendall\* and Michael F. Hochella, Jr.  
NanoGeoscience and Technology Laboratory, Department of Geological Sciences,  
Virginia Tech, Blacksburg, VA 24061 USA

Udo Becker  
University of Michigan, Department of Geological Sciences  
Ann Arbor, MI 48109 USA

TO BE SUBMITTED  
*Geochimica et Cosmochimica Acta or Langmuir*

#### **ABSTRACT**

Molecular and quantum mechanical calculations were completed to further investigate the interaction between azotobactin and iron/aluminum oxide surfaces, and to more fully understand previous force measurements made on the same systems using an atomic force microscope (AFM). The increased force affinity for Fe over Al characteristic of the experimental force signatures was also observed in the simulated siderophore interaction with goethite and diaspore. *Ab initio* calculations on siderophore fragment analogs suggest the iron affinity can in part be attributed to increased electron density associated with the Fe-O bond compared to the Al-O bond; an observation that correlates with iron's larger electronegativity compared to aluminum. Attachment of the ligand to each surface was directed by steric forces within the molecule and coulombic interactions between the siderophore oxygens and the metals in the mineral surface. Chelating ligand pairs, which consisted of both backbone and amino acid side chain oxygen atoms, coordinated with neighboring iron and aluminum atoms to form a binuclear geometry. Upon retraction of azotobactin from each surface, simulated Fe-O(siderophore) bonds persisted into a higher force regime than Al-O(siderophore) bonds, and surface metals were removed from both minerals. Extrapolation of the model to more realistic hydrated conditions using a PCM model in quantum mechanical calculations (e.g., solvent is modeled as a continuum of uniform dielectric constant) and water clusters in the molecular mechanical model demonstrated that the presence of water energetically favors and enhances metal extraction, making this a real possibility in a natural system.



## INTRODUCTION

Siderophores are known to dissolve iron-containing minerals (Hersman et al., 1995), a process that proceeds independently of the presence of the microorganisms that produced them (Hersman et al., 1996); however, the nature of this mechanism is unknown. Recent force measurements collected on an atomic force microscope (AFM) (Chapter 2; (Kendall and Hochella, 2003)) show that the siderophore azotobactin exhibits a degree of mineral surface specificity that favors iron over aluminum oxides. From this it was postulated that surface contact, coordination and reactivity were potential components of siderophore-mediated oxide dissolution.

Molecular simulations of azotobactin-diaspore ( $\alpha$ -AlOOH) and azotobactin-goethite ( $\alpha$ -FeOOH)/Fe interactions were completed to examine this hypothesis and to complement and more fully understand, at least in a qualitative framework, force measurements collected with the AFM. Specific aims included determining which siderophore functional groups attach to the surface and to characterize the nature and geometry of these coordinations. Of the groups that coordinated we hoped to discriminate between relatively weak and strong linkages using energy-distance profiles and derived forces. Using these simulated forces we hoped to make a qualitative comparison with experimental forces to see if the same distinction in goethite and diaspore force signatures observed using the AFM was predicted by the model. Quantum mechanical calculations were also completed to complement the molecular simulations and to assess the source of affinity and specificity of chelating O atoms for Fe. The effect of the interaction on the metal in the mineral structure was also examined with a specific question in mind: is “dissolution” observed under any of the simulated, albeit simplified, conditions (e.g. azotobactin in contact with the mineral surface in vacuum, or under hydrated conditions simulated with a constant dielectric field or with added water clusters)?

## METHODS

### Molecular mechanics

Simulations were carried out using the Cerius<sup>2</sup> computational package (Accelrys, Inc.) on a Silicon Graphics, Inc. (SGI) Octane workstation. In order to develop a set of empirical potentials that mimic the physico-chemical properties of goethite and diasporite, we used the program package GULP (Gale, 1998) to derive these potentials. The Catlow potential library (Sanders et al., 1984; Schroder et al., 1992) was used for initial values of the interatomic potentials for the fitting process. Since Cerius<sup>2</sup> can only utilize rigid core models, the Catlow potentials (which use core-shell models) had to be modified into pure core models. For the fitting procedure, the structural parameters (lattice constants and fractional coordinates) of diasporite (Busing and Levy, 1958) and goethite (Gualtieri and Venturelli, 1999), the elastic constants of diasporite (Haussühl, 1993) and the bulk moduli of diasporite (Haussühl, 1993); and goethite (Haussühl, 1993; Smyth et al., 2000) were used as observables. The elastic constants of goethite were estimated using the ones from diasporite and scaling them with the quotient of the bulk moduli of the two minerals. The interactions within the siderophore molecule are simulated by using the so-called Universal Force Field (Rappe et al., 1992) in combination with Coulomb potentials derived by using the Qeq charge equilibration scheme. This method calculates the charges of a particular species by comparing the electronegativities of that species with the electronegativity values of its neighbors in an iterative process.

The force fields between the siderophore were divided in two groups:

- i. The interaction between the functional (chelating) groups of the siderophore with the cation of interest (Fe or Al) on the surface.
- ii. The interaction between all other atoms in the siderophore with all other atoms in the atomic cluster simulating the mineral.

In order to develop a potential that models the siderophore-metal interaction as precisely as possible, quantum mechanical calculations were performed using the program package Gaussian98 (Frisch et al., 1998). The binding energies and partial electron transfer were calculated as described using a HF-DFT (Hartree-Fock/Density Functional Theory) hybrid approach using the Becke3LYP functional (for further details on the quantum mechanical calculation, see section on Quantum Mechanical Calculations). These binding energies were transformed into Morse potentials between the Fe/Al cations and the O atoms of the chelating groups. It should be noted that one disadvantage of using bonded Morse potentials is that some degree of arbitrariness is introduced because it is up to the judgment of the user of the Cerius<sup>2</sup> program where to draw bonds between the functional groups and the cation, depending on the respective geometry of the molecule as a function of separation from the surface.

Most of the molecular mechanics simulations were in vacuum (dielectric constant  $\epsilon = 1$ ) to reduce computation time; however, solvated conditions in selected runs were simulated by increasing the dielectric constant ( $\epsilon = 80$ ) or adding clusters of individual water molecules to the system. The azotobactin  $\delta$  molecule was constructed based on the structure provided by Palanche et al. (1999) and simulated in a fully deprotonated state with a net charge of -5, thus discounting the influence of protonation equilibria on the energetics of the system. This allowed us to focus on the specific interaction between the siderophore O atoms and the Fe atom in the mineral structure. Choice of this condition is further validated by other studies that indicate retraction force measurements on other ligand-receptor systems containing similar functional groups with comparable pKa's are independent of proton equilibria, and instead are driven by the enthalpy associated with specific bonds and interactions (Izrailev et al., 1997; Moy et al., 1994). Similar to the AFM experimental conditions (Kendall and Hochella, 2003), a hydrazide terminated 11 carbon linker molecule was attached to the azotobactin via a peptide bond to the Asp carboxyl group (Figure 3.1). A gold atom was added to the end of the linker molecule to represent the gold coating on the AFM tip. The azotobactin molecule was brought into contact with both a single Fe<sup>3+</sup> atom and the (010) face of a goethite and its isostructural Al-equivalent diaspro (Figure 3.1). In terms of metal atoms, each simulated mineral

surface consisted of a 20 x 11 x 4 cluster that was terminated insuring no net charge existed on the mineral and that the goethite and diasporite stoichiometry remained intact. Structural information for each mineral including cell parameters and fractional coordinates were obtained from the literature (Busing and Levy, 1958; Gualtieri and Venturelli, 1999). In order to separate the influence of compression/stretching force within the azotobactin, as well as azotobactin-mineral surface interactions (included) and surface relaxation and bond formation/breaking in the surface (not included), the positions of atoms in the mineral cluster were fixed during the initial extension of the molecule towards the surface. Prior to the interaction, the siderophore-linker construct was fully extended by fixing the gold atom at the beginning of the linker and advancing the methyl carbon associated with the hydroxamate group towards the C-terminal end of the molecule in 0.5 Å steps and minimizing the structure after each step. The result was a linearized conformation of the molecule (Figure 3.1). This was completed to provide consistency and reproducibility in the interaction simulation, to insure functional groups were not hindered or prevented from interacting with the surface and to facilitate comparison between the two mineral systems. After the stretching of the molecule, and prior to simulating the extension of the molecule toward the mineral surface, the hydroxamate methyl carbon was released, and allowed to move freely during minimizations. The Au atom remained fixed and AFM extension (approach) or retraction motion was modeled by decreasing or increasing, respectively, the distance between the gold atom and the mineral surface. The molecule was advanced in 0.3-1.5 Å steps during extension and 0.5 -1.5 Å steps upon retraction. An optimization was completed after each step and the overall energy of the system plus interatomic distances between siderophore O atoms and surface bound metals were recorded. Molecular dynamics was used on the extension trace only, where the system was ramped to a temperature of 300K followed by anneal dynamics (annealing cycles between 100K and 300K) and a subsequent energy minimization. These additional molecular dynamics simulation steps were performed to ensure that the system does not get trapped in local energy minima that do not represent the fully optimized structure.

Comparison of calculated lattice energies (e.g., determined with GULP) to values predicted by solubility constants and component ion hydration energies for each mineral provides a scaling factor to adjust all model values that incorporated the GULP clusters. As shown in Table 3.1, lattice energies predicted by GULP were higher than those predicted by the solubility constants; presumably due to the overestimation of the electrostatic energy contribution that results from using formal charges in the simulations. This overestimation was partially accounted for by reducing goethite and diasporite energy values by 8% and 6%, respectively.

To facilitate discussion of the siderophore structure, each O atom has been numbered according to Figure 3.2. This numbering system is referred to when describing the O atoms that coordinate and release from each surface or the free Fe<sup>3+</sup> ion. Coordination or bonding to the surface was defined as an Fe/Al-O (siderophore oxygen) distance of less than 2.2 Å.

### **Quantum mechanical/*ab initio* calculations**

Higher level *ab initio* calculations were completed with Gaussian98 (Frisch et al., 1998) to examine hydration and metal (Fe<sup>3+</sup> and Al<sup>3+</sup>) binding energies associated with small ligand fragments that represent analogs of selected azotobactin functional groups. For example, acetohydroxamic acid, a hydroxamate siderophore analog commonly used in previous bulk dissolution studies (Holmen and Casey, 1996), was employed to represent azotobactin's ornithine hydroxamate (O1 and O2 in Figure 3.2) functional group. At this level of theory, smaller fragments (e.g., on the order of a few atoms) are required to render the simulation computationally practical. Initial geometry optimization of each ligand, metal and ligand-metal complex was achieved using a Hartree-Fock Self Consistent Field and a Pople-type 3-21g basis set. Hartree-Fock optimized coordinates were then used as a starting point for a second set of simulations using in the HF/DFT hybrid method using the Becke-style 3-parameter Density Functional Theory and a larger basis (6-31G(d)) set. Hydrated environments were modeled as a continuum of uniform

dielectric constant using Tomasi's Polarized Continuum Model (PCM) (Miertus and Tomasi, 1982).

## RESULTS AND DISCUSSION

Under the modeling conditions the simulated force/energy distance curves can be separated into a number of phenomena during approach/retraction:

- *successive formation/breaking of bonds between the azotobactin molecule and the surface (specifically Fe or Al on the surface),*
- *contraction, twisting and stretching of the azotobactin molecule into various confirmations,*
- *displacement of Fe or Al atom from its equilibrium position in the lattice*
- *release of an Fe or Al atom from the surface,*
- *additional chelation/increased coordination of extracted metal atoms once other azotobactin groups are free of the surface.*

### **Simulated approach force trace - Azotobactin and goethite/diaspore**

Upon extension of the azotobactin molecule to both the goethite and diasporite from a Au-surface separation of 63 Å to ~10Å, the siderophore O atoms coordinated with metals on the surface in a sequence that was consistent with their relative position on the peptide backbone: the C-terminal groups (e.g., the Hse (lactone) and hydroxamate moieties; see Figure 3.2) coordinated first followed by groups closer the ring structure at the pseudo-N terminus. This is expected because each amino acid was aligned, in order, upon stretching the molecule to a maximum contour length prior to the surface approach (see Methods). Although it was not fixed and atomic motion was permitted, the linker molecule remained extended and rigid throughout the simulation. As a result, the linker angled away from the axis of the extension and retraction; serving as a guide to lay the molecule along its length onto the surface. The extension trace for each mineral was similar, with the diasporite curve essentially shifted down in relative energy scale due to

the lowered lattice energy associated with diascore and differences in the definition of the metal-oxygen interaction potentials associated with each mineral. Future refinement of these potentials and, more importantly a quantitative and explicit treatment of water adsorption to the system, should allow better quantitative assessment of the absolute energy values associated with the two systems, but, for now, only qualitative and/or relative comparisons will be made. All O atoms in both the peptide backbone and amino acid side chains had the potential to coordinate with metals in the surface, however, steric constraints imposed by the siderophore structure dictated which ones came close enough to ultimately interact. These included (in order of coordination to the surface): O1/O2 (hydroxamate), O4/O5 (Hse lactone), O3/O7 (backbone O atom and Hse), O11 (Ser hydroxyl), O13/O14 ( $\beta$ -hydroxyacid) (see Figure 3.3). The slashes (“/”) in the previous sentence indicate attachment of the two O atoms in the chelating group was approximately simultaneous.

It was interesting to note that the spacing of siderophore chelating pairs allowed roughly equidistant coordination to neighboring Fe atoms in the lattice (Figure 3.4). This was unexpected, as siderophore-sorption models based on bulk solution experiments predict an oxygen pair coordinating with a single Fe (Holmen and Casey, 1996) and not with neighboring Fe atoms. Also, note that two of three groups known to participate in the stable chelation of Fe(III)(aq) (O1/O2 hydroxamate and O13/O14 hydroxyacid) were sterically allowed to interact with the surface; however, O atoms associated with other groups such as Hse were important to the surface interaction as well. Other functional groups higher up the backbone (e.g. past O13/O14  $\beta$  hydroxyacid and closer to the quinoline group), including the catechol group, which participates in chelation of the free aqueous iron, did not coordinate with the surface. This could be, in part, due to the steric (and coulombic?) restrictions imposed by their proximity to the linker molecule.

Preliminary extension simulations (see Figure 3.5) confirmed this, where at  $\sim 35\text{\AA}$  Au-surface separation, the linker essentially folded the azotobactin molecule back upon itself with the  $\beta$  hydroxyacid (O13/O14) serving as a hinge point. While this behavior is probably unique to the presence of the linker, and not necessarily reflective of a surface conformation typical in nature, it is interesting to note that a similar hydroxyacid hinge

point position is observed in the azotobactin-Fe(III) aqueous complex structure (see Figure 3.2). In contrast to the first set of extension/approach simulations, the approach shown in Figure 3.3 was generated when a lateral component was added to the downward motion (see also schematic in Figure 3.5). This was done to avoid generation of the hinge point and to stretch and lay the upper part of the molecule onto the mineral, thereby giving groups that are above the  $\beta$  hydroxyacid an opportunity to interact with the surface. Nonetheless, additional coordination of groups closer to the Au atom (where the tip is) was not observed. Future simulations with better constraint on the magnitude and direction of this “diagonal” advance will be required to confirm if this lack of interaction is valid.

Significant gains in energy were recorded upon the coordination of each group (Figure 3.3) with noticeable changes associated with the attachment of the hydroxyacid and the C-terminal Hse (lactone) (O4/O5). The final energy of the goethite system at an Au-surface separation of 10.8 Å was -7547.4 kJ/mol, and differentiation of the energy profile showed a maximum force of 923.61 pN. This force peak, qualitatively equivalent to a jump to contact force, was associated with the docking of the Hse lactone group. It may be tenuous to compare these results directly to AFM data collected in solution; however, it is worth noting that the force magnitude and distance at which this jump occurred (~52 Å) compared favorably with averaged AFM data values (at both pH 3.5 and pH 7) collected with relatively high spring constants ( $k_s = 0.123$  N/m) (see Table 3.2). This was not the case with other data sets collected with softer (less stiff) cantilevers ( $k_s \sim 0.06$  N/m) that were perhaps less adept at capturing the steep gradient generated by the Hse lactone jump in the energy profile (see Appendix). Here, with one exception, the lower spring constant resulted in higher distance and force values.

Other factors should be considered when making this semi-quantitative comparison of modeled forces with AFM data. The simulated value is representative of a single azotobactin molecule interacting with the surface. Based on dimensional considerations and a JKR model of adhesion, the capture of a single molecule interaction was not predicted for the prior AFM experiments (Chapter 2; Kendall and Hochella, 2003). Also,



the simulation was completed in a vacuum and the jump to contact energies and distances are expected to be lower in the presence of water due to charge shielding. An assessment of the additive effect of multiple interactions (or a reassessment of the number of interactions captured in the AFM data), together with a characterization of the influence of a solvated environment should be completed to make a more definitive comment on this relationship.

### **Simulated azotobactin and free Fe<sup>3+</sup> interaction**

The bonding sequence during extension towards the goethite is different from the bonding order associated with the interaction of the azotobactin-linker construct with a single ferric iron. This emphasizes the different roles that each functional group may play depending if the siderophore encounters Fe atom in a solid or aqueous form. As the free ferric iron was moved into the siderophore structure parallel to its extended peptide backbone axis (see Figure 3.1), the following attachment and release sequence was revealed: O1,O2,O4/O5,O7, O5 off, O8/O9, O4 off. Again, the hydroxamate (O1,O2) is shown to participate in the coordination, however, steric hindrances precluded attachment of the catechol or the  $\beta$ -hydroxyacid groups (O13/O14), even though the ferric iron was advanced to a separation of 8 Å from the gold atom. The expected hexadentate (hydroxamate, catechol, hydroxyacid) coordination that is suggested for the stable Azb-Fe(III) (aq) complex was not observed, probably as a result of the direction and geometry of the advance of the iron into the structure and the reduction in the degrees of conformational freedom imposed by the linkage. The presence of the available, uncoordinated chelating groups in the model containing free iron, do however, provide the following connection to the experimental data.

During AFM experiments, the azotobactin-goethite interaction was probed after successively adding soluble free Fe<sup>3+</sup> ion (Chapter 2; Kendall and Hochella, 2003). A sharp decrease in adhesion forces with increasing [Fe(III)(aq)] was followed by a plateau of residual adhesion that existed in spite of sufficient iron to satisfy the chelating groups associated with all of the azotobactin molecules attached to the tip, cantilever and

substrate (see Chapter 2; Kendall and Hochella, 2003). The source of the residual adhesion was hypothesized to be free chelating groups or other sidechain or backbone O atoms interacting with the surface; an idea that is now supported by the conformation suggested in the azotobactin-Fe(III) model.

### **Simulated retraction force trace - Azotobactin and goethite/diaspore**

Prior to retracting the azotobactin from the surface, the metals in each mineral lattice in close association ( $<2.2$  Å away) with siderophore O atoms were identified (8 total for goethite and diaspoire) and marked with distance monitors. These metal atoms were allowed to relax and a Morse potential was defined between the metal and the coordinating siderophore O atom. In contrast to a harmonic potential which shows an exponential increase in energy in both directions away from a bond equilibrium distance, a Morse potential flattens out at larger atom separations, thus providing a better representation of the Fe/Al-O energy distance relationship (Cygan, 2001). The interaction between the relaxed metal and the remaining mineral structure was modeled with a combination of Lennard-Jones and Coulomb potentials from the UFF potential scheme. Because no additional short-range interaction of siderophore groups was observed at Au-surface separation distances of less than  $\sim 36$  Å during extension, simulation time was reduced by beginning the retractions at this point.

#### *Goethite*

Metals were removed from both minerals by the siderophore in the simulated retraction. During retraction from the goethite, one Fe atom was completely removed from the structure by the terminal Hse group (O4/O5) and 4 others were displaced significantly from their equilibrium position in the lattice (e.g.,  $0.5$  Å; Fe-O(goethite) bond stretched  $>2.5$  Å) (Figure 3.6). With the exception of the spike in Fe atom displacements associated with O14 ( $\beta$  hydroxyacid; see discussion below), the displacement magnitudes steadily increased as the overall accumulated stress was transferred from one functional group to the next. This trend parallels the energy profile, which is characterized by a large initial

buildup, followed by a steady rise in energy with periodic spikes correlating to the release of specific functional groups (some with a metal attached) (Figure 3.6). As expected, the order of release from the surface was close to the reverse of the extension attachment sequence, with differences in the order of release of the C-terminal groups. The release sequence is as follows (O atoms separated by commas indicate two discrete releases; O atoms joined with slashes “/” indicate simultaneous release): O13, O14, O11, O7/O3, O2, O1, O4/O5. Interesting observations are included in this ordering. One, the Hse OH (O7) and O3, a component of a backbone carbonyl (O3) were coupled in their release, in spite of a separation of almost a nanometer in contour length. Conversely, a lack of coupling was observed between the hydroxamate and hydroxyacid oxygen pairs separated by 1-2 Å.

Although 8 discrete coordinations and releases were observed during the simulations with goethite, only four major energy peaks are identified in the energy profile (Figure 3.7). These are associated with the steady release of O13 and sharp release of O14; 2) the release of O7; 3) O3; and 4) the steady release of O1 followed by the sharp release of O4 and O5 (see Figure 3.6 and Figure 3.7). The release of the hydroxamate hydroxyl (O2) was masked in the energy profile, emerging only as a shoulder (at 91 Å) in the large energy buildup associated with the terminal O1, O4, O5 coordination (see Figure 3.7). This terminal coordination resulted in a maximum absolute jump from contact force of 1867 pN and a full extension of 9.3 nm. Similarly, plateau features in the AFM retraction data (Kendall and Hochella, 2003) show a flattening of the force trace at 6-8 nm of separation from the surface. Previously interpreted as the energy absorption associated with a full stretch of the azotobactin molecule, these features predict a C-terminal association as the final, persistent link to the surface; a geometry that is supported by the simulations.

### *Diaspore*

Morphologically, the diaspore retraction energy profile is similar to that of goethite, in that it shows four major energy peaks associated with the 8 coordinations (Figure 3.7).

However, closer inspection of the Al displacements and the separation distances at which siderophore functional groups release from the surface reveals a significantly different interaction. One Al atom was removed from the structure (again by the terminal Hse group), and only 1 other atom was significantly displaced during retraction of azotobactin from the diaspore surface (Figure 3.8). The large metal displacement observed for the Fe-hydroxyacid coordination was much less pronounced with the diaspore and, overall, the relative metal displacement values were higher for goethite (compare with Figure 3.6). The sequence was essentially the same as that of goethite, however, functional groups released from the diaspore surface at smaller separation distances. This is reflected in the energy profile where shifts in diaspore peak positions (to the left) show lower energy accumulation in the Al-O(siderophore) surface bond prior to release compared to the Fe-O(siderophore) bond. In other words, the Fe-O(siderophore) bonds persist into a higher force regime resulting in relative goethite adhesion values that are  $1.5\text{-}1.7 \times$  higher than diaspore, in spite of the increased pullout energy predicted for Al over Fe (in the absence of the siderophore; see Table 3.3) (e.g., the higher forces appear to result from the Fe-O(siderophore) linkage and not the Fe-O(goethite) bond). This relationship is comparable to AFM goethite/diaspore adhesion ratios ( $2\text{-}3\times$ ), which also show increased adhesion and affinity for goethite. Note that the lowered absolute energy values associated with the diaspore are likely due to the differential stress imposed on the azotobactin molecule by subtle differences in the diaspore metal spacing and by the higher lattice energy of diaspore with respect to goethite. The latter effect lowers the absolute energy due to stronger metal-mineral interactions within diaspore.

### **Quantum mechanical calculations and discussion of metal removal**

Results from the *ab initio* calculations were compared to molecular mechanics to further define the energetics and affinity of the siderophore-mineral interaction and to explain and possibly validate the observed extraction of the metal from the mineral surface. Moreover, by incorporating a dielectric continuum model (Tomasi's PCM) together with comparison and integration of experimentally determined hydration energies, we

continued to advance the modeled interactions toward a more realistic, solvated environment.

Complete removal of metals from each mineral structure by the siderophore was not expected. The lack of time dependence and consistent adhesion values in the AFM force measurements suggested no metal was being removed and that the bond that was being ruptured upon retraction was formed each time during extension (see Chapter 2). This then raises the question of how realistic is the simulated metal removal? The following considerations suggest the surface metal extraction by the siderophore is indeed a distinct possibility.

The molecular mechanics simulation were completed in vacuum (again, to achieve reasonable computation times) and yet, without water present to solvate the displaced metal and intervene as a secondary or “helper” ligand, siderophore extraction from the metal is still observed. The role of water as a secondary ligand was confirmed in early, preliminary molecular mechanics simulations using a universal force field (Rappe et al., 1992) of a  $\beta$ -hydroxycarboxylic acid (O13-O15) analog (lactic acid) interacting with a relaxed Fe atom in a goethite surface. Here, the addition of a cluster of 20-30 water molecules in the simulation facilitated complete removal of the Fe atom by the siderophore analog. Also, in a hydrated environment, it is likely that the metals that were displaced to a  $M^{3+}$ -O(mineral) interatomic separation exceeding  $\sim 2.5\text{\AA}$  would be shielded from underlying lattice by intervening water molecules and therefore completely removed (opposed to unrealistically snapping back to the lattice as shown in Figure 3.6 and Figure 3.8). This would bring up the total metals removed from goethite and diasporite to 5 and 2 respectively; a difference that may reflect siderophore specificity, but more likely represents the lowered simulated pullout energy associated with Fe over Al (Table 3.3). Moreover, during the retraction, a binuclear geometry was modeled for each siderophore O atom that coordinated with the surface. This was in response to the geometry that resulted from the initial extension/attachment of the molecule to the surface and we believe represents a likely scenario in nature. Upon retraction, however, it is possible for a bidentate coordination to form as one O atom of a chelating pair

releases from the surface while the other continues to displace a metal. Even though the model suggests the siderophore is effective in extracting iron with only a binuclear coordination, it was hypothesized that a bidentate geometry, if formed, would be even more effective. This hypothesis was verified in a separate simulation, where the binuclear coordination between the siderophore's  $\beta$ -hydroxycarboxylic acid and the surface was changed to bidentate resulting in complete removal of the Fe atom (e.g. with no snap back of the metal to the lattice).

In an argument developed with U. Becker (U. Michigan), results from the molecular and quantum mechanical calculations indicate that the hydration and relaxation of the defect site represents another energetic component that favors removal of the structural Fe atom upon retraction of the siderophore. The first step is to determine the magnitude of this energy,  $E_{\text{hydration/relaxation (vacancy)}}$ , which is included in the sum of the energy associated with removal of an Fe atom from the lattice,  $E_{\text{pullout}}$ , as shown in the following equation:

$$E_{\text{pullout}} = E_{\text{hydrationFe}^{3+}} + E_{K_{\text{sp}}} + E_{\text{hydration/relaxation (vacancy)}}.$$

$E_{\text{pullout}}$  calculated using the molecular simulations of the goethite cluster equals  $-6127$  kJ/mol.  $E_{\text{hydrationFe}^{3+}}$  represents the energy gained by hydrating the  $\text{Fe}^{3+}$  ion and can be calculated from literature values (Rashin and Honig, 1985; Rosseinsky, 1965) as  $-4398.2$  kJ/mol. The solubility product of goethite ( $K_{\text{sp}} = 10^{-44}$ ; Lindsay, 1979) dictates that  $E_{K_{\text{sp}}} = -RT \ln K_{\text{sp}} = 252.7$  kJ/mol is required for dissolution. Thus the equation can be solved to show that  $E_{\text{hydration/relaxation (vacancy)}} = -1476.5$  kJ/mol is gained by hydrating and relaxing the defect site when removing the iron. There is, however, an energy cost of displacing the water from the ligand to allow coordination with the cation. The magnitude of this value is derived from quantum mechanical calculations completed on fragments representing siderophore functional groups (see Table 3.4). As one example the difference in hydration energy for the hydroxyacid fragment (e.g., the analog to the  $\beta$  hydroxycarboxylic acid; O13, O14, O15) is  $1035.5$  kJ/mol  $- 377.1$  kJ/mol =  $658.4$  kJ/mol. Because this value does not exceed the energy gained by hydrating the defect, a net gain

of  $-1476.5 \text{ kJ/mol} + 658.4 \text{ kJ/mol} = -818 \text{ kJ/mol}$  exists in favor of transfer and bonding to the siderophore.

#### *Siderophore affinity for $\text{Fe}^{3+}$ over $\text{Al}^{3+}$*

The specificity and increased affinity of azotobactin for the Fe atom in the goethite over the aluminum in the diaspore that is evident in force measurements (Chapter 2) and in the molecular mechanics simulations (e.g., increased energy changes upon retraction) is corroborated by the binding energies calculated from first principles. With both siderophore analogs, the acetohydroxamic acid and the hydroxycarboxylic acid, binding energies were more negative for  $\text{Fe}^{3+}$  compared to  $\text{Al}^{3+}$  (Table 3.4). The absolute *ab initio* values show the same relationship as energies calculated from experimentally derived formation constants ( $K_f$ ), however, the latter values are higher (less negative). This is, in part, because the *ab initio* calculations do not include an entropy component, which would drive the energies down to a less negative value.

In Chapter 2 it was hypothesized that part of the observed specificity and increased affinity of azotobactin for Fe atoms was a result of iron's increased electronegativity over Al. This phenomenon can be seen by comparing the optimized Mulliken charge distributions predicted by the Gaussian98 models of the Fe and Al ligand complexes. As shown in Figure 3.9 and Figure 3.10, Fe's larger ionic radius and higher electronegativity causes it to draw more negative charge from the chelating O atoms than aluminum. This results in an Fe atom with lower positive charge associated with less negative O atoms. Conversely, the O atoms associated with the aluminum are more negative, and the cation is more positive. Comparison of the hydration energies associated with the  $\text{Fe}^{3+}$  and  $\text{Al}^{3+}$  ions (Table 3.1) coupled with observations made during the *ab initio* runs present the possibility of surface hydration energies playing a role in the siderophore mineral interaction forces observed with the AFM. While these values have not been measured for goethite and diaspore (K. Rosso, A. Navrotsky, pers. comm.), it is possible that the increased (more negative) hydration energy associated with the aluminum ion (versus  $\text{Fe}^{3+}$ ) could correlate with an increased surface hydration energy for diaspore (over

goethite). Therefore the lowered siderophore affinity observed for the diaspore surface could also reflect the extra energy required to remove water from the surface.

## SUMMARY AND CONCLUSIONS

Molecular and quantum mechanical calculations were effective in providing qualitative and quantitative information on the azotobactin interaction. Computer simulations of the AFM extension force traces showed that both backbone and sidechain azotobactin oxygens had the opportunity to interact with the mineral surface; however, steric considerations, and constraints imposed by the lattice structure dictated which ones ultimately coordinated. Similar functional groups were associated with each mineral surface after extension (partially due to user constraints imposed during the modeling to facilitate comparison), however, upon retraction of the molecule from the surface, the energy profiles for diaspore and goethite were distinct. Specifically, energy peaks associated with the stretching and release of the siderophore-goethite linkage were higher in magnitude and were shifted to larger Au atom-surface separations compared to the peaks associated with diaspore. The goethite coordinations were persisting into a higher force regime compared to the coordinations associated with the diaspore, a phenomenon that was also observed in the experimental force measurements. One source of this specificity can be found when comparing charge distributions predicted by quantum mechanical calculations of Fe(III) and Al(III) complexes with siderophore analogs. Here the electron density associated with the Fe-O(siderophore) bond was much higher than the Al-O(siderophore) bond, presumably a result of the larger electronegativity and ionic radius of the iron atom. Metal removal was predicted in the models, but not observed in previous AFM force measurements (see Chapter 2). Nevertheless, additional simulations that employed a bidentate, mononuclear coordination (opposed to a bidentate, binuclear coordination) or included water to act as a helper ligand confirmed that siderophore metal removal via direct surface contact was a possibility in a natural system.



## TABLES

Table 3.1 Comparison of GULP and experimental lattice energies.

	$\text{Fe}^{3+} + \text{OH}^- + \text{O}^{2-} \rightarrow$ $\text{FeOOH (goethite)}$ $K_{\text{sp}}^1 = 10^{-44}$ $\Delta G = -RT \ln K_{\text{sp}} =$ -252.7 kJ/mol		$\text{Al}^{3+} + \text{OH}^- + \text{O}^{2-} \rightarrow$ $\text{AlOOH (diaspore)}$ $K_{\text{sp}}^1 = 10^{-33}$ -189.5 kJ/mol
	hydration energy <sup>2</sup> [kJ/mol]		hydration energy <sup>2</sup> [kJ/mol]
$\text{Fe}^{3+}$	-4397.4		---
$\text{Al}^{3+}$	---		-4680.4
$\text{OH}^-$	-455.4		-455.4
$\text{O}^{2-}$	-1161.2		-1161.2
<b>TOTAL</b>	-6015.2		-6298.2
<b>Exptl Lattice energy [kJ/mol]<sup>3</sup></b>	-6267.9		-6487.7
<b>GULP Lattice energy [kJ/mol]<sup>4</sup></b>	-6782.4		-6908.2
<b>Scaling factor</b>	0.924		0.939

<sup>1</sup> References: (Langmuir, 1997; Lindsay, 1979)

<sup>2</sup> References: (Rashin and Honig, 1985; Rosseinsky, 1965)

<sup>3</sup>  $\Delta H_{\text{lattice}} = \Delta H_{\text{Ksp}} - \Delta H_{\text{hydr}}$ ; neglects positive entropy change associated with the decrease in the number of species upon formation of mineral (so far, no direct calorimetric measurements of the lattice energies were found for diaspore and goethite)

<sup>4</sup> Value is adjusted for number of formula units (4)/unit cell and the internal energy of the OH bond which was calculated using GULP as 643 kJ/mol.

Table 3.2 Comparison of jump to contact distances (jtcd) and forces (jtcf) associated with extending azotobactin towards goethite surface with simulated values (see text). Experimental values are shown for various pH and ionic strength (I).

**Azb-goethite**

	pH	log I	jtcf (pN)	jtcd (Å)	$k_s$ (N/m)
simulation	vacuum	vacuum	923	52	na
expmt 1	3.5	-3.5	680	53.6	0.123
expmt 2	7	-1	810	71.4	0.1262
expmt 3	3.5	-3.5	980	84.6	0.123

Table 3.3 Differentiated energy peak values (dE/dx) associated with simulated siderophore release from the surface. Pullout energies represent energy required to position metal atom to an infinite distance from the lattice (in the absence of a siderophore).

peak	1 [pN]	2 [pN]	3 [pN]	4 [pN]		Sim. $E_{\text{pullout}}$ [kJ/mol]
diaspore	381	97	133	1238	Al	-6417
goethite	600	159	215	1867	Fe	-6128

Table 3.4 Quantum mechanical calculations of fully deprotonated siderophore fragments (analog) binding  $\text{Fe}^{3+}$  and  $\text{Al}^{3+}$ .

<b>hydroxyacid (lactic acid) (HA)</b>							
	<b>Fe3+/Al3+</b>	<b>+ HA2-</b>	<b>-&gt;</b>	<b>FeHA1+/AlHA1+</b>	<b>DeltaE [kJ/mol]</b>		
	<b>vacuum (HF, 3-21g) [kJ/mol]</b>						
<b>Fe</b>	-3291655.266	-887812.48		-4184317.775	-4850.02518		
<b>Al</b>	-626243.2129	-887812.48		-1519044.747	-4989.050504		
	<b>vacuum (HF, b3631g) [kJ/mol]</b>						
<b>Fe</b>	-3309837.831	-897933.06		-4212949.055	-5178.162249		
<b>Al</b>	-630714.9499	-897933.06		-1533721.597	-5073.584979		
					<b>BINDING ENERGIES</b>		
						<b>dG=- RTln(Kf) [kJ/mol]</b>	
<b>"hydration" (all species from pcm, HF, b3631gs) [kJ/mol]</b>					<b>DeltaE (tot) [kJ/mol]</b>	<b>log Kf</b>	
<b>Fe</b>	-3519.7981	-1035.4908		-377.07488	4178.21404	-17497.57313	3.6
<b>Al</b>	-4139.57726	-1035.4908		-677.9227	4497.14538	-16740.88134	0.85
<b>acetohydroxamic acid (aHA)</b>							
	<b>Fe3+/Al3+</b>	<b>+ aHA1-</b>	<b>-&gt;</b>	<b>FeaHA2+/AlaHA2+</b>	<b>DeltaE [kJ/mol]</b>		
	<b>vacuum (HF, 3-21g) [kJ/mol]</b>						
<b>Fe</b>	-3291655.266	-736102.82		-4031134.538	-3376.453306		
<b>Al</b>	-626243.2129	-736102.82		-1365774.78	-3428.74808		
	<b>vacuum (HF, b3631g) [kJ/mol]</b>						
<b>Fe</b>	-3309837.831	-744521.34		-4058021.94	-3662.765239		
<b>Al</b>	-630714.9499	-744521.34		-1378712.96	-3476.665555		
					<b>BINDING ENERGIES</b>		
						<b>dG=- RTln(Kf) [kJ/mol]</b>	
<b>"hydration" (all species from pcm, HF, b3631gs) [kJ/mol]</b>					<b>DeltaE (tot) [kJ/mol]</b>	<b>log Kf</b>	
<b>Fe</b>	-3519.7981	-302.4385		-1101.46218	2720.77442	-12611.56087	11.5
<b>Al</b>	-4139.57726	-302.4385		-1449.90482	2992.11094	-11561.21107	8

## FIGURES

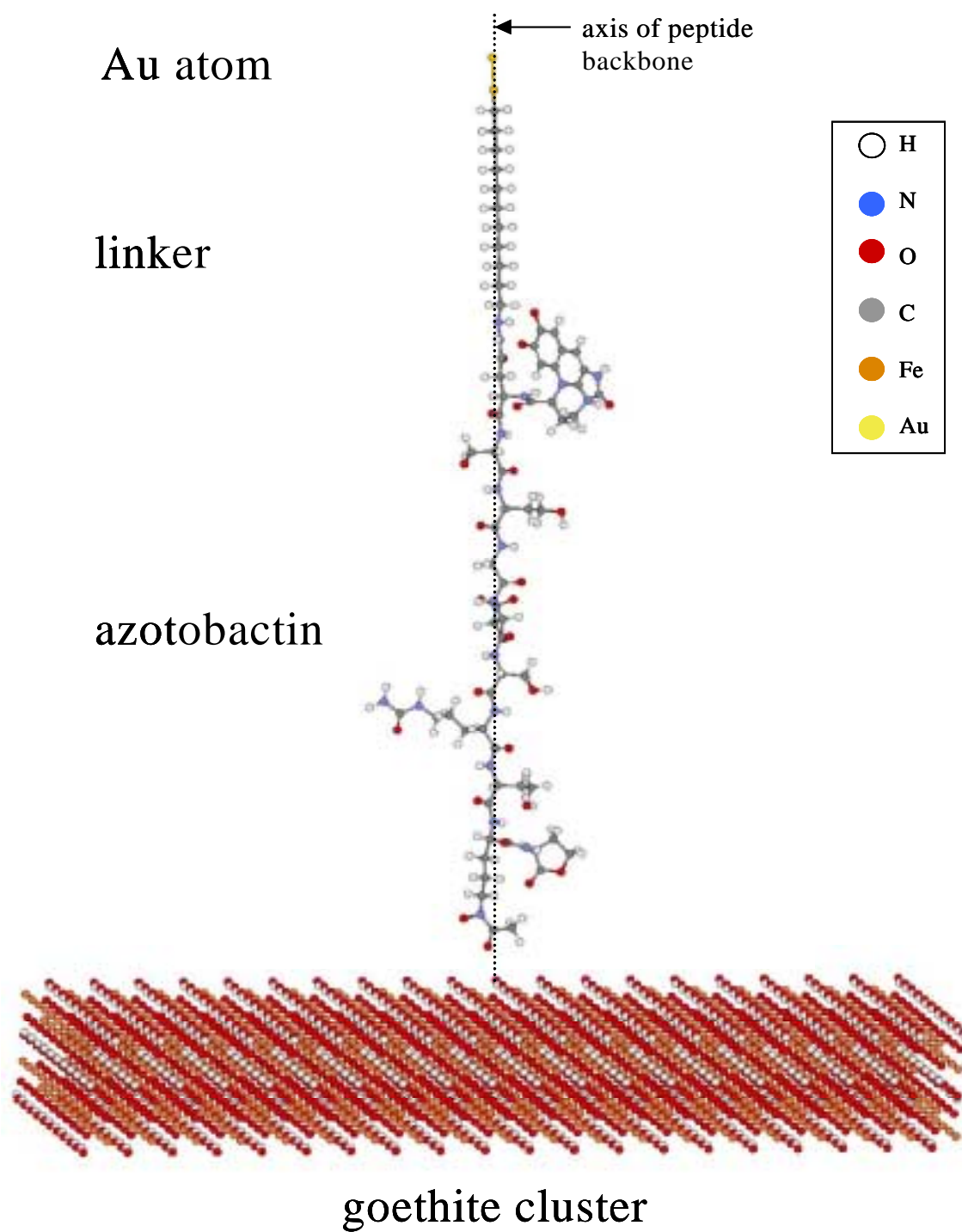


Figure 3.1 Starting point of extension simulation with linearized azotobactin molecule, approaching the goethite cluster.

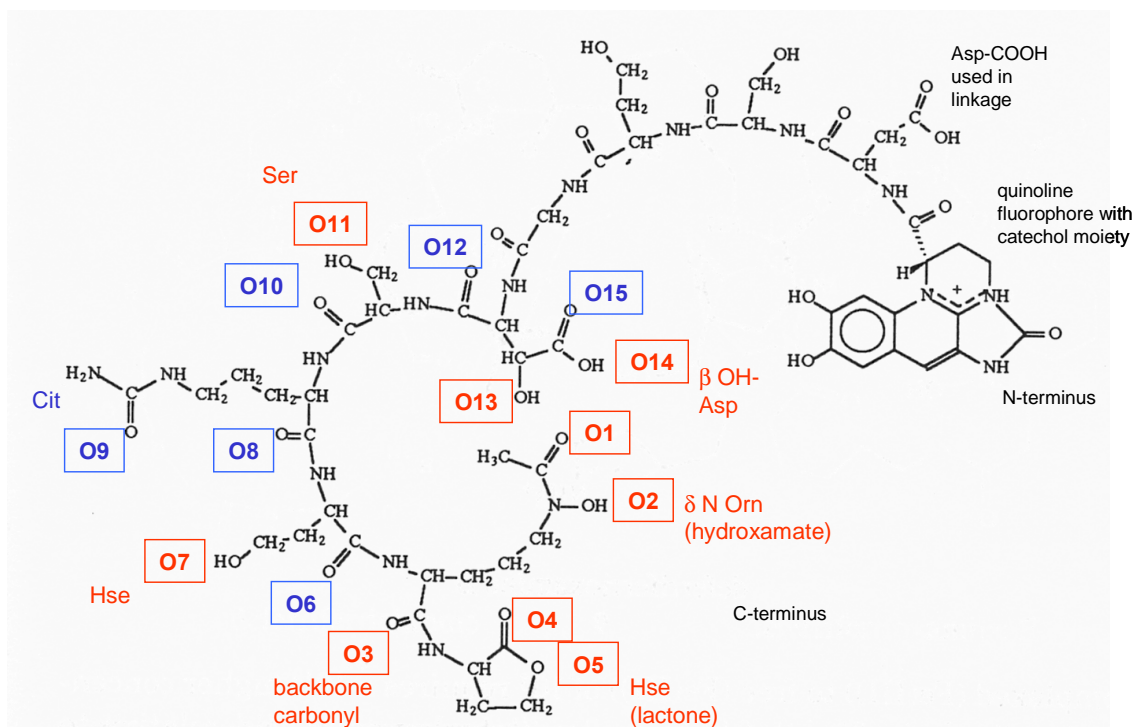


Figure 3.2 Annotated azotobactin  $\delta$  structure (Palanche, 1999) with oxygens numbered in series; those highlighted in red coordinated with metals on the mineral surface during the simulation.

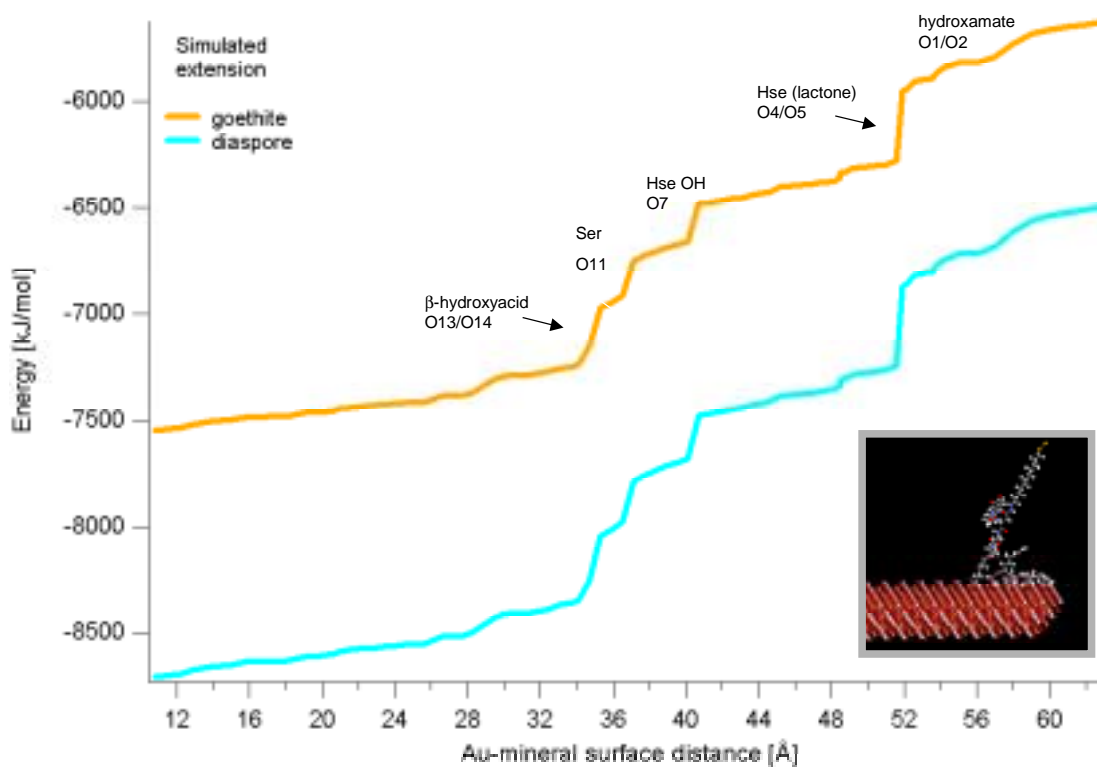


Figure 3.3 Simulated energy profile showing the successive attachment of azotobactin groups upon extension (approach) to the goethite and diaspore. Inset is a screen shot from the simulation showing the extension of the molecule onto the surface. Oxygen numbers (O1,O2,O4, etc.) refer to numbering system shown in Figure 3.2.

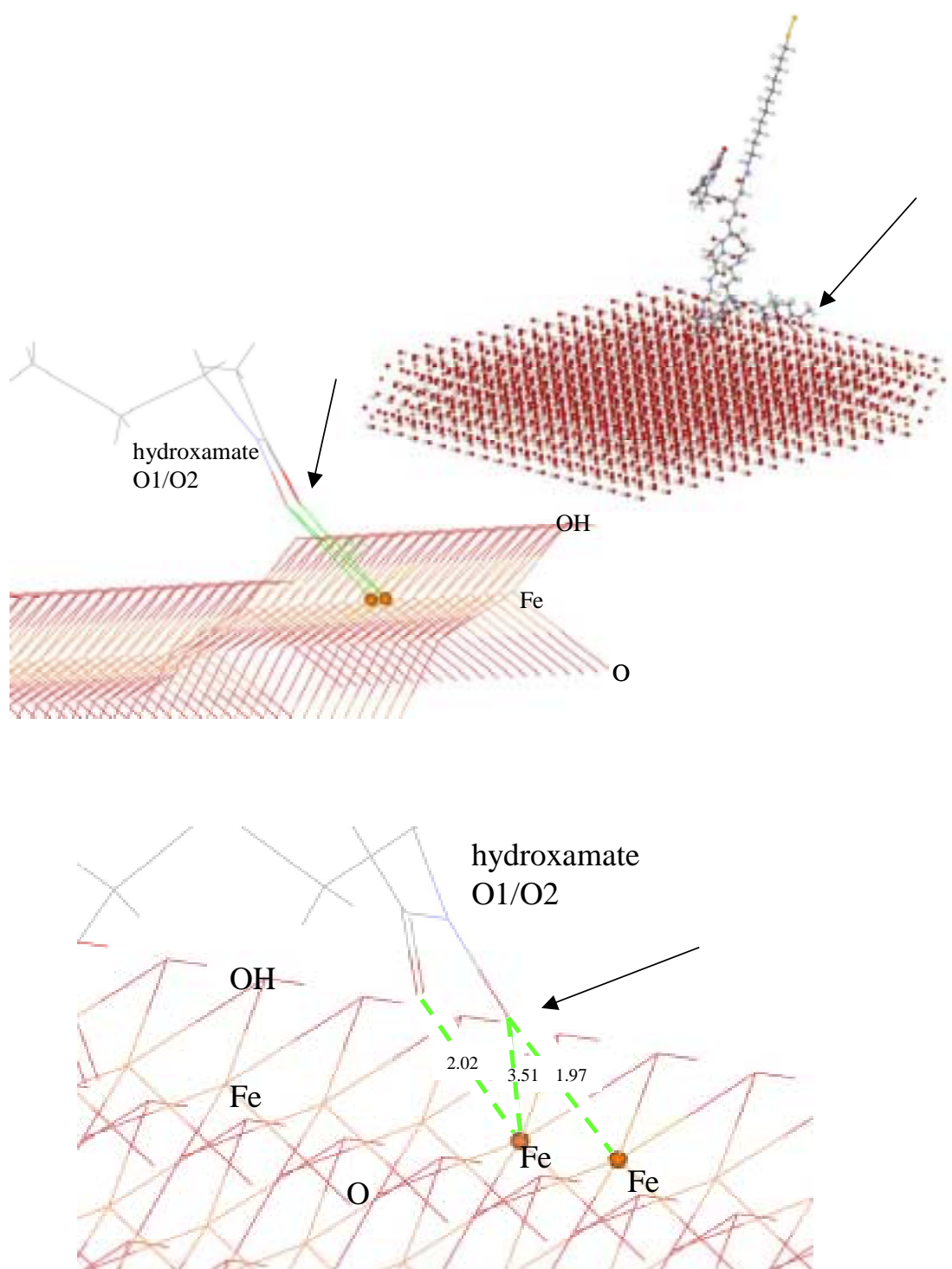


Figure 3.4 Molecular models of azotobactin interacting with a goethite surface. Arrows point to terminal hydroxamate group oxygens coordinating with irons in the lattice in a binuclear fashion. Note the spacing of the siderophore oxygens allow for “bonds” (i.e., Fe-O(siderophore) distances  $\sim 2$  Å) with neighboring irons. With this coordination, the distance between a siderophore oxygen and an iron diagonally across is over  $3$  Å.

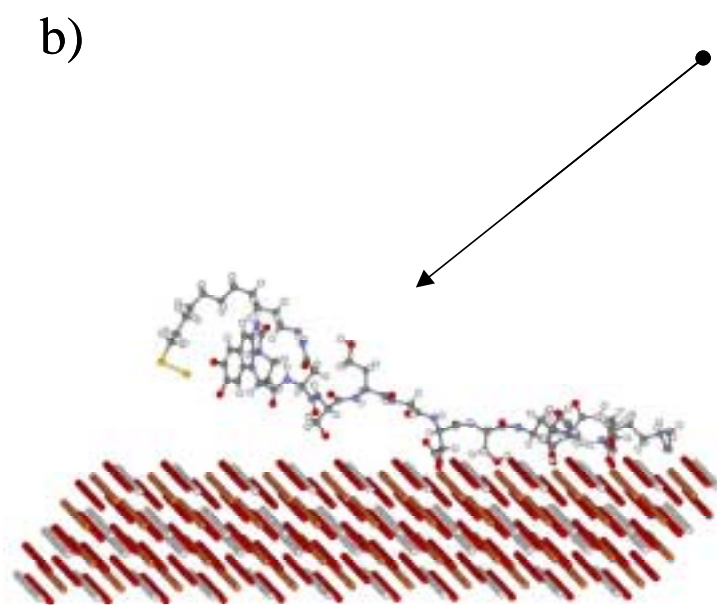
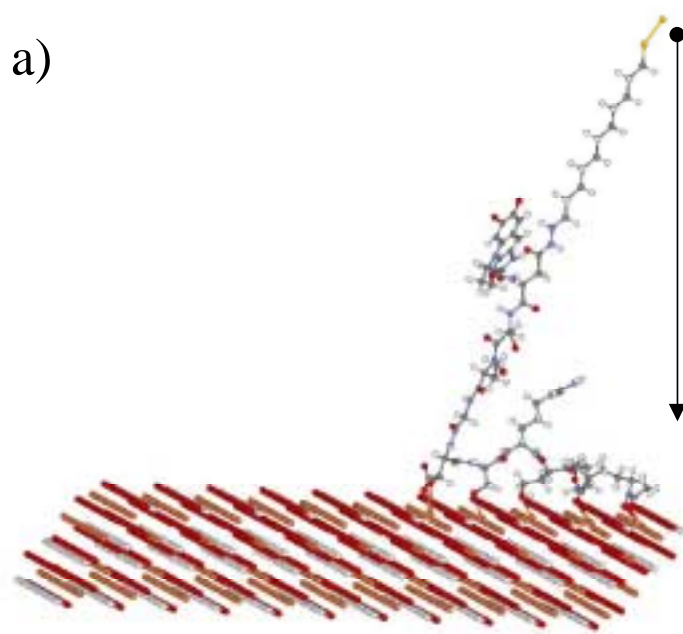


Figure 3.5 Arrow indicates extension of the Au atom/molecule towards the mineral surface with a) no lateral component and b) an arbitrary and varied lateral component. The dot at the beginning of the arrow indicates the starting position of the Au atom.



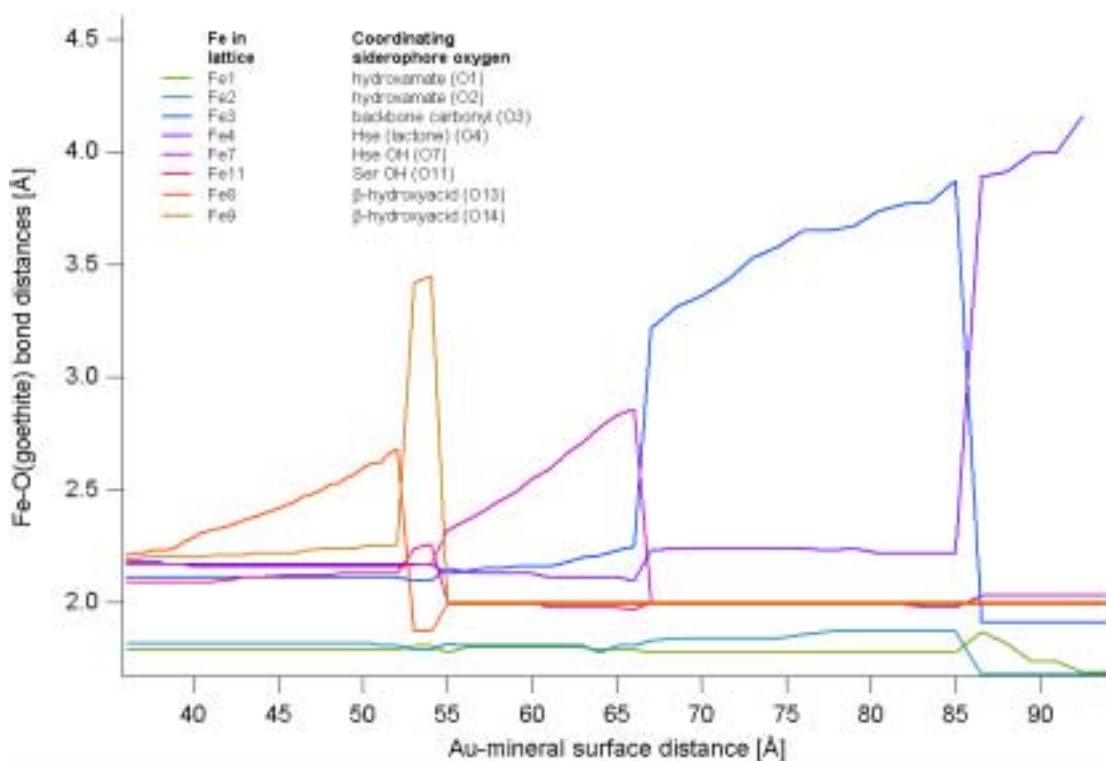


Figure 3.6 Fe displacements from the goethite lattice upon retraction of the siderophore from the surface. Y-axis shows bond distances between the metal and a lattice oxygen directly beneath it. Note the large displacement associated with the  $\beta$ -hydroxyacid group and total removal of an Fe by the Hse (lactone).

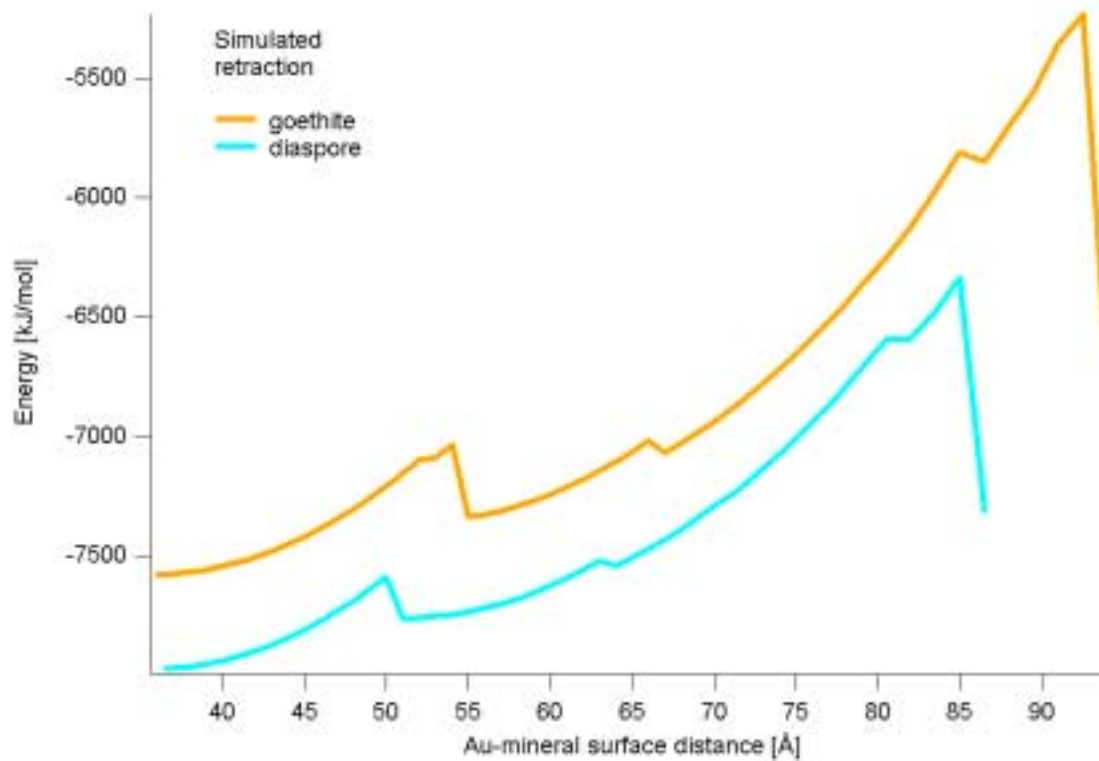


Figure 3.7 Simulated energy profile of siderophore retraction from goethite and diasporite.

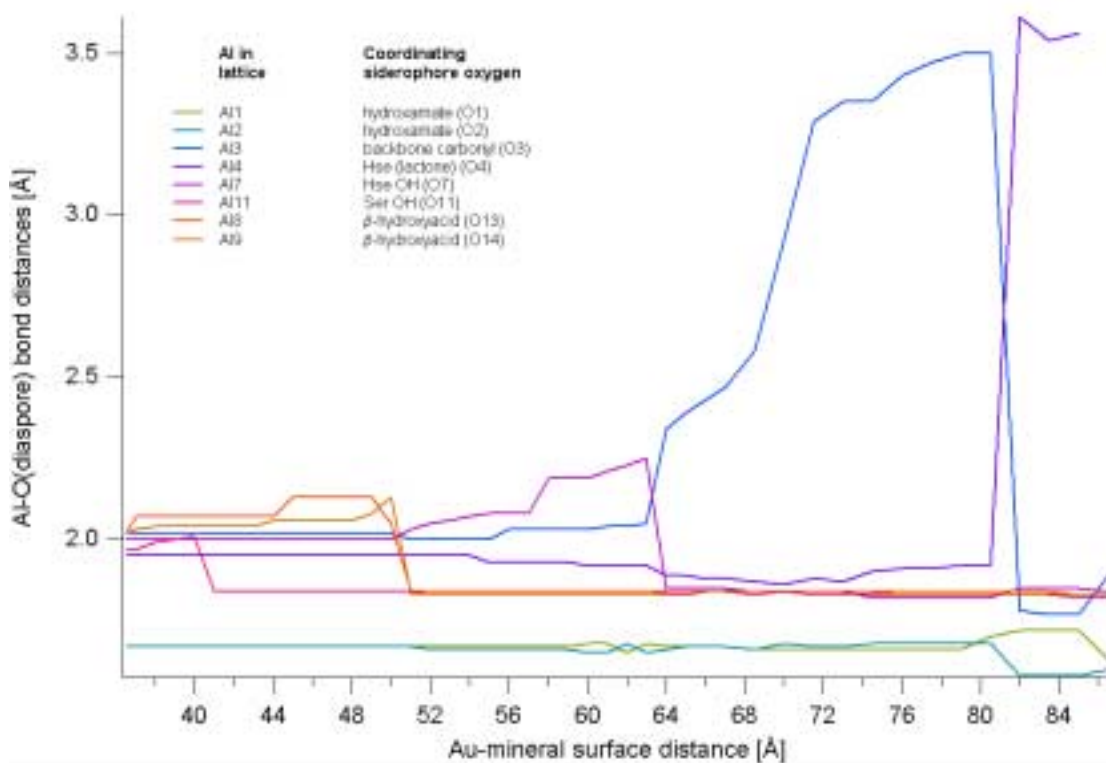


Figure 3.8 Al displacements from the diasporite lattice upon retraction of the siderophore from the surface. Y-axis shows bond distances between the metal and a lattice oxygen directly beneath it.

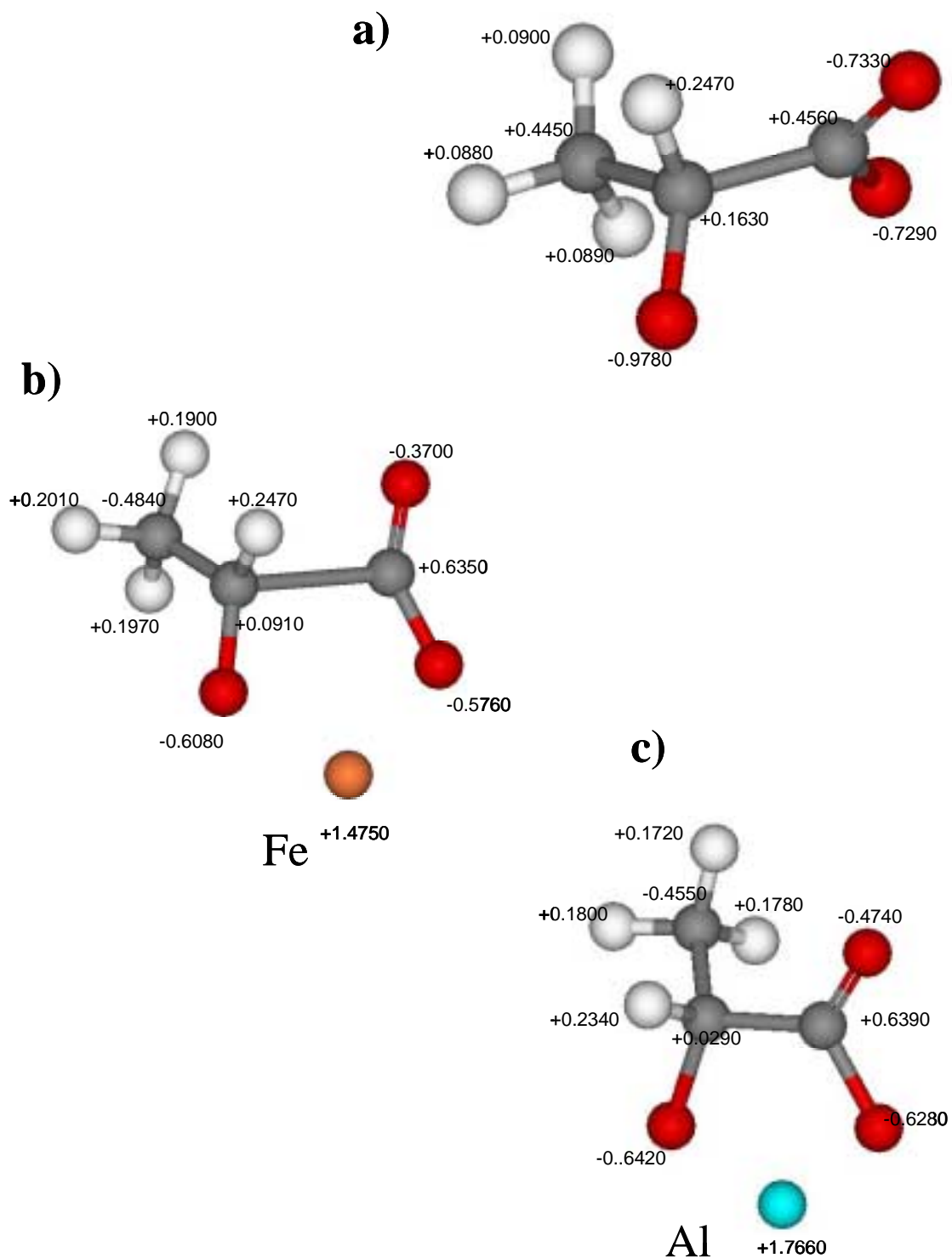


Figure 3.9 Molecular conformation and Mulliken charges predicted for a) hydroxycarboxylic acid and its associated b) Fe and c) Al complexes.

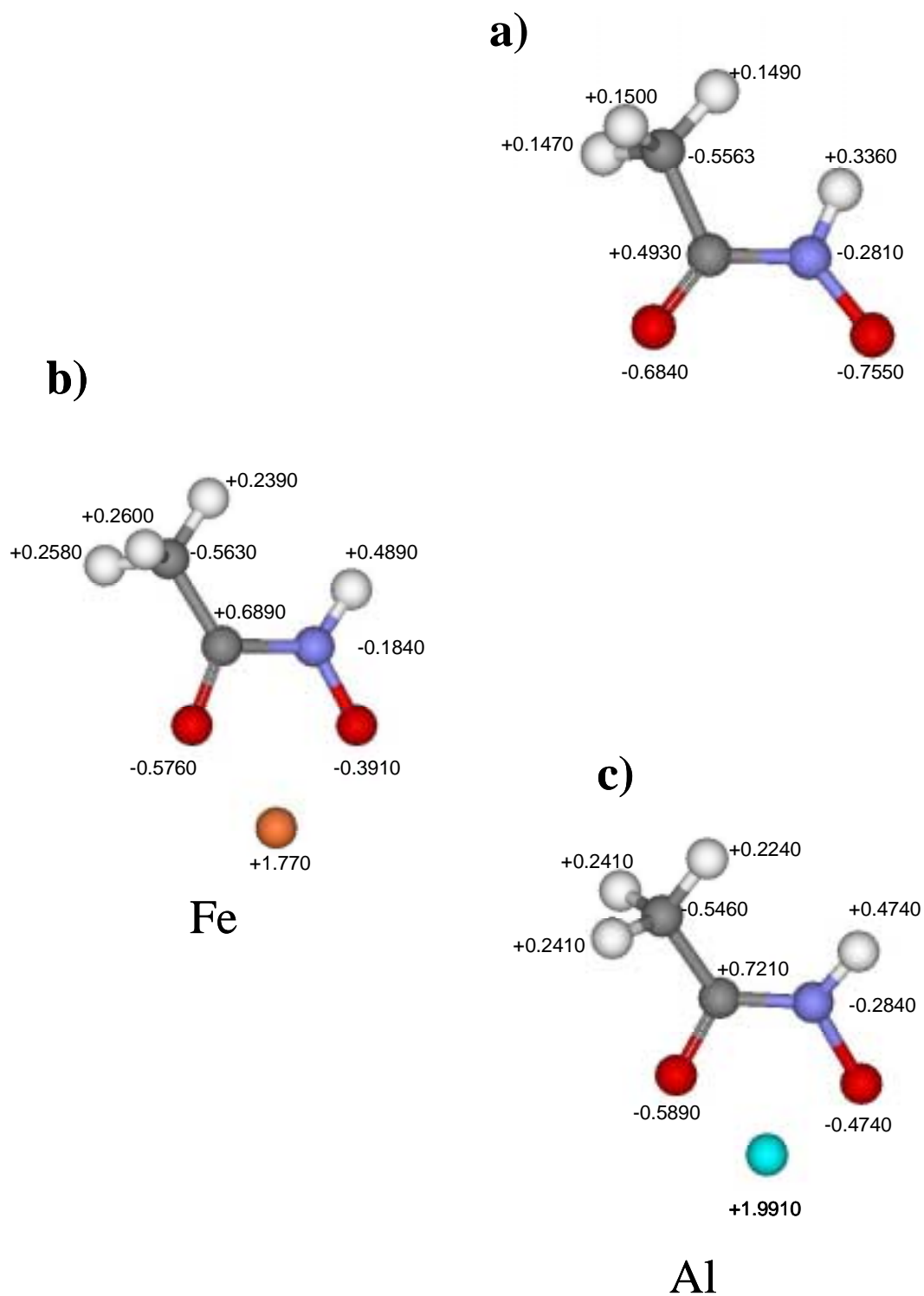


Figure 3.10 Molecular conformation and Mulliken charges predicted for a) acetohydroxamic acid and its associated b) Fe and c) Al complexes.

## REFERENCES

- Busing W. R. and Levy H. A. (1958) A single-crystal neutron-diffraction study of diaspore,  $\text{AlO}(\text{OH})$ . *Acta Cryst.* **11**, 798-803.
- Cygan R. T. (2001) Molecular Modeling in Mineralogy and Geochemistry. In *Molecular Modeling Theory: Applications in the Geosciences*, Vol. 42 (ed. R. T. Cygan and J. D. Kubicki), pp. 531. Mineralogical Society of America and Geochemical Society.
- Frisch M. J., Tomasi J., and Pople J. (1998) Gaussian 98, Revision A.7. Gaussian, Inc.
- Gale J. (1998) General Utility Lattice Program (GULP). Imperial College/Royal Institution of Great Britain.
- Gualtieri A. F. and Venturelli P. (1999) In situ study of the goethite-hematite phase transformation by real time synchrotron powder diffraction. *American Mineralogist* **84**(5-6), 895-904.
- Haussühl S. (1993) Thermoelastic Properties of Beryl, Topaz, Diaspore, Sanidine and Periclase. *Zeitschrift Fur Kristallographie* **204**, 67-76.
- Hersman L., Lloyd T., and Sposito G. (1995) Siderophore-promoted dissolution of hematite. *Geochimica et Cosmochimica Acta* **59**, 3327-3330.
- Hersman L., Maurice P., and Sposito G. (1996) Iron acquisition from hydrous Fe(III)-oxides by an aerobic *Pseudomonas* sp. *Chemical Geology* **132**(1-4), 25-31.
- Holmen B. A. and Casey W. H. (1996) Hydroxamate ligands, surface chemistry, and the mechanism of ligand-promoted dissolution of goethite [ $\alpha\text{-FeOOH(s)}$ ]. *Geochimica et Cosmochimica Acta* **22**, 4403-4416.
- Izrailev S., Stepaniants S., Balsera M., Oono Y., and Schulten K. (1997) Molecular dynamics study of unbinding of the avidin-biotin complex. *Biophysical Journal* **72**(4), 1568-1581.
- Kendall T. A. and Hochella M. F., Jr. (2003) The measurement and interpretation of molecular level forces of interaction between the siderophore azotobactin and mineral surfaces. *Geochimica et Cosmochimica Acta*.
- Langmuir D. (1997) *Aqueous Environmental Geochemistry*. Prentice Hall.
- Lindsay W. L. (1979) *Chemical Equilibria in Soils*.
- Miertus S. and Tomasi J. (1982) Approximate evaluations of the electrostatic free energy and internal energy changes in solution processes. *Chemical Physics* **65**(2), 239-45.
- Moy V. T., Florin E. L., and Gaub H. E. (1994) Intermolecular forces and energies between ligands and receptors. *Science* **266**(5183), 257-9.
- Palanche T., Marmolle F., Abdallah M. A., Shanzer A., and Albrecht-Gary A. M. (1999) Fluorescent siderophore-based chemosensors: iron(III) quantitative determinations. *Journal of Biological Inorganic Chemistry* **4**(2), 188-198.
- Rappe A. K., Casewit C. J., Colwell K. S., Goddard W. A., and Skiff W. M. (1992) UFF, a Full Periodic-Table Force-Field for Molecular Mechanics and Molecular-

- Dynamics Simulations. *Journal of the American Chemical Society* **114**(25), 10024-10035.
- Rashin A. A. and Honig B. (1985) Reevaluation of the Born model of ion hydration. *Journal of Physical Chemistry* **89**(26), 5588-93.
- Rosseinsky D. R. (1965) Electrode potentials and hydration energies. Theories and correlations. *Chem. Rev.* **65**(4), 467-90.
- Sanders M. J., Leslie M. J., and Catlow C. R. A. (1984) Interatomic potentials for SiO<sub>2</sub>. *J. Chem. Soc. Chem. Com.*, 1271-1273.
- Schroder K. P., Sauer J., Leslie M., Catlow C. R. A., and Thomas J. M. (1992) Bridging Hydroxyl-Groups in Zeolitic Catalysts - a Computer- Simulation of Their Structure, Vibrational Properties and Acidity in Protonated Faujasites (H-Y Zeolites). *Chemical Physics Letters* **188**(3-4), 320-325.
- Smyth J. R., Jacobsen S. D., and Hazen R. M. (2000) Comparative Crystal Chemistry of Dense Oxide Minerals. In *High Temperature and High Pressure Crystal Chemistry*, Vol. 40 (ed. R. M. H. a. R. T. Downs). Mineralogical Society of America.

## **APPENDIX - Intermolecular Forces at the Interface of Biological and Mineralogical Particles**

Treavor A. Kendall  
Department of Geological Sciences  
Virginia Polytechnic Institute and State University  
Blacksburg, Virginia 24061

Steven K. Lower\*  
Department of Geology  
The University of Maryland  
College Park, Maryland 20742  
Email: [lower@geology.umd.edu](mailto:lower@geology.umd.edu)

*IN REVIEW*  
*Advances in Agronomy*  
*February 2003*

\*corresponding author



## TABLE OF CONTENTS - APPENDIX

<b>Table of contents - Appendix .....</b>	<b>73</b>
<b>List of Tables .....</b>	<b>74</b>
<b>List of Figures.....</b>	<b>74</b>
<b>Abstract.....</b>	<b>77</b>
<b>Introduction – Forces in nature.....</b>	<b>78</b>
<b>II. Fundamental forces at the interface of biological particles and inorganic surfaces .....</b>	<b>79</b>
<i>A. The van der Waals Force.....</i>	<i>79</i>
<i>B. The Electrostatic Force .....</i>	<i>81</i>
<i>C. The Solvation Force .....</i>	<i>82</i>
<i>D. The Steric Force and Bridging Polymers .....</i>	<i>84</i>
<b>III. Force Curve Theory and Collecting Force Data .....</b>	<b>86</b>
<i>A. Force-distance Curves, Capturing a Potential With Force vs. Separation Plot.....</i>	<i>87</i>
<i>B. Hysteresis .....</i>	<i>89</i>
<i>C. Tip Shape.....</i>	<i>90</i>
<i>D. Spring Constant Determination .....</i>	<i>90</i>
<i>E. Artifacts in Force Measurements .....</i>	<i>91</i>
<i>F. Data Processing and Statistics .....</i>	<i>92</i>
<i>G. Advanced Algorithms .....</i>	<i>93</i>
<i>H. Relating Bond Chemistry and Energies to Force Measurements .....</i>	<i>94</i>
<i>I. Relevance of Dynamic Force Spectroscopy to Biological-Inorganic Interface .....</i>	<i>98</i>
<b>IV. Forces at the biomolecule-mineral interface.....</b>	<b>100</b>
<i>A. Ligand Linkage Schemes .....</i>	<i>102</i>
<i>B. Siderophores and Oxide Surfaces .....</i>	<i>103</i>
<b>V. Forces at the bacterium-mineral interface .....</b>	<b>106</b>
<i>A. Force Microscopy Technique Using Whole Cells.....</i>	<i>106</i>
<i>B. Forces between Escherichia coli and Muscovite .....</i>	<i>109</i>
<i>C. Forces between Shewanella oneidensis and Goethite or Diaspore .....</i>	<i>111</i>
<b>VI. Future Work .....</b>	<b>114</b>
<b>References.....</b>	<b>117</b>
<b>Table.....</b>	<b>128</b>
<b>Figures.....</b>	<b>129</b>

## LIST OF TABLES

Table A. 1	Summary of physical forces of interaction between particles and/or surfaces.* .....	128
------------	---	-----

## LIST OF FIGURES

Figure A. 1	Log-log plot of the theoretical forces describing (1) gravitational attraction between a particle and the Earth (solid “Earth-particle” line), (2) gravitational attraction between two particles of the same size (dashed “particle-particle” line), and (3) van der Waals attraction between two particles of the same size (dashed “vdw” lines). In all instances the particles are assumed to be in “contact” with the Earth (for 1) or another particle (for 2 and 3). For gravitational attraction, mass was determined by assuming each particle was a solid homogeneous sphere with a density of $1 \text{ g cm}^{-3}$ , and contact was defined as the radius of the Earth ( $\sim 6.4 \times 10^6 \text{ m}$ radius; “Earth-particle” interaction) or the sum of the radii of two interacting particles (“particle-particle” interaction). The shaded region outlines the boundaries of the expected van der Waals force using values for Hamaker constant of $10^{-20}$ to $10^{-21} \text{ J}$ , which is appropriate for biological and inorganic phases (Israelachvili, 1992; Leckband and Israelachvili, 2001; Vigeant et al., 2002), and defining “contact” as an effective separation between particles of $\sim 0.2$ (for one hydration layer) to $2 \text{ nm}$ , according to (Israelachvili, 1992; Leckband and Israelachvili, 2001). Only the magnitudes of the forces are shown. By convention, attractive forces (shown here) are negative. For reference, the three diamond symbols represent gravitational forces between the Earth ( $\sim 10^{24} \text{ kg}$ ) and each of three bodies (from left to right): a bacterium ( $10^{-15} \text{ kg}$ ), a human ( $50 \text{ kg}$ ), or the moon ( $10^{22} \text{ kg}$ ). .....	129
Figure A. 2	A typical force versus piezo movement plot showing three general regions – contact, interaction, and no contact. For clarity a single trace is shown (e.g. an approach curve); however, force plots with both approach and retraction traces are also common. In the region of no contact the tip and sample are separated at distances large enough that no interaction occurs. Hysteresis between the approach and retraction curve in the region of no contact may be a function of solution viscosity, or inelastic deformation of the cantilever. As the piezo advances the sample closer, the tip begins to “feel” the surface. In the example plot we see an initial repulsion followed by an attraction recorded as a sharp jump to contact that generates a minimum in the curve. Once in contact, the slope trace is typically constant as the cantilever is moving with the piezo. Information from this region may be used to determine detector sensitivity or elastic properties of the sample or tip.....	130
Figure A. 3	a) Differentiated Lennard-Jones potential provided as an example interaction to be captured with force microscopy or AFM. During AFM operation the forces associated with the potential are recorded as deflections in the cantilever. If the force gradient (tangent to the solid trace) exceeds the spring constant, $k_s$ , the cantilever becomes mechanically unstable and will jump along a slope equal to $k_s$ (dashed line). b) Force-tip sample separation curve showing jumps to and from contact along slope = $k_s$ . Unlike Figure A. 2, the x-axis represents separation distance between the tip and the sample. Here, both the approach (open circles) and the retraction (closed circles) traces are shown. Note that the hysteresis between the two traces is absent in the Lennard-Jones curve where the solid line represents both approach and retraction forces. Points to the left of zero separation (i.e., lowest	

most point on the approach or retraction curves) represent movement of the piezo while the tip and sample are in contact. c) Increasing the spring constant (e.g., using a stiffer cantilever) from $k_{sA}$ to $k_{sB}$ will capture more of the potential (region A <sub>2</sub> -B <sub>2</sub> ), however force resolution is lost and smaller magnitude forces will go undetected. ....	131
Figure A. 4 Screen shot of one module (Sensitivity Tweaks) in the force curve processing routine AFM 4.4 written in Igor Pro, 4.04, WaveMetrics, Inc. (Kendall and Hochella, 2003; some of the base code was provided by H. Skulason). It is designed primarily for handling force data produced Digital Instrument's Nanoscope IIIa MultiMode system. The Sensitivity Tweaks module is designed to rapidly review and assess how well the normalization routine automatically registers and normalizes force data to an origin. The normalization procedure includes the identification of a baseline in the region of no contact, calculating the detector sensitivity from the region of constant compliance and detecting when the tip and the sample are in contact. The latter is determined using peaks in the differentiated force wave that are selected based on threshold/sensitivity settings shown in the panel in the lower right. If initial normalization is unsatisfactory, these settings may be optimized and an auto-normalization may be run again; or features can be identified manually.....	132
Figure A. 5 UV-vis spectra showing the transition of Al into and out of the azotobactin (Azb) structure; corrected for dilution. Upon the addition of Al to the system a characteristic shoulder appears in the spectra. This shoulder could be eliminated with high concentrations of EDTA. A similar process was employed to protect and then regenerate the azotobactin chelating groups during linkage of the siderophore to a hydrazide terminated AFM tip (see also Chapter 2; Tip Activation).....	133
Figure A. 6 Force spectra showing the interaction of two siderophores a) azotobactin and b) deferoxamine (DFO) with goethite (FeOOH) and diaspore (AlOOH) surfaces. Note the large increase in the adhesion force between each siderophore and goethite and versus the adhesion value for diaspore. ....	134
Figure A. 7 Plot showing decrease in azotobactin-goethite adhesion forces with increasing concentrations of added soluble iron (FeCl <sub>3</sub> 6H <sub>2</sub> O). Measurements were collected at pH 3.5 to minimize precipitation of solid iron phases upon the addition of the iron chloride. Taken from Kendall and Hochella (2003); Copyright Elsevier Science Ltd. 2003.....	135
Figure A. 8 Plateau feature common in many retraction curves while probing oxide surfaces with an azotobactin activated AFM. It is suggested that this feature may represent the extension of the azotobactin and linker molecule during separation from the mineral surface as shown in the inset (not to scale). Also shown in the inset is the geometry of the linkage of the siderophore to the tip. Modified from Kendall and Hochella (2003) Copyright Elsevier Science Ltd. 2003. ....	136
Figure A. 9 Molecular models of azotobactin (with linker molecule) interacting with a goethite surface. Simulations were completed using Cerius2, Accelrys, Inc. Arrows point to terminal hydroxamate group oxygens interacting and coordinating with irons (balls) in the lattice. Note the spacing of the siderophore oxygens allow for "bonds" (i.e., Fe-O distances <2.1 Angstroms) with neighboring irons. With this coordination, the cross-distance between a siderophore oxygen and an iron diagonally across is over 3 Angstroms.....	137
Figure A. 10 Force-distance relationship between the basal plane surface of muscovite and <i>E. coli</i> in solutions of high (open symbols across lower portion of figure) or low (closed symbols across upper portion of figure) ionic strength. Shown for each solution condition are five data curves that span the entire range of measurements for literally hundreds of	

force-distance curves. The lines correspond to the DLVO model prediction at high (dotted) or low (solid) ionic strength. Repulsive forces have a positive sign; whereas attractive forces have a negative sign. Only those forces measured upon approach of the mineral towards the bacteria are shown. See text for discussion..... 138

## ABSTRACT

At the most fundamental level, intermolecular forces (e.g., van der Waals, electrostatic, solvation, steric) control interactions between biological molecules and mineral surfaces. These are forces with magnitudes of picoNewtons to nanoNewtons, which operate in a space that is on the order of nanometers. We have used force microscopy to quantitatively probe forces, energies, and distances between crystal surfaces and living microbial cells or biological molecules in their native state. The systems we have studied include those involving: *Escherichia coli*, *Shewanella oneidensis*, siderophores, muscovite, goethite, and/or diaspore, in aqueous solutions of varying composition. Direct force measurements at the organic-inorganic interface have been interpreted with theoretical models describing interfacial forces, adhesion, and molecular dynamic calculations. A new perspective on bacterium-mineral interactions is emerging from these studies. We have discovered a world that operates under a very different set of principles than macroscopic bodies. A world where the intermolecular force, rather than gravitational attraction, is the preeminent force controlling the evolution of processes at the bacterium-mineral interface.

## INTRODUCTION – FORCES IN NATURE

The bacterium-mineral interface is ubiquitous near the surface of the Earth. As many as 97% of the  $\sim 10^{30}$  prokaryotes on Earth live in close proximity to minerals in soil, marine, and terrestrial subsurface environments (Whitman et al., 1998). As we will show in this manuscript, the fundamental forces at this interface are very small, seemingly insignificant. This review will provide evidence that forces on the order of nanoNewtons ( $10^{-9}$  N) to picoNewtons ( $10^{-12}$  N) dominate properties/processes at bacterium-mineral and biomolecule-mineral interfaces. For comparison, there is  $\sim 0.2$  nN of gravitational attraction between a person (50 kg) and the paper (5 g) upon which these words are written. Despite their small magnitude, these forces are at the heart of all interactions between biologically produced polymers and mineral surfaces in nature.

It is now well established that there are four fundamental forces in nature: the strong and weak nuclear forces, the gravitational interaction, and electromagnetic forces, which are the source of all intermolecular forces (Israelachvili, 1992). Because the first two (i.e., nuclear forces) have a range of action that is less than  $10^{-5}$  nm (Israelachvili, 1992), we need not consider these for interactions between biological molecules, microbial cells, and/or mineral surfaces. The question then becomes, under what conditions do gravitational forces or electromagnetic forces (more specifically, intermolecular forces) dominate bacteria-mineral or biomolecule-mineral interactions?

In nature, living organisms exist in communities that are in contact with one another, in contact with mineral surfaces, and they are also in contact with the surface of the Earth (i.e., the upper crust). For simplicity, let us define a particular species of organism as a spherical particle (having a density of water) with a unique size or radius. Each species may interact with one another and/or the Earth. In both instances, there is a force of gravitational attraction at each interface. Figure A. 1 reveals that the gravitational attraction is much greater between the Earth and a particle of a given size (e.g.,  $\sim 4 \times 10^{-5}$  N for a 1 mm particle) relative to the gravitational attraction between two particles of the same given size (e.g.,  $\sim 3 \times 10^{-16}$  N between two 1 mm particles). Also shown on this figure is a theoretical prediction for another type of attractive force, the so-called van der Waals force. This intermolecular force was determined using Equation 1 (see below) to describe the attraction between two similar objects of equal size in contact with one another. For example, two identical 1 mm (radius) particles are expected to

have an attractive, adhesion force at contact (due solely to the van der Waals force) equal to  $\sim 3 \times 10^{-5}$  N (Hamaker constant =  $10^{-20}$  J; effective separation = 0.165 nm, i.e., the “universal” cut-off separation, Israelachvili, 1992). This force magnitude is approximately the same as the gravitational force between the Earth’s surface and one of these 1 mm particles. While it is debatable whether the van der Waals force applies in the same manner to both a particle the size of an atom and an object the size of the moon, the predictions shown in Figure A. 1 for objects smaller than  $\sim 1$  cm are in agreement with others (e.g., Israelachvili, 1992). Consequently, the force of gravity may dominate the interactions between macroscopic bodies (e.g., plants and animals), but intermolecular forces (e.g., van der Waals and others, see below) are the prevailing forces with which microscopic bacteria must contend. This is particularly true when one considers that the van der Waals force is significantly weaker and shorter range than other intermolecular forces, such as electrostatic and hydrophobic interactions as discussed below.

## **II. FUNDAMENTAL FORCES AT THE INTERFACE OF BIOLOGICAL PARTICLES AND INORGANIC SURFACES**

“All intermolecular forces are essentially electrostatic in origin” (page 11, Israelachvili, 1992). In theory, classical electrostatics could be used to calculate intermolecular forces if one could determine the spatial distribution of the electron cloud by solving the Schrödinger equation (Israelachvili, 1992). Unfortunately this is challenging for even simple atomic interactions in vacuum, never mind molecular or organism scale interactions between different functional groups on bacteria and minerals in water. For this reason, it is useful to classify four types of intermolecular forces that are expected to dominate the bacterium-mineral and biomolecule-mineral interfaces. These include the van der Waals force, electrostatic forces, solvation interactions, and steric or entropic forces (Israelachvili and McGuiggan, 1988). – The reader is referred to a number of excellent reviews on these types of forces (e.g., Butt et al., 1995; Israelachvili and McGuiggan, 1988; Leckband and Israelachvili, 2001). This review will touch on all four types of intermolecular forces, although the van der Waals and electrostatic forces will be explored in more detail.

### **A. The van der Waals Force**

The van der Waals force, like the force of gravity, acts between all particles (Israelachvili, 1992). It is quantum mechanical in origin and arises because of time dependent

fluctuations in the electric dipole moment of a particle as it comes into contact with other particles nearby. Even nonpolar particles, which have a time averaged dipole moment of zero, have instantaneous dipoles due to the movement of electrons relative to protons in a nucleus. Dipoles generate an electric field that polarizes adjacent particles and gives rise to an instantaneous force between neighboring particles. Two terms describe the van der Waals force: the first polarization potential, which represents the energy necessary to ionize an atom (i.e., a dipole moment due to interactions between electrons and protons *within* a single particle); and the so-called dispersion term, which describes the dipole induced interactions between two or more atoms (Israelachvili, 1992). Because the dispersion term dominates the van der Waals force, it is sometimes referred to as (London) dispersion forces (Butt et al., 1995).

The van der Waals force has an inverse power law dependence on the separation between two particles. For atoms and small molecules the van der Waals force is  $\sim D^{-7}$ , where  $D$  is the separation distance between particles. It can be attractive or repulsive (e.g., it is always attractive between two similar particles immersed in a third liquid) and is described in terms of the Hamaker constant ( $H_a$ ), which depends upon the refractive indices and dielectric constants of the interacting particles and intervening media (see Israelachvili, 1992). Hamaker constants are on the order of  $10^{-20}$  to  $10^{-21}$  J, for biological cells or molecules interacting with themselves or minerals across an aqueous solution (Bhattacharjee et al., 2000; Butt et al., 1995; Ducker et al., 1991; Leckband and Israelachvili, 2001; Ong et al., 1999; Vigeant et al., 2002).

For simple geometries, the forces between atoms or molecules can be assumed to be additive (Butt et al., 1995; Israelachvili, 1992) such that equations can be derived for larger particles (e.g., organic and inorganic surfaces). Two commonly encountered geometric configurations include interactions between two spheres or a sphere and a flat surface, both of which are given by (Butt et al., 1995; Israelachvili, 1992; Leckband and Israelachvili, 2001):

$$F(D) = \frac{-H_a R_x}{6D^2} \quad (1)$$

where,  $H_a$  = the Hamaker constant (J),  $D$  = separation distance (m) between the two spheres or a sphere and a plane, and  $R_x$  (m) equals the radius of the sphere for the sphere-plane configuration, or it is equal to  $\left( \frac{R_1 R_2}{R_1 + R_2} \right)$  for the interaction between two spheres of radius  $R_1$  and  $R_2$ . A positive Hamaker constant indicates attraction (negative force sign).



## B. The Electrostatic Force

The electrostatic force arises through a variety of mechanisms leading to development of surface charge (e.g., see Sposito, 1989). Water, which has a high dielectric constant, causes the dissociation of surface functional groups. These functional groups display protonation / deprotonation reactions that are dependent upon pH. For example, in water silanol groups on a silica surface undergo the following reaction:  $\text{>SiOH} = \text{>SiO}^- + \text{H}^+$ . Similar acid-base reactions take place on carboxylic groups, amine groups, and other reactive moieties on biological molecules and inorganic surfaces. Hence, many inorganic and biological surfaces develop a charge that is dependent upon pH. Other factors such as the adsorption of charged ions and presence of permanent structural charge (e.g., for clays) are additional contributors to surface charge. The overall charge on a surface is balanced by dissolved counterions in solution, which are attracted to the surface by its electric field and dispersed such that they (i.e., the counterions) increase entropy (Butt et al., 1995). This creates the so-called electric double-layer around surfaces immersed in aqueous solution (Stumm, 1992). When two charged surfaces approach one another, the electric double-layers are perturbed resulting in an electrostatic interaction. This interaction may be attractive (if surfaces are of opposite charge) or repulsive (if surfaces are similarly charged).

The electrostatic force varies exponentially with distance between particles. It depends strongly upon the surface charge densities of the interacting particles and the ionic strength of the intervening solution. Similar to the van der Waals force (see above) equations can be derived to describe the electrostatic force for various geometric configurations. The model for electrostatic forces between two spheres or a sphere and flat surface is (Butt et al., 1995; Leckband and Israelachvili, 2001; Muller and Engel, 1997):

$$F(D) = \frac{4\pi\sigma_1\sigma_2R_x}{\epsilon\epsilon_0\kappa} e^{-\kappa D} \quad (2)$$

where  $\sigma$  is surface charge density ( $\text{C m}^{-2}$ ) of particles 1 and 2,  $\epsilon$  is the dielectric constant of water (78.54 at 298 K),  $\epsilon_0$  is the permittivity of free space ( $8.854 \times 10^{-12} \text{ C}^2 \text{ J}^{-1} \text{ m}^{-1}$ ),  $R_x$  and  $D$  are defined as above. The Debye length ( $1/\kappa$ ) describes the thickness of the diffuse double layer of counterions that surrounds charged particles in solution. The Debye length depends upon the valence and concentration ( $c$ ,  $\text{mol L}^{-1}$ ) of the electrolyte. For monovalent electrolytes (e.g., NaCl) at a temperature of 298 K, the Debye length (in nm) =  $0.304 / (c)^{1/2}$ ; for 1:2 or 2:1

electrolytes (e.g.,  $\text{CaCl}_2$ ) it is  $0.174 / (c)^{1/2}$ ; for 2:2 electrolytes it is  $0.152 / (c)^{1/2}$  (Muller and Engel, 1997). In many instances, it is easier to determine a particle's surface potential as opposed to surface charge. The Graham equation can be used to relate these two parameters according to (Stumm, 1992),

$$\sigma = \sqrt{8RT\epsilon\epsilon_0 c \times 10^3} \times \sinh\left(\frac{z\psi F}{2RT}\right) \quad (3)$$

where  $R$  is the gas constant ( $8.314 \text{ J mol}^{-1} \text{ K}^{-1}$ ), and  $T$  is temperature (K),  $z$  is the valence of ions in solution,  $\psi$  is the surface potential (V), and  $F$  is the Faraday constant ( $96,490 \text{ C mol}^{-1}$ ). A potential measured across an interface contains contributions from at least two layers, the so-called Stern layer and the “diffuse” layer (see Stumm, 1992). Techniques such as streaming potential and electrophoresis are commonly used to determine a particle's zeta potential, which is used as a proxy for surface potential. However, the zeta potential probably represents only the “diffuse” double layer, which is lower than the true surface potential (Stumm, 1992). Leckband and Israelachvili (2001) describe the differences for surfaces that are assumed to have a constant surface charge versus those that are assumed to have a constant surface potential. Interactions at constant surface charge are expected to occur when surface ionizable groups are fully dissociated and remain as such for all separations ( $D$ ). This may be true when the pH of a solution is much greater than the pK value(s) of a particular protonation / deprotonation reaction(s). In instances where surface functional groups are not fully ionized but in equilibrium with solution ions, interactions at constant potential are expected to occur. In this latter case, as two surfaces come together (i.e., very small  $D$ ) the intervening concentration of solution ions increases locally such that some solution ions bind to a surface thereby reducing that surface's density of charged sites (Leckband and Israelachvili, 2001). For many instances, this distinction influences the interaction only at small separations where these two conditions define the boundaries of the expected electrostatic force.

### C. The Solvation Force

The origin, theory, and force-distance relationships of the remaining two force classes – solvation and steric – are indefinite compared to the forces discussed above. Much work remains to be done before solvation and steric forces can be appreciated to the same extent as the van der Waals and electrostatic forces. However, it is well established that the models developed for the van der Waals and electrostatic forces, which treat the intervening solution as a continuum, break

down when two particles or surfaces are within a few nanometers (Butt et al., 1995; Leckband and Israelachvili, 2001). At such close separations, solvation forces may dominate because the solvent (e.g., water) takes on a more ordered structure. Steric forces may also come into play for surfaces with polymers (e.g., biological cells or particles). Our discussion of solvation and steric forces will be more qualitative however, because general force laws (such as those described above) are relatively sparse for these latter two force classes.

Solvation forces (also called hydration or structural forces when the solvent is water) seem to be the result of interactions of solvent molecules with themselves (e.g., in a confined space between two surfaces) or interactions between solvent molecules and a surface (e.g., the orientation of water molecules at the interface of a strongly hydrophilic surface). As two surfaces approach one another the intervening liquid ceases to behave as a structureless media resulting in a force that can be attractive, repulsive, or oscillatory (Butt et al., 1995). These forces can be further subdivided into those that result from solvent-solvent, solvent-surface, and surface-surface interactions (Israelachvili and McGuiggan, 1988).

For two rigid crystalline surfaces at short range ( $< 2\text{nm}$  for water), water molecules interact with themselves such that they take on a semi-discrete layering or structure, which causes the “structural” forces between the interacting surfaces to oscillate between attraction and repulsion with a periodicity equal to the molecular dimension of water (Leckband and Israelachvili, 2001). Between surfaces with polymers, water cannot form well-defined layers because headgroups on lipids, for example, are “rough” on the scale of a water molecule (Israelachvili, 1992), and macromolecules in surfaces are thermally mobile (Beveridge, 1999). Consequently, any repulsion is smeared out and takes on a monotonic component (Israelachvili, 1992). For strongly hydrophilic surfaces in aqueous solution, there is a strong solvent-surface interaction that leads to the formation of hydration shells. These ordered water molecules within the “shell” generate an electric field that impinges upon another surface as two particles approach to within a few nanometers of one another (Israelachvili and McGuiggan, 1988). For example, water molecules may associate with two, adjacent hydrophilic surfaces such that the water’s hydrogens are oriented towards each surface (attracted via hydrogen bonds) and the water oxygens are exposed to the solution. This confers a negative character (from the lone pairs of the water’s oxygens) to each surface, thereby generating a repulsive force. Conversely, the dipoles may complement one another forming an attractive force if water molecules are

staggered on the two surfaces. This hydration force may extend outwards more than the oscillatory force discussed previously (Leckband and Israelachvili, 2001). Finally, for nonpolar surfaces that cannot bind to water molecules – so-called hydrophobic surfaces (defined as those surfaces having a contact angle with water of 75-115°) – there is often a strong attractive force that extends to separations of tens of nanometers or greater (Leckband and Israelachvili, 2001). Hydrophobic forces can be significantly greater than the van der Waals force and may play an important role in interactions involving hydrophobic molecules and/or surfaces (Israelachvili, 1992; Israelachvili and McGuiggan, 1988).

#### **D. The Steric Force and Bridging Polymers**

A steric force affects surfaces that have flexible polymers extending out into solution (e.g., polysaccharides on biological cells). As two surfaces approach one another, the polymer chains become confined such that they are not free to move at random. This entropic confinement results in a repulsive force whose length scale is approximately equal to the radius of gyration of the polymer (Butt et al., 1995), where the radius of gyration is proportional to the number of monomer segments raised to some power between 0.33 (for poor solvents) and 0.6 (for good solvents) (Leckband and Israelachvili, 2001). Approximations derived for the interaction between two flat surfaces reveal that this force depends upon the surface coverage of the polymer and may take on an exponential form (Israelachvili, 1992; Leckband and Israelachvili, 2001). At close separation, the magnitude of the steric force can be similar to that of the electrostatic force (Leckband and Israelachvili, 2001).

In some instances, surface-bound polymers may form an attractive interaction at close separation as the polymer forms a “bridge” between two particles or surfaces (Leckband and Israelachvili, 2001). The resulting adhesive bond may be very long range (i.e., extend well beyond the radius of gyration of the polymer) and resist separation when the surfaces are pulled apart (Jeppesen et al., 2001). While there is no general description for attractive bridging forces by polymers, the linkage of surfaces via a polymeric tether has been described by so-called freely jointed chain (see e.g., Leckband and Israelachvili, 2001), or worm-like chain models (see e.g., (Bustamante et al., 1994; Flory, 1989). In the case of the latter, the polymer is viewed as an elastic element and the force ( $F$ ) needed to stretch the tethered polymer to a length  $x$  is:

$$F(x) = (k_B T / b) [0.25 (1 - x/L)^{-2} - 0.25 + x/L] \quad (4)$$

where  $k_B$  is the Boltzmann's constant,  $T$  is the temperature,  $b$  is the persistence length (i.e., length of the stiff segment or monomer of the chain), and  $L$  is the contour length (i.e., length of the completely stretched chain).

Polymer bridging is a phenomenon that crosses between the disciplines of colloidal science – which has historically tended to investigate intermolecular forces that dominate the interface between two rigid surfaces that are approaching one another – and adhesion science – which is interested in describing the contact between two surfaces and the forces necessary to pull them apart. While attractive intermolecular and intersurface forces (i.e., the four force classes discussed above) are responsible for adhesion events, real particles (e.g., bacteria and minerals) that make contact will also adhere to one another due to elastic or fluid-like deformation, which is an intrinsic and natural part of contact. There is a wealth of information on adhesion processes and theories including the Johnson-Kendall-Roberts (Johnson et al., 1971) and Derjaguin-Muller-Toporov (Derjaguin et al., 1975) theories, which relate the force required to pull two surfaces apart (i.e., the “pull off” force) to the surface energy, surface tension, or work of adhesion. Suffice it to say that surface energy (or tension or work) is determined from intermolecular forces between surfaces. For particles or surfaces that are incapable of forming hydrogen bonding (e.g., nonmetallic compounds), the surface energy can be related directly to the van der Waals force, where surface tension  $\approx H_a / 2.1 \times 10^{-21}$  (Israelachvili, 1992). The surface energies of more polar surfaces, which tend to be larger, are dependent upon van der Waals interactions, as well as an additional electrostatic-like term that relates surface energy to Lewis acid/base reactions (van Oss, 1993).

These four forces – van der Waals, electrostatic, solvation (hydration and hydrophobic), and steric – operate concurrently at the interfaces between microorganisms, biological molecules, and/or mineral surfaces (see Table A. 1) In some instances, one force may dominate at all separations. In other instances, there is a delicate balance such that each force dominates at its own length scale. These four force classes are often invoked to describe interactions as two surfaces approach one another. Two particles that are pulled apart may experience the same sign, magnitude, and range of forces that existed upon approach. However, there is often a notable hysteresis between the forces measured upon approach versus those that are observed upon retraction for soft biological particles and surfaces. This is due to the formation of adhesive bonds (e.g., see discussion of polymer bridges and adhesion, above) once contact has

been established between surfaces. This review will provide examples that illustrate the various forces and force models discussed above as they pertain to interactions between biological and inorganic particles. Further, we will discuss the differences between those forces measured as surfaces come together relative to surfaces that are pulled apart. As a final point to this section, it should be noted that a force of interaction is related to energy ( $E$ ) according to  $F = -dE/dD$ .

### III. FORCE CURVE THEORY AND COLLECTING FORCE DATA

Force measurements attempt to capture interactions representing the electrostatic interplay between single molecules and atoms that are bound in a solid surface or exist as components of a solvated environment. Given the extraordinarily small dimensional (nanometer to angstrom) scale over which they operate, many challenges exist in capturing molecular level forces. This section reviews how force microscopy (or atomic force microscopy, AFM; also known as scanning probe microscopy) addresses these challenges, describes its operation and assesses how accurately the interactions are captured. Highlighted are some of the basic assumptions associated with force microscopy, while noting some of its advantages and limitations.

An AFM force probe consists of a tip attached to a flexible cantilever, which is modeled mechanically as a single harmonic oscillator. Forces exerted on the tip are registered as a spring-like deflection in the cantilever, which may be recorded with various detection systems, including electron tunneling (Binnig et al., 1986), interferometry (Erlandsson et al., 1988; Rugar et al., 1989) and capacitance (Goddenhenrich et al., 1990). The following summarizes an optical lever collection system (Meyer and Amer, 1990) that is most commonly found in commercially available AFMs, including the widely used Veeco / Digital Instrument system. Here the deflection is typically recorded as a change in voltage resulting from the displacement of a laser spot that is reflected off the top of the cantilever and into a photodiode. Voltage (V) is translated into cantilever deflection (nm) using a detector sensitivity value (V/nm) that is equal to the slope of the line when the tip and sample are in contact (see region of contact on Figure A. 2). Provided the sample stiffness is significantly higher than the cantilever (which is the case when probing mineral surfaces), there should be a 1:1 correlation between piezo movement and cantilever deflection once the (V to nm) conversion is made. Small deviations from an absolute slope equal to one may be an indication of detector drift, and can be corrected by dividing the

deflection values by the slope (H. Skulason, personal communication). A slope less than one may also be an indication of a sample compliance that is less than the cantilever (which may be the case when making measurements on a cell), in which case alternative sensitivity determinations, such as the photodiode shift voltage method may be employed (D'Costa and Hoh, 1995); Lower et al., 2001b).

Hooke's law,  $F = -k_s d$ , then allows conversion of cantilever deflection,  $d$ , into force,  $F$ , using the spring constant of the cantilever,  $k_s$ . Note that sign convention dictates that negative forces reflect attractive interactions and positive forces are repulsive.

### **A. Force-distance Curves, Capturing a Potential With Force vs. Separation Plot**

Figure A. 2 shows a typical plot of force vs piezo movement. Note the x-axis represents relative piezo movement or an indexing of a sample's position relative to the cantilever (tip). It does not reflect tip-sample separation (discussed below). Three main components of the plot are identified: the regions of no contact, interaction and contact. Several sub-features are contained within each region including oscillations, subtle slope changes, linear and non-linear extensions, jumps to and from contact (Cappella and Dietler, 1999; Ducker et al., 1992; Gergely et al., 2001), which, in addition to providing reference points to register the force curve to an origin (discussed below), contain valuable information on the interaction between the tip and the surface, the nature of the intervening solution, tribology, adhesion, and elastic properties of the system.

The focus is now turned to the region of interaction, which is of primary interest when studying intermolecular forces at cell or biomolecule-mineral interfaces. Here a wealth of information on the charge character of a mineral surface or biomolecule; the nature and contour length of a polymer extending from a bacterium; DLVO forces (see below) and Debye lengths associated with a colloidal particle or cell; and the energy landscape and activation barriers of a bond are found. But first, to draw both qualitative and quantitative conclusions from forces of interaction, it is imperative to have an understanding of the mechanical constraints of what is recorded in this region using force microscopy using an AFM. To illustrate this we show a simple, short-range interaction potential for atomic scale particles (note, Part II concentrated mainly on larger particles and/or surfaces) described by the Lennard-Jones equation:

$$E(D) = -A/D^6 + B/D^{12} \quad (5)$$

Energy,  $E$ , has an inverse power law dependence on distance,  $D$ , with the  $-1/D^6$  term representing the attractive component of the van der Waals force. The absolute value of this term is maximized at a distance  $D_e$  where the fluctuations in charge density coincide to result in a potential well. At separations less than  $D_e$ , the potential rises rapidly with distance,  $1/D^{12}$ , as the interaction is repulsive in nature due to electronic overlap and nuclear interaction (Cygan, 2001; Israelachvili, 1992). Force microscopy (or AFM), however, does not record energy values directly, but instead measures force. To compare the Lennard-Jones potential with an AFM data set, we take its derivative, such that graphing the relationship

$$dE/dD = F(D) = -6A/D^7 + 12B/D^{13} \quad (6)$$

produces a theoretical force-separation distance curve similar to the one in Figure A. 3a. To further facilitate comparison with the theoretical curve, an origin is defined for the force microscopy data set as follows. A force equal to zero can be defined as the average force value within the region of no contact, while the point at which the tip and sample come into (for approach) and out (for retraction) of contact can be defined as the zero point on the x-axis. Determining the point of contact is clear when a distinct attractive or adhesive component (e.g., a jump to contact) is present, but ambiguous when such features are absent. In the latter case, the intersection between the slope of region of no contact and constant compliance can be used as a guide (Cappella and Dietler, 1999). In a final important step, the x-axis in the force microscopy data set is adjusted to reflect tip sample separation instead of piezo movement, by adding the cantilever deflection values to the piezo movement distances (Butt et al., 1995; Ducker et al., 1992). Here the selection of the sign convention for the forces becomes intuitive. Addition of positive repulsive deflections to the piezo movement results in larger tip-sample separation, while adding negative attractive deflections result in a decrease in the separation. Unlike the Lennard-Jones curve, note that the values in Figure A. 3b left of the point of contact are essentially meaningless in terms of interaction force because the tip and sample are in direct contact. The end result is a force vs. tip-sample separation plot with a region of interaction that can be compared to the theoretical curve (see Figure A. 3a and b; also see Section V, below).

Two main differences exist between the force microscopy data and the potential: 1) the slope of the attractive component of each curve, and 2) the hysteresis that exists between the approach and retraction forces in the force microscopy plot. With the force microscope, it is not uncommon to record an attractive force as a characteristic jump to contact on approach. These



“jumps” represent mechanical instability in the cantilever due to a force gradient that exceeds its spring constant,  $k_s$ . Clearly, interaction information is lost as the cantilever encounters a force gradient (tangent to the theoretical curve) at point  $A_1$  that is greater than its stiffness and consequently jumps to point  $A_2$  along a slope equal to  $k_{sA}$  (see Figure A. 3c). More of the attractive potential can be sampled with a stiffer cantilever (e.g.,  $k_{sB}$ ), however, force resolution is lost, and the region along the theoretical curve between  $B_2$  and  $A_1/B_1$  remains unsampled. A similar situation may be encountered upon retraction, which, in part, contributes to the hysteresis observed in the force data. Specifically, cantilevers with smaller spring constants generate larger amounts of hysteresis. However, hysteresis between approach and retraction curves is also due to the formation of adhesive bonds once surfaces are in contact. This is common for soft samples such as biological cells (see below). For some investigations excessive hysteresis is undesirable and several techniques have been developed to reduce it thereby recovering the “lost” information (i.e., region A2-B2). These methods employ an opposing force that is external to the system in an attempt to increase the effective stiffness of the cantilever, while retaining force resolution. Electrostatic force (Joyce and Houston, 1991), magnetic feedback (Ashby et al., 2000; Jarvis et al., 1998; Jarvis et al., 1996; Yamamoto et al., 1997) and radiation pressure from a laser (Aoki et al., 1997; Tokunaga et al., 1997) have all been used to supply the steadying force to the cantilever.

## **B. Hysteresis**

Certainly other sources besides the instability of the cantilever contribute to approach-retraction hysteresis. In the theoretical Lennard-Jones relationship given as an example potential, no adhesive reaction between the tip and sample is modeled and the retraction curve retraces the approach curve (Figure A. 3a). However, this is not an appropriate model for soft biological cells, which have biopolymers, designed over millions of years of evolutionary selection, for the express purpose of adhesion. When making force microscopy measurements, the tip comes into contact with the surface allowing for reaction and deformation between the two. The bonds and coordinations that result can then be explored and characterized using the associated adhesion forces and approach-retraction hysteresis (Burnham et al., 1990; Cappella et al., 1997). In some systems, the number of bonds that form (and, thus the level of hysteresis) is correlated with the amount of pressure that is applied on the sample by the tip (Weisenhorn et al., 1992). Specifically, increased pressure leads to sample and tip deformation resulting in

increased contact area (Cappella et al., 1997; Israelachvili, 1992), and in the case of functionalized tips (e.g., those coated with self-assembling organic monolayers), a possible rearrangement of functional groups terminating the monolayer. Both of these phenomena facilitate additional bonding, larger hysteresis and higher adhesion values, as documented by several workers (Ashby et al., 2000; Hutter and Bechhoefer, 1993; Toikka et al., 1996; Weisenhorn et al., 1992). Therefore the amount of indentation must be carefully documented to facilitate the comparison of adhesion data from one study to another. One way of controlling the amount of indentation using commercially available AFMs is by adjusting the scan start position, setpoint or the trigger settings. Varying these parameters can be especially useful when probing many biological systems, where pressure and/or contact time may be a natural mechanism of inducing adhesion (e.g., see Lower et al., 2001a; Leckband and Israelachvili, 2001).

### **C. Tip Shape**

Tip shape is a critical AFM parameter that can dictate the force values and contact geometry between the sample and force probe (Butt et al., 1995; Hartmann, 1991). Constraining this value is essential if experimental force traces are going to be compared to theoretical models such as “DLVO” (see Section V below). Yet, tip shape can be difficult to determine, in part due to the surface roughness, irregularities and asperities that are associated with traditional silicon or silicon nitride tips (Cappella et al., 1997). Moreover, tip shape can change over time as continued use promotes wear (Cappella et al., 1997). Solutions to this problem include careful, periodic characterization of the tip with electron microscopy, better constraint of tip geometry by attaching a spherical colloidal probe (Butt et al., 1995; Ducker et al., 1991), or, as described in more recent work, by attaching a carbon nanotube (Cheung et al., 2000; Hafner et al., 1999; Wong et al., 1998a).

### **D. Spring Constant Determination**

If a quantitative analysis of absolute force values is desired, determination of the spring constant ( $k_s$ ) is critical and nominal values provided by the manufacturer generally cannot be relied upon (Lower et al., 2001b). Many factors affect the spring constant including primary characteristics such as cantilever dimensions, geometry and substrate material; as well as, additional modifications common in force spectroscopy such as gold coating, the addition of an organic monolayers, the attachment of colloidal spheres or cells, or even ion adsorption (Cherian and Thundat, 2002; Craig and Neto, 2001; Sader et al., 1995). As a result a large body of

literature detailing several methods of directly determining  $k_s$  exists. A procedure commonly used because of its simplicity, non-destructive nature, and applicability to common cantilever geometries (e.g., V-shaped, rectangular) is provided by (Cleveland et al., 1993). This method derives the spring constant by measuring changes in the cantilever's resonance frequency after small masses (e.g. W microspheres) are loaded onto the end of the tip. The Cleveland method is further optimized when corrected for errors introduced by off-end loading of the mass (Sader et al., 1995). More recent methods measure hydrodynamic drag of the cantilever through a fluid of known viscosity to determine  $k_s$  for bare rectangular cantilevers (Maeda and Senden, 2000; Sader, 1998; Sader et al., 1999). This concept has also been applied to determining  $k_s$  for cantilevers activated with a colloidal probe (i.e., a silica or polystyrene microsphere) (Craig and Neto, 2001). In the latter method, it is useful to directly measuring  $k_s$  for a cantilever with an attached sphere because it accounts for changes in the spring constant due to the shifts in the point of load associated with the position of the colloid sphere and the change in the stiffness associated with the any adhesive used for microsphere attachment. Other methods measure  $k_s$  using thermal oscillations and the equipartition theorem (Butt and Jaschke, 1995; Hutter and Bechhoefer, 1993), a finite element analysis of the static deflection of a cantilever for which the Young's modulus is known (Sader and White, 1993); unloaded resonant frequency of a cantilever of known mass (which is commonly not the case) (Sader et al., 1995), radiation pressure from an acoustic transducer (Degertekin et al., 2001); microscopic and macroscopic reference cantilevers of known stiffness (Jericho and Jericho, 2002; Rabinovich and Yoon, 1994; Torii et al., 1996); and the change in resonant frequency due to gold coating (Gibson et al., 2001).

## **E. Artifacts in Force Measurements**

Several artifacts can arise during force measurements with the AFM. The inverse path effect represented as an upward, hysteretic shift in the retraction trace in the region of contact arises from nonlinearities of the piezoelectric actuator that positions the sample (or tip) (Cappella et al., 1997; Cappella and Dietler, 1999; Heinz and Hoh, 1999). A shift in the contact portion of the retraction trace such that it is parallel with the extension trace reflects friction as the tip plows or slides along the surface (Heinz and Hoh, 1999). A sinusoidal oscillation in the region of no contact may also be present, representing the interference of stray laser light bouncing off the sample and interfering with the laser light reflected off the top of the cantilever (Cappella et al.,

1997; Weisenhorn et al., 1992). This oscillation can be distinguished from other artifacts, such as noise due to mechanical vibrations, because its wavelength should roughly be equal to  $\sim \lambda/2n$ , where  $\lambda$  is the wavelength of the laser source and  $n$  is the index of refraction of the fluid between the tip and sample (Craig and Neto, 2001; Weisenhorn et al., 1992). Thermal oscillation in the region of contact can be recognized by deflection fluctuations whose standard deviation is roughly equal to  $(k_s k_B T)^{0.5}$ ;  $k_s$  = spring constant;  $k_B$  = Boltzmann's constant and  $T$  = temperature (Gergely et al., 2001). Operational artifacts may include a large slope that is present in the region of no contact, common when making measurements in a fluid cell. The origin of this slope is unclear but can often be remedied by eliminating air bubbles in the system or insuring a flat, even orientation of the gasket used to seal the system. Large plateaus at the extremities of both traces often represent a saturation of the detector, requiring an adjustment of the scale of the plot, the deflection limit of the detector or the starting position of the scan.

## **F. Data Processing and Statistics**

With standard AFMs, the one-click ease with which a single force curve is collected allows hundreds of curves to be recorded at a sample point in only a few minutes. Considering a typical curve can contain 2048 data points, a single experiment can produce an enormous volume of data. Further, the variability between force curves collected at a single location can often be quite high. This raises several questions regarding data processing and interpretation that are often neglected. What is the most efficient way to process these data? What is the minimum number of curves necessary to characterize each sample point or a particular interaction? What level of error and variability is associated with the force measurements? How is force data distributed about its mean? What measurable parameters or features of a force curve are most important in characterizing the interactions (e.g., adhesion force)? What is the best way to identify trends or correlations in these parameters? Clearly, answering these questions requires statistical techniques, tests and models that determine appropriate, significant average values of force curve parameters and facilitate the identification of meaningful force curve features.

This process begins by collecting summary statistics for each data set, including calculation of means, standard deviations, error values (e.g. confidence limits) and by plotting histograms for multiple parameters derived from the curves, including adhesion force and distance of jump to contact. When comparing parameters from the curves, statistical tests (e.g. ANOVA, t-tests; correlative tests) may be performed using a standard statistical and data

processing package (e.g., Igor Pro, Wavemetrics, Inc.). Simple regression models may also be employed to determine important variables that contribute to the shape of a force curve. To this end, a routine has been written (Kendall and Hochella, 2003) that rapidly processes force curve data to produce plots of force vs. piezo movement and force vs. tip sample separation using the procedures discussed above. Automated parameter determination, statistical calculations, whole force curve averaging, and histogram generation are incorporated in this customized routine written using Igor Pro's internal programming environment. The simple parameter extraction module quickly and consistently identifies features and selects the values using basic, objective criteria such as maxima thresholds in the differentiated force data and tolerance limits for specific changes in slope (see Figure A. 4).

### **G. Advanced Algorithms**

These criteria are appropriate when the bond ruptures and snaps to contact are large and/or distinct however, other more advanced algorithms (Baumgartner et al., 2000; Gergely et al., 2001; Kasas et al., 2000) are required when features are small, numerous, less distinct (e.g., multiple ligand-receptor interactions) and/or have the potential to be masked by vibrational and thermal noise. For example Kasas et al. (2000) employ a fuzzy logic algorithm that enables automated discrimination of specific, significant adhesions in a retraction curve that might otherwise be overlooked. The routine assigns a grade to each potential rupture event, ranking it somewhere between non-specific (0) or specific (1). Assignment of the grade relies on *a priori* knowledge of the interaction event morphology, and uses criteria such as the angle between the jump and the background trace, or whether or not the jump is U-shaped or V-shaped. This means the procedure is operationally defined and has to first be “taught” what the features of interest look like in order to calibrate it to the system/features being studied.

(Gergely et al., 2001) present an algorithm that identifies ruptures based on a comparison of the minima with neighboring peaks. Selection is controlled by adjusting an appropriate noise level,  $m$ , such that the difference between a feature and its nearest neighbors must be greater than  $2m$  times the standard deviation of the force values. Additional smoothing of the force curve is also achieved by fitting a second order polynomial to a designated amount,  $p$ , of consecutive points. Using this routine, forces measured between human fibrinogen interacting with a silica surface were processed. By monitoring histograms of inter-rupture distances selected with successively more rigorous (higher)  $m$  values, the authors were able to detect a significant peak

at 20-25 nm, a value that corresponds nicely to the known spacing between two domains in the protein.

## H. Relating Bond Chemistry and Energies to Force Measurements

Force microscopy measurements intuitively have the potential to describe energies,  $E(D)$ , associated with an interaction at small separations,  $D$ , by integrating force over distance,  $E(D) = \int FdD$ . As discussed above, however, differences in spring constants can produce variable hysteresis and, therefore, can lead to drastically different energy values. Without fine control of the effective spring constant, it is difficult to accurately capture a potential in a quantitative fashion, which is critical for single molecule work. Moreover, if reaction occurs upon contact (and provided single interactions can be identified in the force spectra); simple prediction of bond/interaction energies based on rupture forces is non-trivial. Specifically, it might be postulated that the maximum gradient in the potential,  $[dE/dD]_{max}$ , is equal to the adhesion or rupture force from the retraction trace; however, in a seminal paper, Evans and Ritchie (1997) showed that such a simple correlation is not valid for single molecule interactions, and more sophisticated theory is required for quantitative comment on the absolute energetics of a bond using force data.

Before continuing, it must be noted that these findings do not preclude valuable quantitative and qualitative comparison of force measurements and bond ruptures to energy parameters. Indeed, early force experiments with various ligand receptor (e.g., biotin, iminobiotin, avidin, streptavidin combinations) revealed a correlation between the rupture forces and enthalpy values associated with each complex (Moy et al., 1994a). This information together with the lack of correlation between rupture force and total free energy suggested the unbinding was adiabatic and that any entropic contributions to the system (e.g., solvation forces) occurred outside of the binding pocket, and were not recorded with the AFM. Other studies followed relating thermodynamic parameters to interaction forces (Chilkoti et al., 1995), as well as many force experiments that employed “elementary” or averaged rupture forces to compare two or more systems in a relative fashion (Dammer et al., 1996; Fiorini et al., 2001; Florin et al., 1994; Frisbie et al., 1994; Ito et al., 1999; Kendall and Hochella, 2003; Kreller et al., 2002; Lower et al., 2001a; Noy et al., 1997; Schmitt et al., 2000). The true value of these studies is their relative quantitative and qualitative comparisons of force data. These characterize the nature of forces at an interface, demonstrate surface and molecule recognition, and define

relative affinity between two molecules or between a molecule and a surface. However, Evans demonstrated that these rupture forces, as absolute values, represent one point in a continuum of bond strengths (Merkel et al., 1999); and that the detachment force recorded with the AFM (and other force measuring techniques) is not a singular fundamental property of the molecular interaction being probed (Evans, 1998; Evans and Ritchie, 1997; Merkel et al., 1999). Instead, apparent bond strength as estimated by rupture force is a function of loading rate (Evans and Ritchie, 1997).

This relationship represents a refinement of a model proposed by (Bell, 1978) that predicts an exponential amplification of dissociation kinetics in the presence of an external force (Merkel et al., 1999). Dissociation of relatively weak associations can be conceptualized as a particle moving out of a potential well (bond), over single (simple interaction) or multiple (complex interaction) activation barriers representing transition states ((Evans and Ritchie, 1997; Merkel et al., 1999). Under a zero force condition the particle will migrate out of the well, through the transition states, and ultimately to complete dissociation on a time scale that is dictated by thermal agitation ( $k_B T$ ). A constant external force on the bond, however, expedites the thermally mediated kinetics and decreases the lifetime of the bond by lowering activation barriers in the energy landscape along a projection that is proportional to the amount of force (Evans and Ritchie, 1997). Under a dynamic load (e.g. a retracting cantilever) where the force,  $F$ , increases over time,  $t$ , as loading rate,  $R_f = dF/dt = k_s v_c$  ( $k_s$  = spring constant of the system,  $v_c$  = velocity of the cantilever), inner activation barriers are revealed as outer activation barriers are progressively lowered by the accumulating force. This phenomenon leads to an intriguing positive correlation between rupture force,  $F_r$ , and  $\log_e(R_f)$ , that is best conceptualized in terms of thermally mediated nature of the bond rupture kinetics. At small loading rates, activation barriers are lowered at a rate slow enough for thermal contributions from the medium to be effective in helping the molecule diffuse out of the well and over the barrier before higher forces are reached (Gergely et al., 2002). Thus, with an effective thermal contribution, a lower rupture force is recorded at the time of dissociation. Under large loading rates (e.g., those typical of many AFM experiments), activation barriers are lowered fast enough such that dissociation proceeds with minimal thermal contribution, resulting in a higher rupture force (Gergely et al., 2002). At ultrafast loading rates on the time scale typical of molecular dynamics (MD) simulations ( $10^{12}$  s), the entire bonding potential is compromised quick enough that only

frictional drag is recorded as the molecule traverses a completely “stretched” and coarsened energy landscape (Evans and Ritchie, 1997). Here, loading rates commonly exceed the time scale of unencumbered, diffusive passage of a molecule from its bonded state, leaving the complex kinetically trapped as force continues to rise. This was observed during molecular dynamic simulations of the biotin-streptavidin complex (Grubmuller et al., 1996). For the biotin system, the time for diffusive passage,  $t_D$  (e.g., the lifetime of the bond) is estimated to be 500 ps under a constant force of 280 pN (Evans and Ritchie, 1997). All activation barriers are lowered at this force such that the initial minimum (e.g. the original potential well representing the bond) is exposed allowing direct diffusion out of the well. However, the ultrafast molecular dynamic simulation loading rate ( $1.3 \times 10^{12}$  pN/s) exceeds  $280\text{pN}/t_D$ , therefore, leaving the complex kinetically trapped in the bound state as rupture force rises well above 280 pN (Evans and Ritchie, 1997).

With these observations and extensive theory development, Evans recognized that measurements of rupture forces over a large range of loading rates effectively probes the lifetime of the interaction under different levels of force while mapping out energy barrier position and heights in a technique now known as dynamic force spectroscopy (Evans, 1998). A dynamic force spectra is constructed by plotting the most probable rupture force of a single interaction,  $F_r$ , versus  $\log_e[R_f]$ , where  $R_f$  values span several orders of magnitude. Regions of constant slope defined as  $f_b = k_B T/x_\beta$  represent activation barriers at a distance of  $x_\beta$  from the potential well. Barrier heights  $E_b$  can be derived from the intercept of the slopes at zero force defined as (Evans and Ritchie, 1997):

$$\log_e (R_f^0) = - E_b/ k_B T + \log_e (f_b/t_D) \quad (7)$$

where, again  $t_D$  = time of diffusive passage, and thus  $1/t_D$  represents an attempt frequency. The attempt frequency is generally not known, but can be estimated from damping phenomenon (Evans, 1998). Activation barrier positions derived from experimental dynamic force spectra of the biotin-avidin interaction compared well with barriers predicted molecular dynamic simulations (Evans and Ritchie, 1997; Izrailev et al., 1997), further emphasizing the value of coupling force measurements with computer simulations. However, it must be noted that bridging the gap between the orders of magnitude difference in the loading rate of experimental systems versus loading rates used in computer simulations is not straightforward and extrapolation of calculated rupture forces to experimentally determined forces must be done with



caution (Grubmuller et al., 1996; Izrailev et al., 1997; Wong et al., 1999). While this was attempted by Grubmuller (1996); Izrailev (1997) and Evans (1997, 1998) indicate that the real value of molecular dynamic simulations, in this context, is their potential to provide clues as to which structural determinants of the interactions contribute to the activation barriers, thereby providing a qualitative mechanism to account for dynamic force spectra features. For example, Izrailev et al. (1997) used a collection of molecular dynamic simulation packages to demonstrate a ground state avidin-biotin complex that was stabilized by hydrogen bonds between the biotin head group and polar amino acids (e.g., Tyr33) within the binding pocket. With application of an external force, two intermediate states stabilized by H-bonds with amino acids at different positions in and near the pocket (e.g., Ser16 and Arg114) are revealed as the ligand is removed – an observation that was consistent with dynamic force spectroscopy experiments.

(Lo et al., 2002) also used a variation of the Bell model to explore the relationship between rupture force and ambient temperature in the biotin-avidin system. The experiments were conducted on an AFM with a constant, millisecond time scale loading rate that was slow enough, compared to the nano to picosecond time scale of molecular dynamic simulations, to neglect any frictional energy loss due to viscous drag. The slow loading rates also allowed the key assumption that thermal equilibrium is achieved at any moment during the unbinding process. This validated the use of a Maxwell-Boltzmann energy distribution to describe the thermal energy being supplied to the complex. The end result is a relationship (Lo et al., 2002):

$$F_i^2 = 2\Delta E_C k_{bond} - 2k_B T k_{bond} \log_e \left( \frac{\tau_R}{\tau_D} \right) \quad (8)$$

that can be fit to an experimental AFM data set of adhesion forces ( $F_i$ ), to derive bond stiffness ( $k_{bond}$ ), and critical binding energy ( $\Delta E_C$ ). Both derived values reflect a summation of the different types of forces that make up the biotin-avidin interaction (e.g., H-bonds, van der Waals and polar interactions). Other variables include thermal energy ( $k_B T$ ), and the ratio of the rupture time ( $\tau_R$ ; determined from the AFM data) and time required for the ligand to diffuse out of the binding pocket ( $\tau_D$ ; estimated independently). Critical binding energy,  $\Delta E_C$ , may be related to a dissociation energy ( $D_e$ ) by defining a potential to describe the interaction – in this case a Morse potential was used. Their  $D_e$  value based on force measurements, 118.9 kJ/mol, compared favorably with the enthalpy change of the dissociation determined by independent means ( $\Delta H =$

98.0 kJ/mol) (Lo et al., 2002; Swamy, 1995). Moreover, the enthalpy value was combined with bond stiffness in additional calculations to determine a critical displacement magnitude (0.1 nm) that was close to inner barrier position,  $x_\beta$ , value determined with dynamic force spectroscopy ( $x_\beta = 0.12$  nm).

Both temperature dependent and load dependent dynamic force spectroscopy rely on force measurements of the interaction of a *single* ligand-receptor pair. This is accomplished by reducing the density of sites that are present and available for bonding (similar to protocols outlined by (Florin et al., 1994; Grandbois et al., 1999; Marszalek et al., 1998; Rief et al., 1997a; Rief et al., 1997b)), such that 1 in 7-10 touches results in attachment (Evans, 1998). Governed by Poisson statistics (Williams et al., 1996), 90-95% of the attachments are predicted to be single bonds. In addition to the biotin-avidin linkage, Poisson distributions are common in force measurements associated with several other systems (Han et al., 1995; Lo et al., 1999; Stevens et al., 1999; Wenzler et al., 1997; Williams et al., 1996). The probability,  $P(n)$ , of an attachment representing  $n$  linkages follows a defined, Poisson distribution, making it possible to extract the  $n=1$  case from a large number of rupture force measurements (Lo et al., 2002). Feedback mechanisms are also employed to control impingement on the sample thereby insuring each approach and retraction cycle has the same magnitude and history of contact force (Evans, 2001). This is especially important when making measurements with biomolecules secured to monolayers that can easily deform on contact to produce various contact areas and configurations, and ultimately different numbers of attachment (Evans, 2001).

Although successful dynamic force spectroscopy experiments have been carried out on a single force measuring instrument (AFM) with a range of loading rates from 100 – 5000 pN/s (Yuan, 2000), due to the exponential relationship on kinetic rates and barrier energies (discussed above), dynamic force spectroscopy is optimized when collecting force measurements over a range of loading rates that are different by orders of magnitude. This can require the use of several force measuring techniques including laser/optical tweezers for slow loading rates 1-10 pN/s, a biomembrane force probe (BFP) for intermediate rates (10-1000 pN/s) and AFM for fast loading rates ( $10^4$ - $10^6$  pN/s) (Evans and Ritchie, 1997).

## **I. Relevance of Dynamic Force Spectroscopy to Biological-Inorganic Interface**

Techniques to extract energy information from force spectroscopy were developed primarily using the biotin-(strept)avidin system (Evans and Ritchie, 1997; Moy et al., 1994a) due

to its relevance to biological systems, non-covalent nature, high affinity and extensive history of experimentation and study. Since then, dynamic force spectroscopy has been applied to other systems, primarily non-covalent and biological in nature. These include DNA base pair interactions (Strunz et al., 1999), unfolding of muscle protein domains (Rief et al., 1997a), antibody-antigen interactions (Schwesinger et al., 2000) and lipid anchoring in membranes (Evans and Ludwig, 2000) to name a few. (Grandbois et al., 1999) also made an attempt at using the dynamic force spectroscopy concept to measure the strength of a single covalent bond. Although they produced values for only one loading rate due to the difficulty of collecting individual covalent interactions (H. Gaub, personal communication). Their calculation of rupture force probabilities based on dynamic force spectroscopy methods allowed them to identify the covalent attachment being terminated as a Si-C bond.

Applying dynamic force spectroscopy concepts to AFM data collected on environmental systems has great potential to provide new insight on the interaction energetics and bond chemistry associated with biogeochemical interfaces. This is, in part, because experimental data collected at the molecular level to describe surface reactions between single biomolecules and mineral surfaces is lacking. Traditionally confined to computer simulation (Cygan, 2001), dynamic force spectroscopy now affords a unique, direct examination of energy landscapes associated with some of the non-covalent mechanisms (e.g., H-bonding) assumed to initiate sorption reactions between minerals and ligands (Holmen and Casey, 1996), the possible ionic or covalent binding of a metal in a mineral surface associated with dissolution (Stumm, 1992), reversible and non-reversible adhesion states of colloids or cells to a surface (Absolom et al., 1983; Ryan and Elimelech, 1996; Ryan and Gschwend, 1994), mineral and or metal recognition of a mineral structure by membrane bound proteins (Lower et al., 2001a).

Perhaps, the true advantage of using dynamic force spectroscopy is realized when used in a comparative framework, for example, dynamic force spectra of cell or biomolecule-mineral interaction before and after structural and functional changes in either 1) the cell surface (e.g., via altered gene expression due to imposed environmental conditions) or the biomolecule (e.g., via point mutations in proteins, functional group substitutions/inactivation in ligands) or 2) the mineral via metal substitution or by comparing isostructural mineral equivalents or different crystal growth faces. Changes in slopes of the dynamic force spectra resulting from structural modifications can provide clues as to which proteins, functional groups or even crystallographic

constraints contribute to surface complex stability or specific activation barriers to binding or detachment. Concomitant correlation of force values with independently determined thermodynamic parameters can also provide insight as to whether a surface attachment or detachment or metal extraction is enthalpy driven or entropically dominated. And as seen above, a common theme when using dynamic force spectroscopy is to supplement and validate characteristics of a particular energy landscape with mechanistic information derived from computer simulations. The role of these simulations is anticipated to be just as important when applying these techniques to biogeochemical systems.

#### **IV. FORCES AT THE BIOMOLECULE-MINERAL INTERFACE**

Organic ligands produced by microorganisms such as low molecular weight organic acids and siderophores have the potential to greatly impact the geochemistry and ecology of soil environments (Hersman, 2000; Stone, 1997). These ligands interact with mineral surfaces to form a critical interface that has implications on biological nutrient/metals acquisition, control of metal toxicity or even ecological competition (Bossier et al., 1988; Brantley et al., 2001; Kraemer et al., ; Kraemer et al., 2002; Neubauer et al., 2000; Stone, 1997). Ligands enter into sorption and desorption reactions with minerals that enhance dissolution or surface passivation, mediate contaminant mobility, or alter the charge character of the mineral surface (Barker et al., 1997; Stumm, 1992). As a result this interface has been studied extensively with bulk experiments and sorption studies (e.g., Kummert and Stumm, 1980; Ludwig et al., 1995; Yao and Yeh, 1996), and with surface sensitive techniques such as XPS (Kalinowski et al., 2000), and Fourier Transform Infrared (FTIR) Spectroscopy (Hansen et al., 1995; Holmen et al., 1997). Key to sorption and desorption reactions between ligands and minerals, however, are the forces that bring the ligand into and out of contact with the surface. Such forces are dependent on the charge character, structure and reactivity of the ligand, the mineral surface and the intervening solution. Characterization of these forces using force microscopy holds great potential to complement information from the existing methodologies listed above in addition to providing new insight on how ligands interact and coordinate with mineral bound metals.

In pioneering work, activation of an AFM tip with a specified chemistry was carried out to examine the biotin-avidin interaction (Florin et al., 1994; Lee et al., 1994b). Florin et al., (1994) sorbed biotin (an organic ligand) to an AFM tip, and probed a surface coated with the

protein receptor avidin. Force measurements of this high affinity ligand-receptor system showed a positive correlation between elementary quantized adhesion forces detected with an autocorrelation analysis and thermodynamic binding affinities. Specifically, biotin adhesion to the avidin substrate measured 160 pN, while iminobiotin, which contains an N substitution in place of an oxygen and has a lower binding affinity, exhibited adhesions closer to 85 pN. Several force spectroscopy studies of the biotin system followed (Chilkoti et al., 1995; Lo et al., 2002; Moy et al., 1994a; Moy et al., 1994b; Wong et al., 1999), along with other force investigations of biomolecules, including examination of: interactions between antibodies and antigens (Dammer et al., 1996; Hinterdorfer et al., 1996; Schwesinger et al., 2000); enzyme activity (Fiorini et al., 2001); proteoglycans (Dammer et al., 1995); observations on the stretching of polysaccharides (Marszalek et al., 1998; Rief et al., 1997b) and muscle proteins (Rief et al., 1997a); and the hybridization of oligonucleotides (Lee et al., 1994a; Mazzola et al., 1999). Simple functional groups have also been covalently attached to AFM tips in order to explore more fundamental interactions, such as the forces between methyl, carboxyl or methyl-carboxyl pairs (Frisbie et al., 1994; Noy et al., 1997). Specifically, this technique, termed chemical force microscopy (CFM), was used to identify the nature of the interacting force (H bond, van der Waals, electrostatic), characterize surface energies and charge distributions, and generate force maps that showed the spatial arrangement of simple functional groups or hydrophobic regions on a monolayer or surface, sometimes with nanometer resolution (Noy et al., 1997).

Collectively, these studies provide a foundation, which allows application of force spectroscopy to additional, more complex, natural systems, such as the ligand/biomolecule-mineral interface that is characteristic of soil environments. Indeed the same forces (e.g., H-bonding, hydrophobic/hydrophilic forces, the van der Waals force, steric forces, non-specific and specific interactions) that allow molecular recognition between biomolecules are also present in ligand mineral interaction (Israelachvili, 1992; Stumm, 1992). However, to our knowledge, only two studies, one of which is summarized below, have probed ligand interaction with a mineral surface using force microscopy (Kendall and Hochella, 2003; Kreller et al., 2002). A discussion of this burgeoning application begins with a description of protocols enabling linkage of a ligand to an AFM tip.

## A. Ligand Linkage Schemes

Devising a suitable linkage scheme to attach the ligand of interest to the AFM probe can present a significant challenge. Each scheme should be appropriately tailored to the relevant experimental goal; however, the following summarizes general considerations. Successful linkage will provide a strong (e.g., covalent or stronger than the interaction of interest), reproducible bond between the ligand and the tip while avoiding non-specific interactions associated with the cantilever material, tip or linker molecule (Fiorini et al., 2001; Wagner, 1998).

Simple ligands such as carboxylate and phosphate groups are commonly linked as terminations of alkylthiol monolayers that coat the tip (Kreller et al., 2002; Noy et al., 1997). The amphiphilic molecules of the monolayer provides an anchor for the ligand but also serves as a spacer, providing separation between the ligand and the tip material thereby reducing non-specific interactions. Larger ligands and proteins that contain either a free amino or carboxyl group may be attached using an active ester technique commonly used to couple two proteins (Cheung et al., 2000; Fiorini et al., 2001; Hinterdorfer et al., 2002; Kendall and Hochella, 2003). In the presence of an carboxyl group, 1-Ethyl-3-(3-Dimethylaminopropyl) carbodiimide (EDC) together with N-hydroxysuccinimide (NHS) will form a stable, hydrolysis resistant, active succinimidyl ester that readily forms a peptide bond with an available amino group (Grabarek and Gergely, 1990). Note that the position of the amino and carboxyl groups can vary with one being supplied as a self assembling monolayer (SAM) terminal group on the tip and the other contributed by the molecule to be attached, or vice versa. Other linkage protocols employ polyethylene glycol (PEG) as a cross-linking spacer that is terminated with various functional groups such as pyridyldithiopropionate (PDP). PDP coordinates with thiol groups and nitrilotriacetic acid (NTA) which, in combination with various divalent metals, binds to consecutive histidine residues (Hinterdorfer et al., 2002; Kienberger et al., 2000; Schmitt et al., 2000). One advantage to using PEG-NTA- $\text{Me}^{2+}$ -His linkage system is that selection of the divalent metal ( $\text{Cu}^{2+}$ ,  $\text{Co}^{2+}$ ,  $\text{Ni}^{2+}$ ) permits control of the binding force, and, to a certain extent, the probability of the linkage. In addition, the NTA- $\text{Me}^{2+}$ -His bond is easily reversible, such that it can be terminated with the use of EDTA, and then regenerated with the reintroduction of the free metal (Schmitt et al., 2000). Other workers propose attaching ligands or molecules via carbon nanotubes that extend from the AFM tip (Hafner et al., 2001; Wong et al., 1998a; Wong et al.,

1998b). This provides ideal spacing between the molecule and the tip, but more importantly, drastically increases the resolution of the force spectroscopy (and imaging) due to the nanotube's extremely small radius of curvature compared to a traditional  $\text{Si}_3\text{N}_4$  tip. Because nanotubes can only be functionalized at the end termination of the carbon lattice this also places an important constraint on the orientation and localization of the molecules being linked. As a result, the probability of capturing a single molecule interaction is increased, especially when working with lower molecular weight molecules.

It is important that the linkage must not directly interfere with the activity of ligand (Fiorini et al., 2001), and thus, electron donor functional groups should be protected during the linkage reaction. Kendall and Hochella (2003) accomplished this by inserting a metal ( $\text{Al}^{3+}$ ) into the ligand (azotobactin) structure to occupy and protect the chelating groups, while carrying out the linkage reaction. Once attached to the tip, the azotobactin was reactivated by removing the Al with high concentrations of a competing ligand (EDTA), a process that was monitored in a test solution with UV-vis spectroscopy (Figure A. 5).

Unfortunately, inherent to fixing a molecule to a surface is a reduction in the degree of freedom afforded to the molecule's conformation. This can result in an alteration or loss of chelation or ligand activity and should be considered. To this end, control activations are often run in parallel to tip activations, where monolayers, linker molecules and the biomolecule of interest are reacted with a flat,  $\text{Si}_3\text{N}_4$  or  $\text{SiOH}$  substrate (Fiorini et al., 2001; Hinterdorfer et al., 2002). Similar in composition to the tip, the flat test substrates serve as a proxy for tip that are readily probed with AFM imaging, fluorescence and confocal microscopy, surface plasmon resonance (SPR) and various enzyme and ligand assays in an effort to assess the success of the linkage reaction; estimate coverage, density and footprint area of the monolayer-biomolecule construct; and evaluate activity retention in the immobilized biomolecule (Fiorini et al., 2001).

## **B. Siderophores and Oxide Surfaces**

Kendall and Hochella (2003) collected force signatures between a ligand (siderophore) and two mineral bound metals ( $\text{Fe(III)}$  and  $\text{Al(III)}$ ) in an attempt to examine the mechanism of siderophore-mediated dissolution of oxide surfaces. Siderophores are ligands produced by microorganisms to assimilate the essential nutrient ferric iron, in spite of its extreme insolubility in near surface, circumneutral environments. The aqueous chemistry of siderophores has long been studied (Winkelmann, 1991), and it is recognized that siderophores' effectiveness in

acquiring iron, can, in part, be attributed to a thermodynamic binding affinity for Fe(III) (aq) that is orders of magnitude above that for other metals, including Al(III). Only recently, however, was it recognized that, in addition to the formation of stable, aqueous iron complexes, siderophores can release iron from minerals (Hersman et al., 1995; Holmen and Casey, 1996; Liermann et al., 2000; Maurice et al., 2000; Seaman et al., 1992; Watteau and Berthelin, 1994). The mechanism of this release, however, is not clearly defined.

Force microscopy of the pyoverdinin type siderophore azotobactin interacting with iron and aluminum oxide surfaces showed a unique relationship between ligand-metal affinity and adhesion forces (Kendall and Hochella, 2003). Average adhesion forces between azotobactin and goethite ( $\alpha$ -FeOOH) at pH 7 were 2-3 times the value between azotobactin and goethite's isostructural Al-equivalent, diaspore ( $\alpha$ -AlOOH) (Figure A. 6a). A similar force relationship was also observed between the trihydroxamate siderophore deferoxamine (DFO) and each oxide surface (Figure A. 6b). Control experiments where each mineral surface was probed with a SAM coated tip lacking the azotobactin molecule produced force signatures that were almost identical, indicating the distinction in the force signature between diaspore and goethite could be attributed to the presence of the azotobactin on the tip.

Force measurements collected under various solution conditions (e.g., pH, ionic strength and soluble iron concentrations) and at different sample locations on the mineral extended the characterization of the ligand-mineral interaction and helped identify the source of discrepancy in adhesion values associated with each oxide. As a first guess, it could be hypothesized that the forces of interaction are dominated by an electrostatic component; and that the difference in the adhesion values between diaspore and goethite, simply reflects variation in the charge character of each mineral. Although point-of-zero-charge (pzc) literature values for goethite (pzc 7-9) and diaspore (pzc 7-8) are similar, suggesting both should be neutral or slightly positively charged (Cornell and Schwertmann, 1996; Kosmulski, 2001), it's possible that our model system deviates from pristine charge conditions, such that the goethite is positive and the diaspore is slightly negative. With a net negative charge predicted for azotobactin at pH 7 ( $pK_a$  hydroxycarboxylate = 4-5; (Telford and Raymond, 1996), this could result in a larger adhesion force for goethite presumably due to a stronger electrostatic interaction. Measurements at lower pH and different sample locations, however, suggest otherwise. At pH 3.5, far from the pzc value of each mineral, and where the azotobactin is anticipated to be neutral, the same 2-3 fold increase in



adhesion values is observed. Moreover, the azotobactin-goethite/azotobactin-diaspore force relationship remained intact when comparing adhesion distributions representative of different sample locations on each mineral surface, where anomalous charge distributions and changes in microtopography are expected. Overall, similar to observations made with the biotin ligand system (Chilkoti et al., 1995; Izrailev et al., 1997; Moy et al., 1994a), adhesion values upon retraction appear to be relatively independent of protonation equilibria, and may reflect a specific interaction between the siderophore oxygens and the metal contained in each mineral. The discrepancy in adhesion for goethite versus diaspore can then be explained by differences in electronic character of each metal (e.g., Fe(III) versus Al(III)), where the more electronegative ferric iron will behave as a harder acid with a higher affinity for the oxygens. In additional experiments with goethite only, this surface affinity was readily disrupted with the addition of soluble iron (Figure A. 7). Here, increased  $[\text{FeCl}_3 \cdot 6\text{H}_2\text{O}]$  (pH 3.5) led to a saturation of the ligand as the soluble iron out competed the mineral iron for the siderophore oxygens, resulting in lowered adhesion values.

This does not discount an electrostatic component to the azotobactin-oxide interaction. Indeed, decreases in the jump to contact distance with increasing ionic strength thought to reflect a collapse in the double layer associated with the mineral surface (Lower et al., 2000; Noy et al., 1997), confirm the effect of charge, especially upon approach. Instead, force evidence suggests a balance between electrostatics dominating the approach and more specific interactions directing surface adhesion; a scheme that is embodied in the following observation - goethite force signatures at pH 7 often show a long range, electrostatic repulsion on approach that was equal to or significantly lower in the diaspore signatures; yet, the goethite adhesion force averaged 3.81 nN compared to 1.38 nN for diaspore.

Force data also provided information on which azotobactin functional groups might be important in the interaction. Distinctive plateaus were commonly observed after retracting the tip ~6-7 nm from the surface (Figure A. 8). These features are thought to represent the energy absorption associated with the combined extension and stretching of azotobactin's polypeptide chain and the molecule used to link the ligand the tip. Using an approximation of 0.38 nm/amino acid, a quick calculation shows that azotobactin's fully outstretched length of ~3.8 nm, together with an additional 3 nm from the linker molecule gives a value that is close to the 6-7 nm observed in the force signatures. This distance, then, requires that azotobactin's terminal

homoserine group serve as an anchor to the surface, providing a strong, persistent link in the interaction. This coincides with other reports that, in aqueous systems, the adjacent hydroxamate group initiates chelation (Albrecht-Gary and Crumbliss, 1998; Telford and Raymond, 1996). Additionally, considering its terminal position on the molecule, it is feasible that the homoserine group is a dominant component during surface interaction.

Finally, these force microscopy results give cause to reassess the role of large ligands, such as azotobactin, in dissolving minerals. Instead of serving as an Fe shuttle between smaller ligands that interact with the surface and the cell, the force evidence demonstrating azotobactin's strong surface affinity presents a distinct possibility of the relatively large molecule entering into a strong, stable complex with the mineral. As seen above, the force data also allow comment on the nature of the association with the surface. Steric constraints imposed by ligand size, structure and conformation, together with the limited access to an iron atom contained on a mineral surface, would certainly preclude the hexadentate coordination characteristic of the siderophore-aqueous complex (Cocozza et al., 2002; Hersman, 2000; Holmen and Casey, 1996). Instead, plateau features in the retraction curves suggest a strong coordination formed by a single oxygen pair that terminates the azotobactin molecule as one possibility. Recent, ongoing molecular dynamics (MD) simulations, in collaboration with U. Becker (Univ. of Michigan), confirm this possibility, as well as the extended dimensions of the azotobactin-linker construct. Interestingly enough, however, simulations reveal that the spacing between the two, chelating hydroxamate oxygens is sufficient to allow individual coordination with neighboring irons in the goethite structure (Figure A. 9). Siderophore-oxide interaction continues to be examined with molecular dynamic simulation as well as dynamic force spectroscopy.

## **V. FORCES AT THE BACTERIUM-MINERAL INTERFACE**

### **A. Force Microscopy Technique Using Whole Cells**

The fundamental forces between a bacterium and mineral surface are central to understanding the intricacies of interfacial phenomena such as bacterial adhesion to minerals and dispersal in the environment (Fletcher, 1996; van Loosdrecht et al., 1989), mineral growth and dissolution (Fortin et al., 1997; Hiebert and Bennett, 1992; Myers and Nealson, 1988; Roden and Zachara, 1996; Schultze-Lam et al., 1992), biofilm formation (Davies et al., 1998; Lawrence et al., 1991), and bacterial affinity for or recognition of specific mineral surfaces (Bhosle et al.,

1998; Dziurla et al., 1998; Edwards et al., 1998; Fleminger and Shabtai, 1995; Ohmura et al., 1993). A myriad of physicochemical interactions occur at biological-mineral interfaces in nature, due to (i) the mosaic of spatially discrete macromolecular cell wall structures on bacteria, (ii) the dynamic nature of these structures, and (iii) the diversity of mineral surface functionality, topography, and crystallography (Lower et al., 2000). As discussed above in section II, these interactions are expected to be governed by the cumulative effects of intermolecular forces (Butt et al., 1995; Fletcher, 1996; Gay and Leibler, 1999; Israelachvili, 1992; Israelachvili and McGuiggan, 1988; Kendall, 1994). However, acquiring even an elementary appreciation of these forces presents a daunting challenge, primarily due to the minute scale at which these interfaces must be probed, and the difficulty in developing a technique that preserves the natural intricacies of the bacteria surface (Lower et al., 2000).

Measurement of fundamental forces between whole bacterial cells and inorganic phases can be conducted in one of two ways with force microscopy. The first involves “fixing” cells to a solid substrate (e.g., a glass slide) and probing these cells with a force-sensing cantilever. The simplest setup makes use of the sharp tip that is integrated into most force microscopy cantilevers (see above). In many instances, however, this is not ideal because these tips are not well constrained with respect to their geometry and/or area of contact. As shown in section II, this greatly influences force measurements thereby making it difficult to compare measured data to theoretical force models, and impedes the comparison of data collected with different tips. To overcome the limitations imposed by using a sharp tip, Ducker et al (1991) devised a simple yet ingenious solution. They created a “colloidal tip” by attaching a glass bead to the end of a force-sensing cantilever. This bead was then used to probe a flat silicon surface (Ducker et al., 1991, 1992), although such a “colloidal tip” could also be used to probe microbial cells on a glass surface. A number of companies, such as Duke Scientific Corporation, Polysciences Incorporated, and Bangs Laboratories Incorporated, sell spheres ranging in size from nanometers to micrometers. A major drawback to this scenario, however, is that it limits the inorganic phases that can be utilized to those materials commonly used to make tips (e.g., silicon and silicon nitride) or beads (e.g., plastic and glass). With the exception of silica (e.g., glass beads), minerals or other inorganic phases cannot be attached to a force-sensing cantilever. Therefore, interactions between bacteria and minerals much employ another technique. That is, the cells

must be linked to the force-sensing cantilever, which is then used to probe a particular face on a mineral crystal or other surface.

The first cell to be linked to a force-sensing cantilever was a large mammalian cell (Antonik et al., 1997). This cell was not actually “attached”, rather it was induced to grow on the cantilever. The researchers conducting this experiment were not interested in measuring forces, which was fortunate because cells grew on both the top and bottom surfaces of the cantilever. Hence, the cell growth would have affected not only the spring constant of the lever, but it would also alter the optical lever detection system. None-the-less, this opened the door to a number of other protocols of linking cells to a force microscope cantilever.

It is a difficult challenge to link microbial cells on the order of 1  $\mu\text{m}$  to the end of a cantilever. Early attempts relied on the attachment of cells that had been chemically fixed or treated with harsh chemicals (e.g., glutaraldehyde) (Razatos et al., 1998a; Razatos et al., 1998b). While these investigations produced some very intriguing force measurements, this type of linkage protocol is often undesirable because the cells are killed in the process. Further, chemicals such as glutaraldehyde are known to denature proteins and other macromolecules. Another method was developed that allowed the force-sensing cantilever to support bacterial cells in a living, native, fully functional state – thereby creating “biologically active force probes” (Lower et al., 2000, 2001b). A polycationic linker molecule (e.g., aminopropyltriethoxysilane or poly-lysine) can be used to link living bacteria to a small glass bead that is then attached to the cantilever, or the bacteria can be linked directly onto the cantilever itself (Lower et al., 2001b). Polycationic linkers work well because most bacteria are negatively charged over a wide range of pH conditions. Hydrophobic molecules (e.g., octadecyltrichlorosilane) are also attractive linkers because many microorganisms have hydrophobic surfaces. Techniques similar to affinity chromatography (e.g., see (Egger et al., 1992; Pleuddemann, 1991; Rezanian et al., 1999)) may be employed to design tailor-made linker molecules (e.g., ligand-receptor or antibody-antigen) that work on virtually any bacterial species. The use of polycationic linkers, or similar molecules, preserves the natural conformation, structure, and function of the macromolecules on the microbial surface. When live cells are used (i.e., a biologically active force probe), force measurements may be collected under different physiological or environmental conditions in real time (Lower et al., 2001a; Lower et al., 2000, 2001b). Finally, for larger microbial cells such as yeast or fungal cells, the “colloidal tip”

technique (see above) can be used to glue a single cell to the end of a cantilever (Bowen et al., 1998b).

Using these techniques, a number of groups have used force microscopy to measure intermolecular forces at the bacterium-mineral interface (Bowen et al., 1998a; Bowen et al., 2000a, b; Camesano and Logan, 2000; Lower et al., 2001a; Lower et al., 2000, 2001b; Ong et al., 1999; Razatos et al., 1998a; Razatos et al., 1998b). In our laboratories, we have used biological force microscopy (Lower et al., 2000) to measure intermolecular forces between living bacteria (e.g., *Escherichia coli*, *Burkholderia cepacia*, and *Shewanella oneidensis*) and inorganic phases (e.g., muscovite, goethite, diaspore, graphite, and glass) in solutions of varying ionic strength, pH, and oxygen concentration (Lower et al., 2001a; Lower et al., 2000, 2001b). Below we will examine the force-distance relationships at the *E. coli*-muscovite and *S. oneidensis*-goethite interfaces. We will concentrate on the forces measured upon approach of a bacterium towards a mineral in the case of the former. For the latter system (i.e., *S. oneidensis*-goethite), we will explore forces measured as the two surfaces are pulled apart or retracted from one another.

## **B. Forces between *Escherichia coli* and Muscovite**

Figure A. 10 shows the interaction between *E. coli* and the (001) surface of muscovite as the sodium chloride (NaCl) solution was exchanged five times between low ( $\sim 10^{-5}$  M) and high ( $\sim 10^{-1}$  M) ionic strength. While both approach and retraction forces were measured, shown in Figure A. 10 are only the forces detected upon approach of the mineral towards living cells on a biologically active force probe. At low ionic strength, repulsive (positive sign) forces were detected at a separation of approximately 100 nm. This repulsive interaction increased exponentially (see below) to a maximum value of  $\sim 30$ -35 nN at contact. At high ionic strength, the magnitude of repulsion was significantly less as was the range of separation over which force interactions took place. The two surfaces did not “feel” one another until they were within 15-20 nm of separation. As with the measurements at low ionic strength, an exponential force appears to dominate at high ionic strength. It is important to note that these data shown in Figure A. 10 span the entire range of measurements for literally hundreds of force-distance curves taking as a solution was exchanged several times between high and low ionic strength. Hence, the measurements are reproducible.

Results can be interpreted with the so-called DLVO theory (Derjaguin and Landau, 1941; Verwey and Overbeek, 1948). This theory describes forces ( $F$ ) as a function of the distance ( $D$ )

(e.g., between a bacterium, treated as a sphere and a mineral, treated as a flat plane) as the sum of the electrostatic and van der Waals forces (Butt et al., 1995; Ducker et al., 1991; Israelachvili, 1992; Muller and Engel, 1997):

$$F_{DLVO}(D) = F_{electrostatic}(D) - F_{vdw}(D) = \frac{4\pi\sigma_{bacteria}\sigma_{mineral}R}{\epsilon\epsilon_0\kappa} e^{-\kappa D} - \frac{HR}{6D^2}$$

where  $\sigma$  is surface charge density ( $C\ m^{-2}$ ),  $R$  is the radius of a cell (or in this case the radius of the bacteria coated bead attached to the cantilever),  $\epsilon$  is the dielectric constant of water (78.54 at 298K)  $\epsilon_0$  is the permittivity of free space ( $8.854 \times 10^{-12}\ C^2\ J^{-1}\ m^{-1}$ ),  $\kappa$  is the inverse Debye length (Debye length  $\sim 1\ nm$  at  $10^{-1}\ M$  and  $\sim 100\ nm$  at  $10^{-5}\ M$ ; see above), and  $H$  is the Hamaker constant. For the model results plotted in Figure A. 10, Hamaker's constant was  $10^{-21}\ J$  (Vigean et al., 2002); surface charge density of the bacterium was estimated using Equation 3 as  $-0.001$  or  $-0.04\ C\ m^{-2}$  at low or high IS, respectively (surface potential measurements were taken from, (Camesano and Logan, 2000; Ong et al., 1999; Vigean et al., 2002); and the surface charge density of the mineral was estimated using Equation 3 as  $-0.004$  or  $-0.2\ C\ m^{-2}$  at low or high ionic strength, respectively (surface potential measurements were taken from (Ducker et al., 1992; Ong et al., 1999).

Figure A. 10 compares measured forces to those predicted by DLVO theory. Ionic strength (approx.  $10^{-1}$  versus  $10^{-5}\ M$ ) appears to have a strong effect on the interactions between *E. coli* and muscovite. This is because higher salt concentrations cause the electrostatic double-layer to become thinner (i.e., surfaces cannot “feel” one another until they get very close). Further, the increased concentration of counter ions at high ionic strength effectively screens the negative charges on both surfaces, thereby resulting in smaller magnitude forces of repulsion. These particular measurements are fairly consistent with DLVO theory. However, there are some important discrepancies. For example, at low ionic strength the attractive van der Waals force is expected to dominate the interaction at separations less than 5 nm. However, measurements reveal that *E. coli* and muscovite do not exhibit attraction even at the closest approach. Indeed, adhesion forces were not detected when *E. coli* and muscovite were forced together and subsequently pulled apart at low ionic strength (Lower et al., 2000). This suggests that electrostatic and/or other repulsive forces (e.g., solvation interactions) dominate this particular interaction.

Many other force measurements conducted in our laboratories, suggest that electrostatic and van der Waals forces are not the only intermolecular forces at the bacterium-mineral interface (S. Lower, unpublished results). Others have attempted to invoke extended-DLVO models to explain deviations from purely van der Waals and electrostatic forces and fit model predictions to measurements (see e.g., Camesano and Logan, 2000; Ong et al., 1999). While these investigations may be valid, one needs to remember that force models are sensitive to the geometric shapes of interacting particles as well as the roughness of surfaces and contact area (Israelachvili, 1992), all of which are difficult to rigorously define or control for minerals and cells with biopolymers. Further, DLVO was developed to describe phenomena between inanimate particles rather than living cells that have exquisite control over the expression of surface macromolecules. Seemingly simple concepts such as “contact” become difficult to define for cells having polymers of varying length, which extend for some distance beyond the cell wall. Further, living cells and/or surfaces with polymers are expected to show a time dependent adhesion (measured by Lower et al., 2001a) as biopolymers diffuse in the cell wall and reorient with respect to another surface (Beveridge, 1999; Leckband and Israelachvili, 2001). The true value may not be in whether a model perfectly fits data, but the most definite answer comes when the measurements contradict the theory, thereby disproving a particular construct and suggesting that other forces are responsible for a particular bacteria-mineral interaction. As stated by (Oreskes et al., 1994), scientific investigations are at their best when one combines experimental measurements and model predictions to challenge existing formulations. Hence, there is a great need to test such models by comparing theories to precise force measurements using “model” microorganisms and minerals. Only then will we be able to understand how *all* of the various intermolecular forces (e.g., electrostatic, van der Waals, hydration, hydrophobic, and steric interactions) govern interactions at the bacterium-mineral interface.

### **C. Forces between *Shewanella oneidensis* and Goethite or Diaspore**

Not shown in Figure A. 10 are the forces required to pull the mineral and bacteria apart (i.e., retraction data). In fact, a very strong adhesion force was detected between *E. coli* and muscovite, but only at high ionic strength (Lower et al., 2000). Aside from being a notable example of a situation that DLVO theory often cannot explain, retraction data provide an immense amount of information about the adhesive strength and structural properties of specific biopolymers on a cell’s surface. Recently, we interpreted these retraction data for studies of

bacterial adhesion and electron transfer reactions between *Shewanella oneidensis* (a dissimilatory-iron-reducing-bacteria) and the minerals goethite (FeOOH) or diaspore (AlOOH) under aerobic and anaerobic solution conditions (Lower et al., 2001a; Lower et al., 2002). *S. oneidensis* is capable of using either oxygen or ferric iron in the crystal structure of iron oxyhydroxides as a terminal electron acceptor (Nealson and Saffarini, 1994). We used force microscopy to determine whether a microorganism could discriminate between two very similar minerals (diaspore and goethite) under anaerobic conditions, when electron transfer is expected to occur between *S. oneidensis* and iron containing minerals.

A mineral crystal, mounted on a piezoelectric scanner, approached live bacteria on a biologically active force probe at a rate that was comparable to the natural velocity of motile bacteria. Once contact was established, the two surfaces were pulled apart resulting in retraction data. Figure illustrates the retraction profile for *S. oneidensis* and goethite versus diaspore under anaerobic or aerobic conditions (Lower et al., 2001a). The intricate details of these curves and the entire data set provide valuable information about intermolecular forces and structures at the bacterium-mineral interface. Initially the entire retraction data were characterized by integrating force with respect to distance. This provided quantitative energy values associated with adhesion. The retraction curves were further analyzed by the worm-like chain model (see above) to establish a correlation between specific bridging polymers and unique signatures in the retraction curves.

Energy values determined from retraction curves similar to those shown in (Lower et al., 2001a) revealed that *S. oneidensis* had an higher affinity for diaspore (vs. goethite) under aerobic conditions (Lower et al., 2001a). However, under anaerobic conditions the bacteria exhibited a significant increase in affinity for goethite (see Lower et al., 2001a); whereas the adhesion energy for diaspore was indifferent to oxygen concentrations (Lower et al., 2001a). The attractive energy between *S. oneidensis* and goethite was 30 attoJoules ( $\text{aJ} = 10^{-18}\text{J}$ ) and 130 attoJoules under aerobic and anaerobic conditions, respectively. Further, the energetic affinity between goethite and *S. oneidensis* also increased with contact time under anaerobic conditions. This provided quantitative evidence suggesting that this microorganism recognized a particular inorganic surface such that it localized and/or produced biopolymers to mediate contact with goethite under anaerobic conditions.



This idea was further tested by using a “bridging polymer” model to interrogate the intricate details (e.g., the saw-tooth pattern) in the retraction data. As shown above for the worm-like chain model, linear polymers such as proteins are expected to unravel according to Equation 4. According to this model, one needs only the persistence length and the contour length to describe the force as a function of the distance a polymer is extended. This model describes a physical process similar to that which is recorded in the retraction data of force microscopy. A protein, for example, in the cell wall of a bacterium makes contact with a mineral. The mineral is then pulled away from the bacterium causing the protein to unravel until it is completely extended at which point the protein is either ripped from the cell wall or it breaks free of the mineral surface and recoils into the cell surface.

The outer surface proteins of *Shewanella* are well characterized. *Shewanella* is known to have proteins on its outer membrane that mediate contact with iron oxyhydroxides (Caccavo, 1999; Caccavo et al., 1997; Das and Caccavo, 2000). Several of these proteins are putative iron reductases, which are expected to make physical contact with goethite such that they can transfer electron across the organic-inorganic interface (Arnold et al., 1990; DiChristina and Delong, 1994; Myers and Myers, 1992, 1993, 1997; Myers and Nealson, 1990; Myers and Myers, 1998, 2000, 2001; Nealson and Saffarini, 1994; Roden and Zachara, 1996). In fact, four putative iron reductase proteins have been characterized according to their mass and/or genetic sequence (Myers and Myers, 1997; Myers and Myers, 1998, 2000, 2001, 2002). The worm-like chain model was used to predict the way in which each of these four proteins (ranging in size from ~50 to 150 kDa; (Myers and Myers, 1997; Myers and Myers, 1998) would unfold. The molecular mass of each protein was used to estimate its overall length according to the following conversion, ~110 Da per amino acid residue (Voet and Voet, 1995). The persistence length of each amino acid, defined as the distance between two adjacent  $C_{\alpha}$ , was equal to 0.38 nm (Karlsson et al., 1996; Muller et al., 1999; Myers and Myers, 2001). As shown in Figure 1 contained in Lower et al., 2001, *Science*, the saw-tooth pattern at approximately 500 nm corresponds to the force-extension profile of one of the four putative iron reductase proteins. This profile was reproducible suggesting that the cell wall protein was not ripped from the bacterium, but rather retained its native conformation after multiple extensions. This unique signature was present only for goethite under anaerobic conditions where it was detected in ~80% of the retraction curves, but only when the bacterium was given some period of time to

make contact with the surface of goethite (Lower et al., 2001a). This suggests that the bacterium required time to “recognize” the mineral surface and subsequently create and/or mobilized a specific protein to the area of contact with goethite.

## **VI. FUTURE WORK**

On Earth, literally millions of different species of prokaryotes may interact with any of thousands of different minerals. An interface is formed at the junction of a bacterium and a mineral surface that is complex, dynamic, and by its very nature, nanoscale in size. This is because bacteria are living cells that have mastered the art of synthesizing fully functional structures (e.g., lipids, proteins, polysaccharides) and utilizing properties that exist only at the nanometer scale. The study of the interface between minerals and microorganisms requires a unique fusion of geomicrobiology and nanoscale science. What are the fundamental forces that control the binding of a silanol group on a mineral surface to a carboxylic group in a bacterium’s cell wall? How does the density and distribution of functional groups on a crystal face influence the way microorganisms sense mineral surfaces? Do bacteria express specific outer surface proteins to interact with certain minerals? How do bacteria modulate forces of interaction between themselves and minerals (or other bacteria) to either enhance or inhibit adhesion and subsequent biofilm formation? Researchers must be able to thoroughly explore both sides of the interface (i.e., the bacterium and the mineral) and the fundamental nanoscale forces in the intervening region to discover phenomena that exist only in the nanospace between a microorganism (or microbially produced polymers) and a mineral surface.

As mentioned earlier, application of force microscopy to the biogeosciences is in its infancy, and there exists many other uses and unexplored possibilities of force experiments with ligands, microorganisms, and minerals. Structural elements within a particular biomolecule/ligand may contribute to its ability to bind to a surface or promote dissolution, or chelate dissolved or mineral bound metals (Ludwig et al., 1995; Nubel et al., 1996; Stumm, 1992). One can envision collecting a force signature for a large ligand interacting with a mineral, followed by collection of spectra associated with several, individual cognate functional groups associated with the ligand. Comparison of the whole ligand, baseline spectrum with the individual component spectra could reveal which functional groups are dominating the interaction with the mineral. Or, a similar process could be achieved by making force

measurements after successive chemical modification of the original ligand structure. Such modification might include inactivation of a specific functional group with a residue-specific reactive reagent (Voet and Voet, 1995), or an amino acid substitution resulting from alteration of the genes associated with the biosynthesis of the molecule. Again changes in the force signature with each modification might help determine the critical moieties contributing to the interaction.

Force maps (Noy et al., 1997) are also possible using ligand activated tips. Here, the contrast in the map may be supplied by the differential adhesion between the ligand and various metals that are associated with a surface. For example, a map constructed with a siderophore activated tip might show large adhesions in areas of high concentrations of trivalent metals such as Fe(III) or Al(III) and lower adhesions for divalent metals such as Cu(II), Zn(II) or ferrous iron. Given the spatial resolution of the AFM, such images could be useful for identifying contaminant distribution on a surface or pinpointing impurity concentrations on a mineral growth face, both on a nanometer scale.

Chemical force microscopy is traditionally carried out in a fluid cell (Digital Instruments) that allows direct observation of ligand-surface interaction under environmentally relevant conditions with pico- to nanoNewton force resolution and a spatial resolution of tens of nanometers down to potentially the atomic level. Changes in the forces of interaction with solution composition provide important information about the structure and charge character of the ligand and mineral surface, and the nature of the interaction between the two. While the effect of solution composition (e.g. pH) on ligand sorption can be monitored with force measurements using a force titration (Kreller et al., 2002). The sensitivity of this technique also allows small changes in mineral solubility and associated metal concentrations, pH, and ionic strength to be detected (Kendall and Hochella, 2003). Given the spatial resolution mentioned above, this opens up the possibility of using this technique to detect localized solution micro- or even nanoenvironments associated with a surface.

Finally, force investigations with living microorganisms are rich with possibilities. For example, one could measure forces of adhesion using wild-type stains versus mutants that are incapable of producing specific cell wall macromolecules. These data may result in unique force signatures characteristic of particular biomolecules. Force measurements could also be coupled to other techniques such as confocal scanning laser microscopy. This provides the potential to

collect force measurements concurrent with fluorescence observations of the distribution and localization of cell wall macromolecules.

**Acknowledgements** – SKL acknowledges the support of the National Science Foundation, the Department of Energy, the American Chemical Society, and the General Research Board of the University of Maryland. SKL would also like to thank J. Tak for support. Funding was provided to TAK by a GAAN Fellowship (U.S. Dept. of Education), the NSF's Nanoscale Science and Engineering (NSE) Program (EAR 01-03053), and the Department of Energy's OBES Geosciences Program (DE-FG02-99ER 15002). TAK acknowledges the support of Michael F. Hochella, Jr. (Virginia Tech).

## REFERENCES

- Absolom, D. R., Lamberti, F. V., Policova, Z., Zingg, W., van Oss, C. J., and Neumann, A. W. (1983). Surface thermodynamics of bacterial adhesion. *Applied and Environmental Microbiology* 46, 90-97.
- Albrecht-Gary, A.-M., and Crumbliss, A. L. (1998). Coordination chemistry of siderophores: Thermodynamics and kinetics of iron chelation and release. In "Iron transport and storage in microorganisms, plants, and animals" (H. Sigel, ed.), Vol. 35, pp. 239-327. Marcel Dekker, New York.
- Antonik, M. D., D'Costa, N. P., and Hoh, J. H. (1997). A biosensor based on micromechanical interrogation of living cells. *IEEE Engineering in Medicine and Biology* 16, 66-72.
- Aoki, T., Hiroshima, M., Kitamura, K., Tokunaga, M., and Yanagida, T. (1997). Non-contact scanning probe microscopy with sub-piconewton force sensitivity. *Ultramicroscopy* 70, 45-55.
- Arnold, R. G., Hoffmann, M. R., DiChristina, T. J., and Picardal, F. W. (1990). Regulation of dissimilatory Fe(III) reductase activity in *Shewanella putrefaciens*. *Applied and Environmental Microbiology* 56, 2811-2817.
- Ashby, P. D., Chen, L., and Lieber, C. M. (2000). Probing Intermolecular Forces and Potentials with Magnetic Feedback Chemical Force Microscopy. *Journal of the American Chemical Society* 122, 9467-9472.
- Barker, W. W., Welch, S. A., and Banfield, J. F. (1997). Biogeochemical weathering of silicate minerals. In "Geomicrobiology: Interactions Between Microbes and Minerals" (K. H. Nealson, ed.), Vol. 35, pp. 448. Mineralogical Society of America, Washington D.C.
- Baumgartner, W., Hinterdorfer, P., and Schindler, H. (2000). Data analysis of interaction forces measured with the atomic force microscope. *Ultramicroscopy* 82, 85-95.
- Bell, G. I. (1978). Models for specific adhesion of cell to cells. *Science* 200, 618-627.
- Beveridge, T. J. (1999). Structures of Gram-negative cell walls and their derived membrane vesicles. *Journal of Bacteriology* 181, 4725-4733.
- Bhattacharjee, S., Chen, J. Y., and Elimelech, M. (2000). DLVO interaction energy between spheroidal particles and a flat surface. *Colloids and Surfaces A: Physicochemical and Engineering Aspects* 165, 143-156.
- Bhosle, N., Suci, P. A., Baty, A. M., Weiner, R. M., and Geesey, G. G. (1998). Influence of divalent cations and pH on adsorption of a bacterial polysaccharide adhesin. *Journal of Colloid and Interface Science* 205, 89-96.
- Binnig, G., Quate, C. F., and Gerber, C. (1986). Atomic force microscope. *Physical Review Letters* 56, 930-933.
- Bossier, P., Hofte, M., and Verstraete, W. (1988). Ecological Significance of Siderophores in Soil. In "Advances in Microbial Ecology" (K. C. Marshall, ed.), Vol. 10, pp. 385-414. Plenum Press, New York.
- Bowen, R. W., Hilal, N., Lovitt, R. W., and Wright, C. W. (1998a). Direct measurement of interactions between adsorbed protein layers using an atomic force microscope. *Journal of Colloid and Interface Science* 197, 348-352.

- Bowen, R. W., Hilal, N., Lovitt, R. W., and Wright, C. W. (1998b). Direct measurement of the force of adhesion of a single biological cell using an atomic force microscopy. *Colloids and Surfaces A: Physicochemical and Engineering Aspects* 136, 231-234.
- Bowen, W. R., Lovitt, R. W., and Wright, C. J. (2000a). Direct quantification of *Aspergillus niger* spore adhesion in liquid using an atomic force microscope. *Journal of Colloid and Interface Science* 228, 428-433.
- Bowen, W. R., Lovitt, R. W., and Wright, C. J. (2000b). Direct quantification of *Aspergillus niger* spore adhesion to mica in air using an atomic force microscope. *Colloids and Surfaces a-Physicochemical and Engineering Aspects* 173, 205-210.
- Brantley, S. L., Liermann, L., and Bau, M. (2001). Uptake of trace metals and rare earth elements from hornblende by a soil bacterium. *Geomicrobiology Journal* 18, 37-61.
- Burnham, N. A., Dominguez, D. D., Mowery, R. L., and Colton, R. J. (1990). Probing the surface forces of monolayer films with an atomic-force microscope. *Physical Review Letters* 64, 1931-4.
- Bustamante, C., Marko, J. F., Siggia, E. D., and Smith, S. (1994). Entropic elasticity of lambda-phage DNA. *Science* 265, 1599-1600.
- Butt, H. J., and Jaschke, M. (1995). Calculation of Thermal Noise in Atomic-Force Microscopy. 6, 1-7.
- Butt, H. J., Jaschke, M., and Ducker, W. (1995). Measuring surface forces in aqueous electrolyte solution with the atomic force microscope. *Bioelectrochemistry and Bioenergetics* 38, 191-201.
- Caccavo, F. (1999). Protein-mediated adhesion of the dissimilatory Fe(III)-reducing bacterium *Shewanella alga* BrY to hydrous ferric oxide. *Applied and Environmental Microbiology* 65, 5017-5022.
- Caccavo, F., Jr., Schamberger, P. C., Keiding, K., and Nielsen, P. H. (1997). Role of hydrophobicity in adhesion of the dissimilatory Fe(III)-reducing bacterium *Shewanella alga* to amorphous Fe(III) oxide. *Applied and Environmental Microbiology* 62, 3837-3843.
- Camesano, T. A., and Logan, B. E. (2000). Probing bacterial electrosteric interactions using atomic force microscopy. *Environmental Science & Technology* 34, 3354-3362.
- Cappella, B., Baschieri, P., Frediani, C., Miccoli, P., and Ascoli, C. (1997). Force-distance curves by AFM: A powerful technique for studying surface interactions. *IEEE Engineering In Medicine And Biology Magazine* 16, 58-65.
- Cappella, B., and Dietler, G. (1999). Force-distance curves by atomic force microscopy. *Surface Science Reports* 34, 1-104.
- Cherian, S., and Thundat, T. (2002). Determination of adsorption-induced variation in the spring constant of a microcantilever. *Applied Physics Letters* 80, 2219-2221.
- Cheung, C. L., Hafner, J. H., Chen, L. W., and Lieber, C. M. (2000). Direct growth of single-walled carbon nanotube scanning probe microscopy tips and application to ultrahigh-resolution chemical force microscopy and structural imaging. 219, 182-PHYS.
- Chilkoti, A., Boland, T., Ratner, B. D., and Stayton, P. S. (1995). The relationship between ligand-binding thermodynamics and protein-ligand interaction forces measured by atomic force microscopy. *Biophysical Journal* 69, 2125-30.

- Cleveland, J. P., Manne, S., Bocek, D., and Hansma, P. K. (1993). A nondestructive method for determining the spring constant of cantilevers for scanning force microscopy. *Review of Scientific Instruments* 64, 403-405.
- Cocozza, C., Tsao, C. C. G., Cheah, S. F., Kraemer, S. M., Raymond, K. N., Miano, T. M., and Sposito, G. (2002). Temperature dependence of goethite dissolution promoted by trihydroxamate siderophores. 66, 431-438.
- Cornell, R. M., and Schwertmann, U. (1996). "The Iron Oxides: Structure, Properties, Reactions, Occurrence and Uses," VCH.
- Craig, V. S. J., and Neto, C. (2001). In Situ Calibration of Colloid Probe Cantilevers in Force Microscopy: Hydrodynamic Drag on a Sphere Approaching a Wall. *Langmuir* 17, 6018-6022.
- Cygan, R. T. (2001). Molecular Modeling in Mineralogy and Geochemistry. In "Molecular Modeling Theory: Applications in the Geosciences" (J. D. Kubicki, ed.), Vol. 42, pp. 531. Mineralogical Society of America Geochemical Society, Washington D.C.
- Dammer, U., Hegner, M., Anselmetti, D., Wagner, P., Dreier, M., Huber, W., and Guentherodt, H. J. (1996). Specific antigen/antibody interactions measured by force microscopy. *Biophys. J.* 70, 2437-2441.
- Dammer, U., Popescu, O., Wagner, P., Anselmetti, D., Guntherodt, H. J., and Misevic, G. N. (1995). Binding Strength Between Cell-Adhesion Proteoglycans Measured By Atomic-Force Microscopy. *Science* 267, 1173-1175.
- Das, A., and Caccavo, F. (2000). Dissimilatory Fe(III) oxide reduction by *Shewannella alga* BrY requires adhesion. *Current Microbiology* 40, 344-347.
- Davies, D. G., Parsek, M. R., Pearson, J. P., Iglewski, B. H., Costerton, J. W., and Greenberg, E. P. (1998). The involvement of cell-to-cell signals in the development of a bacterial biofilm. *Science* 280, 295-298.
- D'Costa, N. P., and Hoh, J. H. (1995). Calibration of optical lever sensitivity for atomic force microscopy. *Review of Scientific Instruments* 66, 5096-5097.
- Degertekin, F. L., Hadimioglu, B., Sulchek, T., and Quate, C. F. (2001). Actuation and characterization of atomic force microscope cantilevers in fluids by acoustic radiation pressure. *Appl. Phys. Lett.* 78, 1628-1630.
- Derjaguin, B. V., and Landau, L. (1941). *Acta Physiochim URSS* 14, 633.
- Derjaguin, B. V., Muller, V. M., and Toporov, Y. P. (1975). *Journal of Colloid and Interface Science* 53.
- DiChristina, T. J., and Delong, E. F. (1994). Isolation of anaerobic respiratory mutants of *Shewanella putrefaciens* and genetic analysis of mutants deficient in anaerobic growth on  $\text{Fe}^{3+}$ . *Journal of Bacteriology* 176, 1468-1474.
- Ducker, W. A., Senden, T. J., and Pashley, R. M. (1991). Direct measurement of colloidal forces using an atomic force microscope. *Nature* 353, 239-241.
- Ducker, W. A., Senden, T. J., and Pashley, R. M. (1992). Measurement of forces in liquids using a force microscope. *Langmuir* 8, 1831-6.
- Dziurla, M., -A., Achouak, W., Lam, B., -T., Heulin, T., and Berthelin, J. (1998). Enzyme-linked immunofiltration assay to estimate attachment of *Thiobacilli* to pyrite. *Applied and Environmental Microbiology* 64, 2937-2942.

- Edwards, K. J., Schrenk, M. O., Hamers, R., and Banfield, J. F. (1998). Microbial oxidation of pyrite: Experiments using microorganisms from an extreme acidic environment. *American Mineralogist* 83, 1444-1453.
- Egger, M., Heyn, S.-P., and Gaub, H. E. (1992). Synthetic lipid-anchored receptors based on the binding site of a monoclonal antibody. *Biochimica et Biophysica Acta* 1104, 45-54.
- Erlandsson, R., McClelland, G. M., Mate, C. M., and Chiang, S. (1988). Atomic force microscopy using optical interferometry. *Journal of Vacuum Science & Technology, A: Vacuum, Surfaces, and Films* 6, 266-70.
- Evans, E. (1998). Energy landscapes of biomolecular adhesion and receptor anchoring at interfaces explored with dynamic force spectroscopy. 1-16.
- Evans, E. (2001). Probing the relation between force-lifetime-and chemistry in single molecular bonds. *Annual Review of Biophysics and Biomolecular Structure* 30, 105-128.
- Evans, E., and Ludwig, F. (2000). Dynamic strengths of molecular anchoring and material cohesion in fluid biomembranes. *Journal of Physics: Condensed Matter* 12, A315-A320.
- Evans, E., and Ritchie, K. (1997). Dynamic strength of molecular adhesion bonds. 72, 1541-1555.
- Fiorini, M., McKendry, R., Cooper, M. A., Rayment, T., and Abell, C. (2001). Chemical force microscopy with active enzymes. *Biophysical Journal* 80, 2471-2476.
- Fleminger, G., and Shabtai, Y. (1995). Direct and rapid analysis of the adhesion of bacteria to solid surfaces: Interaction of fluorescently labeled *Rhodococcus* strain GIN-1 (NCIMB 40340) cells with titanium-rich particles. *Applied and Environmental Microbiology* 61, 4357-4361.
- Fletcher, M., ed. (1996). "Bacterial Adhesion: Molecular and Ecological Diversity." Wiley-Liss, New York.
- Florin, E. L., Moy, V. T., and Gaub, H. E. (1994). Adhesion Forces Between Individual Ligand-Receptor Pairs. *Science* 264, 415-417.
- Flory, P. J. (1989). "Statistical Mechanics of Chain Molecules," Hanser Publishers, Munich.
- Fortin, D., Ferris, F. G., and Beveridge, T. J. (1997). Surface-mediated mineral development by bacteria. In "Geomicrobiology: Interactions between Microbes and Minerals" (K. H. Nealson, ed.), Vol. 35, pp. 161-180. Mineralogical Society of America, Washington D. C.
- Frisbie, C. D., Rozsnyai, L. F., Noy, A., Wrigton, M. S., and Lieber, C. M. (1994). Functional-Group Imaging By Chemical Force Microscopy. *Science* 265, 2071-2074.
- Gay, C., and Leibler, L. (1999). On stickiness. *Physics Today* 52, 48-52.
- Gergely, C., Hemmerle, J., Schaaf, P., Horber, J. K. H., Voegel, J.-C., and Senger, B. (2002). Multi-bead-and-spring model to interpret protein detachment studied by AFM force spectroscopy. *Biophysical Journal* 83, 706-722.
- Gergely, C., Senger, B., Voegel, J. C., Horber, J. K. H., Schaaf, P., and Hemmerle, J. (2001). Semi-automatized processing of AFM force-spectroscopy data. *Ultramicroscopy* 87, 67-78.
- Gibson, C. T., Weeks, B. L., Lee, J. R. I., Abell, C., and Rayment, T. (2001). A nondestructive technique for determining the spring constant of atomic force microscope cantilevers. *Review of Scientific Instruments* 72, 2340-2343.
- Goddenhenrich, T., Lemke, H., Hartmann, U., and Heiden, C. (1990). Force microscope with capacitive displacement detection. *Journal of Vacuum Science & Technology, A: Vacuum, Surfaces, and Films* 8, 383-387.



- Grabarek, Z., and Gergely, J. (1990). Zero-length crosslinking procedure with the use of active esters. *Anal. Biochem.* 185, 131-5.
- Grandbois, M., Beyer, M., Rief, M., Clausen-Schaumann, H., and Gaub, H. E. (1999). How strong is a covalent bond? *Science* 283, 1727-1730.
- Grubmuller, H., Heymann, B., and Tavan, P. (1996). Ligand binding: molecular mechanics calculation of the streptavidin-biotin rupture force. *Science* 271, 997-999.
- Hafner, J. H., Cheung, C. L., and Lieber, C. M. (1999). Growth of nanotubes for probe microscopy tips. 398, 761-762.
- Hafner, J. H., Cheung, C. L., Woolley, A. T., and Lieber, C. M. (2001). Structural and functional imaging with carbon nanotube AFM probes. 77, 73-110.
- Han, T., Williams, J. M., and Beebe, T. P. (1995). Chemical-Bonds Studied with Functionalized Atomic-Force Microscopy Tips. 307, 365-376.
- Hansen, D. C., McCafferty, E., Lins, C. W., and Fitzpatrick, J. J. (1995). An FT-IR investigation of parabactin adsorbed onto aluminum. *Appl. Surf. Sci.* 84, 85-90.
- Hartmann, U. (1991). van der Waals interactions between sharp probes and flat sample surfaces. *Physical Review B* 43, 2404-2407.
- Heinz, W. F., and Hoh, J. H. (1999). Spatially resolved force spectroscopy of biological surfaces using the atomic force microscope. *Trends in Biotechnology* 17, 143-150.
- Hersman, L., Lloyd, T., and Sposito, G. (1995). Siderophore-promoted dissolution of hematite. *Geochimica et Cosmochimica Acta* 59, 3327-3330.
- Hersman, L. E. (2000). The role of siderophores in iron oxide dissolution. In "Environmental microbe-metal interactions" (D. R. Lovley, ed.), pp. 395. ASM Press, Washington D.C.
- Hiebert, F. K., and Bennett, P. C. (1992). Microbial control of silicate weathering in organic-rich ground water. *Science* 258, 278-281.
- Hinterdorfer, P., Baumgartner, W., Gruber, H. J., Schilcher, K., and Schindler, H. (1996). Detection and localization of individual antibody-antigen recognition events by atomic force microscopy. *Proc. Natl. Acad. Sci. U. S. A.* 93, 3477-81.
- Hinterdorfer, P., Gruber, H. J., Kienberger, F., Kada, G., Riener, C., Borken, C., and Schindler, H. (2002). Surface attachment of ligands and receptors for molecular recognition force microscopy. *Colloids and Surfaces, B: Biointerfaces* 23, 115-123.
- Holmen, B. A., and Casey, W. H. (1996). Hydroxamate ligands, surface chemistry, and the mechanism of ligand-promoted dissolution of goethite [ $\alpha$ -FeOOH(s)]. *Geochimica et Cosmochimica Acta* 22, 4403-4416.
- Holmen, B. A., Tejedor-Tejedor, M. I., and Casey, W. H. (1997). Hydroxamate Complexes in Solution and at the Goethite-Water Interface: A Cylindrical Internal Reflection Fourier Transform Infrared Spectroscopy Study. *Langmuir* 13, 2197-2206.
- Hutter, J. L., and Bechhoefer, J. (1993). Calibration of atomic-force microscope tips. *Review of Scientific Instruments* 64, 1868-73.
- Israelachvili, J. N. (1992). "Intermolecular and Surface Forces," 2nd/Ed. Academic Press, San Diego.
- Israelachvili, J. N., and McGuiggan, P. M. (1988). Forces between surfaces in liquids. *Science* 241, 795-800.

- Ito, T., Citterio, D., Buehlmann, P., and Umezawa, Y. (1999). Observation of Silver and Hydrogen Ion Binding to Self-Assembled Monolayers Using Chemically Modified AFM Tips. *Langmuir* 15, 2788-2793.
- Izrailev, S., Stepaniants, S., Balsera, M., Oono, Y., and Schulten, K. (1997). Molecular dynamics study of unbinding of the avidin-biotin complex. *Biophysical Journal* 72, 1568-1581.
- Jarvis, S. P., Duerig, U., Lantz, M. A., Yamada, H., and Tokumoto, H. (1998). Feedback-stabilized force sensors. A gateway to the direct measurement of interaction potentials. *Applied Physics A: Materials Science & Processing* A66, S211-S213.
- Jarvis, S. P., Yamada, H., Yamamoto, S. I., Tokumoto, H., and Pethica, J. B. (1996). Direct mechanical measurement of interatomic potentials. *Nature (London)* 384, 247-249.
- Jeppesen, C., Wong, J. Y., Kuhl, T. L., Israelachvili, J., Mullah, J. N., Zalipsky, S., and Marques, C. M. (2001). Impact of polymer tether length on multiple ligand-receptor bond formation. *Science* 293, 465-468.
- Jericho, S. K., and Jericho, M. H. (2002). Device for the determination of spring constants of atomic force microscope cantilevers and micromachined springs. *Review of Scientific Instruments* 73, 2483-2485.
- Johnson, K. L., Kendall, K., and Roberts, A. D. (1971). Surface energy and the contact of elastic solids. *Proceedings of the Royal Society of London A* 324, 301-313.
- Joyce, S. A., and Houston, J. E. (1991). A new force sensor incorporating force-feedback control for interfacial force microscopy. *Review of Scientific Instruments* 62, 710-15.
- Kalinowski, B. E., Liermann, L. J., Brantley, S. L., Barnes, A., and Pantano, C. G. (2000). X-ray photoelectron evidence for bacteria-enhanced dissolution of hornblende. *Geochimica Et Cosmochimica Acta* 64, 1331-1343.
- Karlsson, J.-J., Kadziola, A., Rasmussen, A., Rostrup, T. E., and Ulstrup, J. (1996). Electron transfer of the di-heme protein: *Pseudomonas stutzeri* cytochrome *c*<sub>4</sub>. In "Protein Folds: A Distance-Based Approach" (S. Brunak, ed.), pp. 56-67. CRC Press, Boca Raton.
- Kasas, S., Riederer, B. M., Catsicas, S., Cappella, B., and Dietler, G. (2000). Fuzzy logic algorithm to extract specific interaction forces from atomic force microscopy data. *Review of Scientific Instruments* 71, 2082-2086.
- Kendall, K. (1994). Adhesion: Molecules and mechanics. *Science* 263, 1720-1725.
- Kendall, T. A., and Hochella, M. F., Jr. (2003). The measurement and interpretation of molecular level forces of interaction between the siderophore azotobactin and mineral surfaces. *Geochimica et Cosmochimica Acta*.
- Kienberger, F., Kada, G., Gruber, H. J., Pastushenko, V. P., Riener, C., Trieb, M., Knaus, H.-G., Schindler, H., and Hinterdorfer, P. (2000). Recognition force spectroscopy studies of the NTA-His6 bond. *Single Molecules* 1, 59-65.
- Kosmulski, M. (2001). "Chemical properties of material surfaces," Marcel Dekker, New York.
- Kraemer, S. M., Cheah, S. F., Zapf, R., Xu, J. D., Raymond, K. N., and Sposito, G. (1999). Effect of hydroxamate siderophores on Fe release and Pb(II) adsorption by goethite. *Geochimica Et Cosmochimica Acta* 63, 3003-3008.
- Kraemer, S. M., Xu, J. D., Raymond, K. N., and Sposito, G. (2002). Adsorption of Pb(II) and Eu(III) by oxide minerals in the presence of natural and synthetic hydroxamate siderophores. *Environmental Science & Technology* 36, 1287-1291.

- Kreller, D. I., Gibson, G., vanLoon, G. W., and Horton, J. H. (2002). Chemical Force Microscopy Investigation of Phosphate Adsorption on the Surfaces of Iron(III) Oxyhydroxide Particles. *Journal of Colloid and Interface Science* 254, 205-213.
- Kummert, R., and Stumm, W. (1980). The surface complexation of organic acids on hydrous .gamma.-alumina. *J. Colloid Interface Sci.* 75, 373-85.
- Lawrence, J. R., Korber, D. R., Hoyle, B. D., Costerton, J. W., and Caldwell, D. E. (1991). Optical sectioning of microbial biofilms. *Journal of Bacteriology* 173, 6558-6567.
- Leckband, D., and Israelachvili, J. (2001). Intermolecular forces in biology. *Quarterly Reviews of Biophysics* 34, 105-267.
- Lee, G. U., Chrisey, L. A., and Colton, R. J. (1994a). Direct Measurement of the Forces Between Complementary Strands of Dna. *Science* 266, 771-773.
- Lee, G. U., Kidwell, D. A., and Colton, R. J. (1994b). Sensing Discrete Streptavidin-Biotin Interactions with Atomic Force Microscopy. *Langmuir* 10, 354-7.
- Liermann, L. J., Kalinowski, B. E., Brantley, S. L., and Ferry, J. G. (2000). Role of bacterial siderophores in dissolution of hornblende. *Geochimica Et Cosmochimica Acta* 64, 587-602.
- Lo, Y. S., Huefner, N. D., Chan, W. S., Stevens, F., Harris, J. M., and Beebe, T. P. (1999). Specific interactions between biotin and avidin studied by atomic force microscopy using the Poisson statistical analysis method. 15, 1373-1382.
- Lo, Y. S., Simons, J., and Beebe, T. P. (2002). Temperature dependence of the biotin-avidin bond-rupture force studied by atomic force microscopy. 106, 9847-9852.
- Lower, S. K., Hochella, M. F., and Beveridge, T. J. (2001a). Bacterial recognition of mineral surfaces: Nanoscale interactions between *Shewanella* and  $\alpha$ -FeOOH. *Science* 292, 1360-1363.
- Lower, S. K., Hochella, M. F., Jr., Banfield, J. F., and Rosso, K. (2002). Nanogeoscience: From the movement of electrons to lithosphere plates. *Eos: Transactions of the American Geophysical Union* 83, 53-56.
- Lower, S. K., Tadanier, C. J., and Hochella, M. F. (2000). Measuring interfacial and adhesion forces between bacteria and mineral surfaces with biological force microscopy. *Geochimica Et Cosmochimica Acta* 64, 3133-3139.
- Lower, S. K., Tadanier, C. J., and Hochella, M. F. (2001b). Dynamics of the mineral-microbe interface: Use of biological force microscopy in biogeochemistry and geomicrobiology. *Geomicrobiology Journal* 18, 63-76.
- Ludwig, C., Casey, W. H., and Rock, P. A. (1995). Prediction of ligand-promoted dissolution rates from the reactivities of aqueous complexes. *Nature (London)* 375, 44-7.
- Maeda, N., and Senden, T. J. (2000). A Method for the Calibration of Force Microscopy Cantilevers via Hydrodynamic Drag. *Langmuir* 16, 9282-9286.
- Marszalek, P. E., Oberhauser, A. F., Pang, Y.-P., and Fernandez, J. M. (1998). Polysaccharide elasticity governed by chair-boat transitions of the glucopyranose ring. *Nature (London)* 396, 661-664.
- Maurice, P. A., Lee, Y. J., and Hersman, L. E. (2000). Dissolution of Al-substituted goethites by an aerobic *Pseudomonas mendocina* var. bacteria. *Geochimica Et Cosmochimica Acta* 64, 1363-1374.
- Mazzola, L. T., Frank, C. W., Fodor, S. P. A., Mosher, C., Lartius, R., and Henderson, E. (1999). Discrimination of DNA hybridization using chemical force microscopy. *Biophysical Journal* 76, 2922-2933.

- Merkel, R., Nassoy, P., Leung, A., Ritchie, K., and Evans, E. (1999). Energy landscapes of receptor-ligand bonds explored with dynamic force spectroscopy. *Nature* 397, 50-53.
- Meyer, G., and Amer, N. M. (1990). Simultaneous measurement of lateral and normal forces with an optical-beam-deflection atomic force microscope. *Applied Physics Letters* 57, 2089-91.
- Moy, V. T., Florin, E. L., and Gaub, H. E. (1994a). Intermolecular forces and energies between ligands and receptors. *Science* 266, 257-9.
- Moy, V. T., Florin, E.-L., and Gaub, H. E. (1994b). Adhesive forces between ligand and receptor measured by AFM. *Colloids and Surfaces, A: Physicochemical and Engineering Aspects* 93, 343-8.
- Muller, D. J., Baumeister, W., and Engel, A. (1999). Controlled unzipping of a bacterial surface layer with atomic force microscopy. *Proceedings of the National Academy of Sciences of the United States of America* 96, 13170-13174.
- Muller, D. J., and Engel, A. (1997). The height of biomolecules measured with the atomic force microscope depends on electrostatic interactions. *Biophysical Journal* 73, 1633-1644.
- Myers, C. R., and Myers, J. M. (1992). Localization of cytochromes to the outer membrane of anaerobically grown *Shewanella Putrefaciens* MR-1. *Journal of Bacteriology* 174, 3429-3438.
- Myers, C. R., and Myers, J. M. (1993). Ferric reductase is associated with the membranes of anaerobically grown *Shewanella putrefaciens* MR-1. *Fems Microbiology Letters* 108, 15-22.
- Myers, C. R., and Myers, J. M. (1997). Outer membrane cytochromes of *Shewanella putrefaciens* MR-1: Spectral analysis, and purification of the 83-kDa *c*-type cytochrome. *Biochimica et Biophysica Acta* 1326, 307-318.
- Myers, C. R., and Nealson, K. H. (1988). Bacterial manganese reduction and growth with manganese oxide as the sole electron acceptor. *Science* 240, 1319-1321.
- Myers, C. R., and Nealson, K. H. (1990). Respiration-linked proton translocation coupled to anaerobic reduction of manganese(IV) and iron(III) in *Shewanella putrefaciens* MR-1. *Journal of Bacteriology* 172, 6232-6238.
- Myers, J. M., and Myers, C. R. (1998). Isolation and sequence of *omcA*, a gene encoding a decaheme outer membrane cytochrome *c* of *Shewanella putrefaciens* MR-1, and detection of *omcA* homologs in other strains of *S. putrefaciens*. *Biochimica et Biophysica Acta* 1373, 237-251.
- Myers, J. M., and Myers, C. R. (2000). Role of the tetraheme cytochrome CymA in anaerobic electron transport in cells of *Shewanella putrefaciens* MR-1 with normal levels of menaquinone. *Journal of Bacteriology* 182, 67-75.
- Myers, J. M., and Myers, C. R. (2001). Role for outer membrane cytochromes OmcA and OmcB of *Shewanella putrefaciens* MR-1 in reduction of manganese dioxide. *Applied and Environmental Microbiology* 67, 260-269.
- Myers, J. M., and Myers, C. R. (2002). Genetic complementation of an outer membrane cytochrome *omcB* mutant of *Shewanella putrefaciens* MR-1 requires *omcB* plus downstream DNA. *Applied and Environmental Microbiology* 68, 2781-2793.
- Nealson, K. H., and Saffarini, D. (1994). Iron and manganese in anaerobic respiration: Environmental significance, physiology, and regulation. *Annual Review of Microbiology* 48, 311-343.

- Neubauer, U., Nowack, B., Furrer, G., and Schulin, R. (2000). Heavy metal sorption on clay minerals affected by the siderophore desferrioxamine B. *Environmental Science & Technology* 34, 2749-2755.
- Noy, A., Vezenov, D. V., and Lieber, C. M. (1997). Chemical force microscopy. *Annual Review of Materials Science* 27, 381-421.
- Nubel, U., Engelen, B., Felske, A., Snaidr, J., Wieshuber, A., Amann, R. I., Ludwig, W., and Backhaus, H. (1996). Sequence heterogeneities of genes encoding 16S rRNAs in *Paenibacillus polymyxa* detected by temperature gradient gel electrophoresis. *Journal of Bacteriology* 178, 5636-5643.
- Ohmura, N., Kitamura, K., and Saiki, H. (1993). Selective adhesion of *Thiobacillus ferrooxidans* to pyrite. *Applied and Environmental Microbiology* 59, 4044-4050.
- Ong, Y.-L., Razatos, A., Georgiou, G., and Sharma, M. M. (1999). Adhesion forces between *E. coli* bacteria and biomaterial surfaces. *Langmuir* 15, 2719-2725.
- Oreskes, N., Shrader-Frechette, K., and Belitz, K. (1994). Verification, validation, and confirmation of numerical models in the Earth Sciences. *Science* 263, 641-646.
- Pleuddemann, E. P. (1991). "Silane Coupling Agents," Plenum Press, New York.
- Rabinovich, Y. I., and Yoon, R. H. (1994). Use of Atomic Force Microscope for the Measurements of Hydrophobic Forces between Silanated Silica Plate and Glass Sphere. *Langmuir* 10, 1903-9.
- Razatos, A., Ong, Y. L., Sharma, M. M., and Georgiou, G. (1998a). Evaluating the interaction of bacteria with biomaterials using atomic force microscopy. *Journal of Biomaterial Science and Polymer Education* 9, 1361-1373.
- Razatos, A., Ong, Y.-L., Sharma, M. M., and Georgiou, G. (1998b). Molecular determinants of bacterial adhesion monitored by atomic force microscopy. *Proceedings of the National Academy of Sciences USA* 95, 11059-11064.
- Rezania, A., Johnson, R., Lefkow, A., and Healy, K. E. (1999). Bioactivation of metal oxide surfaces. 1. Surface characterization and cell response. *Langmuir* 15, 6931-6939.
- Rief, M., Gautel, M., Oesterhelt, F., Fernandez, J. M., and Gaub, H. E. (1997a). Reversible unfolding of individual titin immunoglobulin domains by AFM. *Science (Washington, D. C.)* 276, 1109-1112.
- Rief, M., Oesterhelt, F., Heymann, B., and Gaub, H. E. (1997b). Single molecule force spectroscopy on polysaccharides by atomic force microscopy. *Science (Washington, D. C.)* 275, 1295-1297.
- Roden, E. E., and Zachara, J. M. (1996). Microbial reduction of crystalline iron(III) oxides: Influence of oxide surface area and potential for cell growth. *Environmental Science & Technology* 30, 1618-1628.
- Rugar, D., Mamin, H. J., and Guethner, P. (1989). Improved fiber-optic interferometer for atomic force microscopy. *Applied Physics Letters* 55, 2588-90.
- Ryan, J. N., and Elimelech, M. (1996). Colloid mobilization and transport in groundwater. *Colloids and Surfaces a-Physicochemical and Engineering Aspects* 107, 1-56.
- Ryan, J. N., and Gschwend, P. M. (1994). Effects of Ionic-Strength and Flow-Rate on Colloid Release - Relating Kinetics to Intersurface Potential-Energy. 164, 21-34.
- Sader, J. E. (1998). Frequency response of cantilever beams immersed in viscous fluids with applications to the atomic force microscope. *J. Appl. Phys.* 84, 64-76.

- Sader, J. E., Chon, J. W. M., and Mulvaney, P. (1999). Calibration of rectangular atomic force microscope cantilevers. *Rev. Sci. Instrum.* 70, 3967-3969.
- Sader, J. E., Larson, I., Mulvaney, P., and White, L. R. (1995). Method for the calibration of atomic force microscope cantilevers. *Review of Scientific Instruments* 66, 3789-98.
- Sader, J. E., and White, L. (1993). Theoretical analysis of the static deflection of plates for atomic force microscope applications. *Journal of Applied Physics* 74, 1-9.
- Schmitt, L., Ludwig, M., Gaub, H. E., and Tampe, R. (2000). A metal-chelating microscopy tip as a new toolbox for single-molecule experiments by atomic force microscopy. *Biophysical Journal* 78, 3275-3285.
- Schultze-Lam, S., Harauz, G., and Beveridge, T. J. (1992). Participation of a cyanobacterial S-layer in fine-grain mineral formation. *Journal of Bacteriology* 174, 7971-7981.
- Schwesinger, F., Ros, R., Strunz, T., Anselmetti, D., Guntherodt, H. J., Honegger, A., Jermutus, L., Tiefenauer, L., and Pluckthun, A. (2000). Unbinding forces of single antibody-antigen complexes correlate with their thermal dissociation rates. *Proceedings of the National Academy of Sciences of the United States of America* 97, 9972-7.
- Seaman, J. C., Alexander, D. B., Loeppert, R. H., and Zuberer, D. A. (1992). The Availability of Iron From Various Solid-Phase Iron Sources to a Siderophore Producing Pseudomonas Strain. *Journal of Plant Nutrition* 15, 2221-2233.
- Sposito, G. (1989). "The Chemistry of Soils," Oxford University Press, New York.
- Stevens, F., Lo, Y. S., Harris, J. M., and Beebe, T. P. (1999). Computer modeling of atomic force microscopy force measurements: Comparisons of Poisson, histogram, and continuum methods. 15, 207-213.
- Stone, A. T. (1997). Reactions of extracellular organic ligands with dissolved metal ions and mineral surface. In "Geomicrobiology: Interactions Between Microbes and Minerals." (K. H. Nealson, ed.), Vol. 35, pp. 309-341. Mineralogical Society of America, Washington D. C.
- Strunz, T., Oroszlan, K., Schafer, R., and Guntherodt, H.-J. (1999). Dynamic force spectroscopy of single DNA molecules. *Proceedings of the National Academy of Sciences of the United States of America* 96, 11277-11282.
- Stumm, W. (1992). "Chemistry of the Solid-Water Interface," John Wiley & Sons, Inc., New York.
- Swamy, M. J. (1995). Thermodynamic analysis of biotin binding to avidin. A high sensitivity titration calorimetric study. *Biochemistry and Molecular Biology International* 36, 219-25.
- Telford, J. R., and Raymond, K. N. (1996). Siderophores. *Comprehensive Supramolecular Chemistry* 1, 245-266.
- Toikka, G., Hayes, R. A., and Ralston, J. (1996). Surface forces between spherical ZnS particles in aqueous electrolyte. 12, 3783-3788.
- Tokunaga, M., Aoki, T., Hiroshima, M., Kitamura, K., and Yanagida, T. (1997). Subpiconewton intermolecular force microscopy. *Biochemical and Biophysical Research Communications* 231, 566-569.
- Torii, A., Sasaki, M., Hane, K., and Okuma, S. (1996). A method for determining the spring constant of cantilevers for atomic force microscopy. *Meas. Sci. Technol.* 7, 179-84.
- van Loosdrecht, M. C. M., Lyklema, J., Norde, W., and Zehnder, A. J. B. (1989). Bacterial adhesion: A physicochemical approach. *Microbial Ecology* 17, 1-15.

- van Oss, C. J. (1993). Acid-base interfacial interactions in aqueous media. *Colloids and Surfaces A: Physicochemical and Engineering Aspects* 78, 1-49.
- Verwey, E. J., and Overbeek, J. T. G. (1948). "Theory of the Stability of Lyophobic Colloids," Elsevier Publishing, Amsterdam.
- Vigeant, M. A.-S., Ford, R. M., Wagner, M., and Tamm, L. K. (2002). Reversible and irreversible adhesion of motile *Escherichia coli* cells analyzed by total internal reflection aqueous fluorescence microscopy. *Applied and Environmental Microbiology* 68, 2794-2801.
- Voet, D., and Voet, J. (1995). "Biochemistry," Second/Ed. John Wiley & Sons, New York.
- Wagner, P. (1998). Immobilization strategies for biological scanning probe microscopy. *FEBS Letters* 430, 112-115.
- Watteau, F., and Berthelin, J. (1994). Microbial Dissolution of Iron and Aluminum From Soil Minerals - Efficiency and Specificity of Hydroxamate Siderophores Compared to Aliphatic Acids. *European Journal of Soil Biology* 30, 1-9.
- Weisenhorn, A. L., Maivald, P., Butt, H. J., and Hansma, P. K. (1992). Measuring Adhesion, Attraction, and Repulsion Between Surfaces in Liquids With an Atomic-Force Microscope. *Physical Review B* 45, 11226-11232.
- Wenzler, L. A., Moyes, G. L., Olson, L. G., Harris, J. M., and Beebe, T. P. (1997). Single molecule bond-rupture force analysis of interactions between AFM tips and substrates modified with organosilanes. 69, 2855-2861.
- Whitman, W. B., Coleman, D. C., and Wiebe, W. J. (1998). Prokaryotes: The unseen majority. *Proceedings of the National Academy of Sciences of the United States of America* 95, 6578-6583.
- Williams, J. M., Han, T. J., and Beebe, T. P. (1996). Determination of single-bond forces from contact force variances in atomic force microscopy. 12, 1291-1295.
- Winkelmann, G., ed. (1991). "CRC Handbook of Microbial Iron Chelates." CRC Press, Boca Raton, Florida.
- Wong, J., Chilkoti, A., and Moy, V. T. (1999). Direct force measurements of the streptavidin-biotin interaction. *Biomolecular Engineering* 16, 45-55.
- Wong, S. S., Joselevich, E., Woolley, A. T., Cheung, C. L., and Lieber, C. M. (1998a). Covalently functionalized nanotubes as nanometre-sized probes in chemistry and biology. *Nature* 394, 52-55.
- Wong, S. S., Woolley, A. T., Joselevich, E., Cheung, C. L., and Lieber, C. M. (1998b). Covalently-functionalized single-walled carbon nanotube probe tips for chemical force microscopy. 120, 8557-8558.
- Yamamoto, S.-i., Yamada, H., and Tokumoto, H. (1997). Precise force curve detection system with a cantilever controlled by magnetic force feedback. *Review of Scientific Instruments* 68, 4132-4136.
- Yao, H.-L., and Yeh, H.-H. (1996). Fumarate, Maleate, and Succinate Adsorption on Hydrous .delta.-Al<sub>2</sub>O<sub>3</sub>. 1. Comparison of the Adsorption Maxima and Their Significance. *Langmuir* 12, 2981-2988.

## TABLE

Table A. 1 Summary of physical forces of interaction between particles and/or surfaces.\*

Type of interaction	Description
van der Waals	<b>force between all particles due to polarization; usually attractive; short range</b>
electrostatic	force between charged particles; attractive (for particles of opposite sign) or repulsive (for particles of similar sign); depends upon ionic strength of solution; short to long range
solvation	structural or hydration forces are typically repulsive due to sorbed water layers; short range
	hydrophobic force is attractive between nonpolar surfaces; short to long range
steric	typically a short range, repulsive force associated with polymers; may be longer range, attractive force for “bridging” polymers

*\*This review has followed the force characterization of Israelachvili (1988). Other force classes, such as hydrogen bonding or thermal fluctuations, may dominate when two particles or surfaces are very close. However, these other classes can often be described as a subset of electrostatic (for hydrogen bonding) or steric (for thermal fluctuations) interactions, according to Leckband and Israelachvili (2001). So-called specific interactions (e.g., ligand-receptor) interactions are typically a result of unique combinations of these four “non specific” physical forces (Israelachvili, 1992).*



## FIGURES

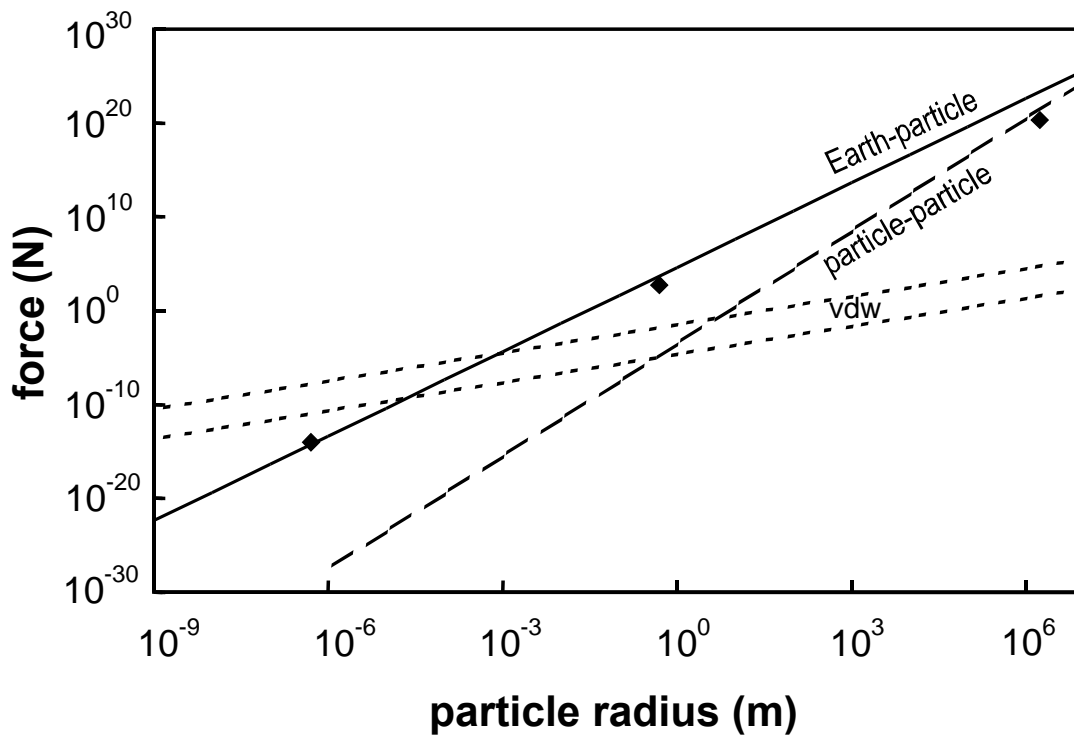


Figure A. 1 Log-log plot of the theoretical forces describing (1) gravitational attraction between a particle and the Earth (solid “Earth-particle” line), (2) gravitational attraction between two particles of the same size (dashed “particle-particle” line), and (3) van der Waals attraction between two particles of the same size (dashed “vdw” lines). In all instances the particles are assumed to be in “contact” with the Earth (for 1) or another particle (for 2 and 3). For gravitational attraction, mass was determined by assuming each particle was a solid homogeneous sphere with a density of  $1 \text{ g cm}^{-3}$ , and contact was defined as the radius of the Earth ( $\sim 6.4 \times 10^6 \text{ m}$  radius; “Earth-particle” interaction) or the sum of the radii of two interacting particles (“particle-particle” interaction). The shaded region outlines the boundaries of the expected van der Waals force using values for Hamaker constant of  $10^{-20}$  to  $10^{-21} \text{ J}$ , which is appropriate for biological and inorganic phases (Israelachvili, 1992; Leckband and Israelachvili, 2001; Vigeant et al., 2002), and defining “contact” as an effective separation between particles of  $\sim 0.2$  (for one hydration layer) to  $2 \text{ nm}$ , according to (Israelachvili, 1992; Leckband and Israelachvili, 2001). Only the magnitudes of the forces are shown. By convention, attractive forces (shown here) are negative. For reference, the three diamond symbols represent gravitational forces between the Earth ( $\sim 10^{24} \text{ kg}$ ) and each of three bodies (from left to right): a bacterium ( $10^{-15} \text{ kg}$ ), a human ( $50 \text{ kg}$ ), or the moon ( $10^{22} \text{ kg}$ ).

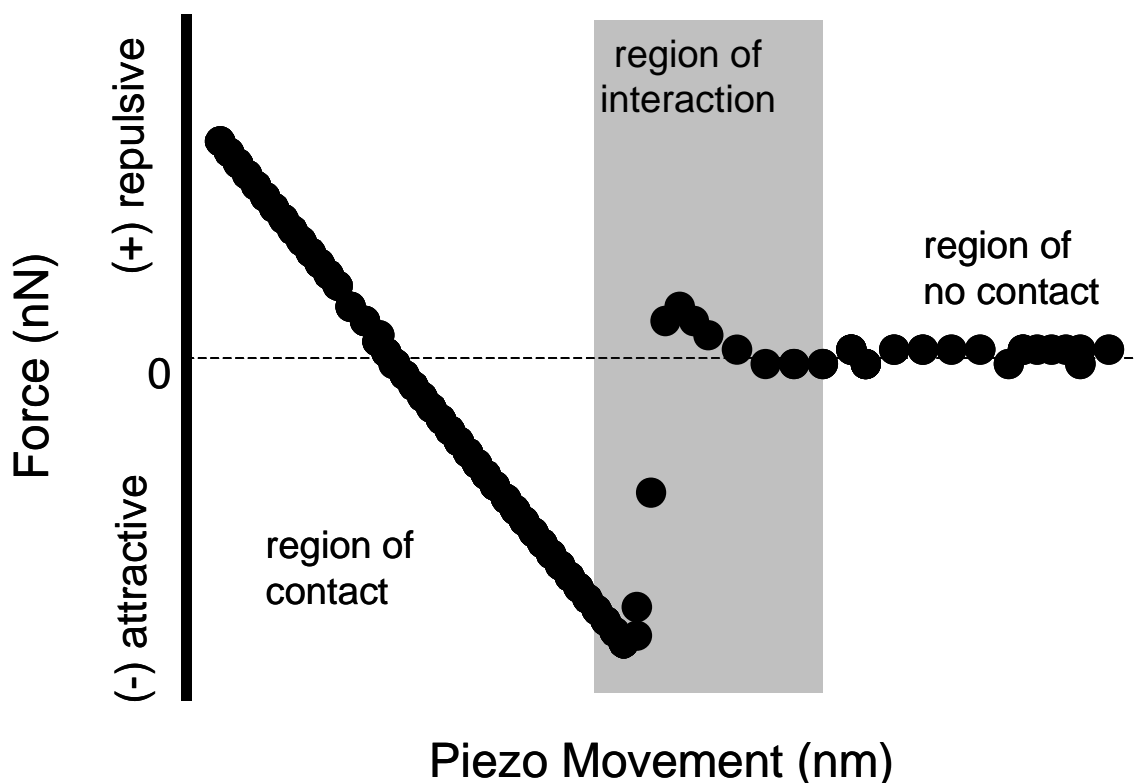


Figure A. 2 A typical force versus piezo movement plot showing three general regions – contact, interaction, and no contact. For clarity a single trace is shown (e.g. an approach curve); however, force plots with both approach and retraction traces are also common. In the region of no contact the tip and sample are separated at distances large enough that no interaction occurs. Hysteresis between the approach and retraction curve in the region of no contact may be a function of solution viscosity, or inelastic deformation of the cantilever. As the piezo advances the sample closer, the tip begins to “feel” the surface. In the example plot we see an initial repulsion followed by an attraction recorded as a sharp jump to contact that generates a minimum in the curve. Once in contact, the slope trace is typically constant as the cantilever is moving with the piezo. Information from this region may be used to determine detector sensitivity or elastic properties of the sample or tip.

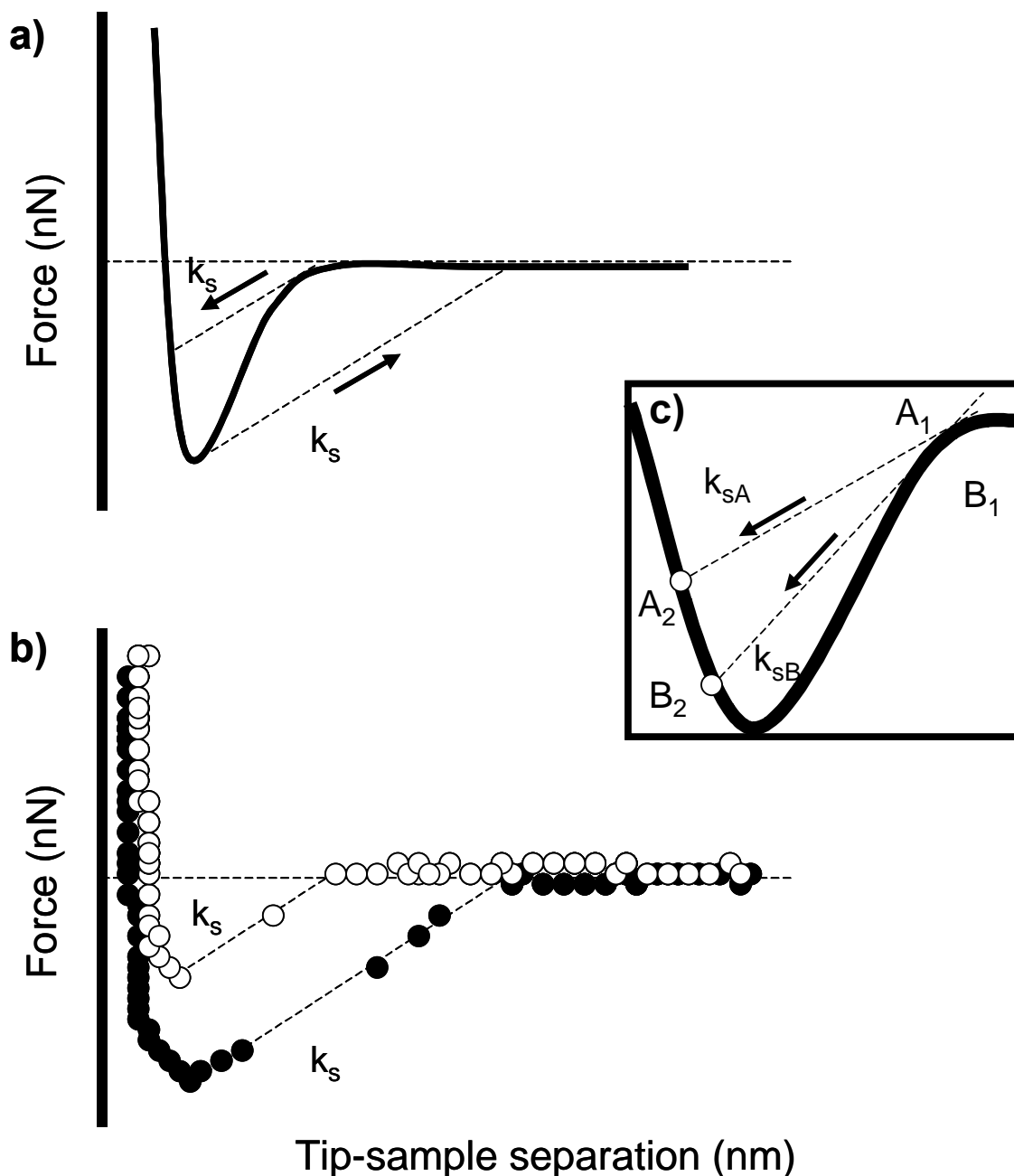


Figure A. 3 a) Differentiated Lennard-Jones potential provided as an example interaction to be captured with force microscopy or AFM. During AFM operation the forces associated with the potential are recorded as deflections in the cantilever. If the force gradient (tangent to the solid trace) exceeds the spring constant,  $k_s$ , the cantilever becomes mechanically unstable and will jump along a slope equal to  $k_s$  (dashed line). b) Force-tip sample separation curve showing jumps to and from contact along slope =  $k_s$ . Unlike Figure A. 2, the x-axis represents separation distance between the tip and the sample. Here, both the approach (open circles) and the retraction (closed circles) traces are shown. Note that the hysteresis between the two traces is absent in the Lennard-Jones curve where the solid line represents both approach and retraction forces. Points to the left of zero separation (i.e., lowest most point on the approach or retraction curves) represent movement of the piezo while the tip and sample are in contact. c) Increasing the spring constant (e.g., using a stiffer cantilever) from  $k_{sA}$  to  $k_{sB}$  will capture more of the potential (region  $A_2$ - $B_2$ ), however force resolution is lost and smaller magnitude forces will go undetected.

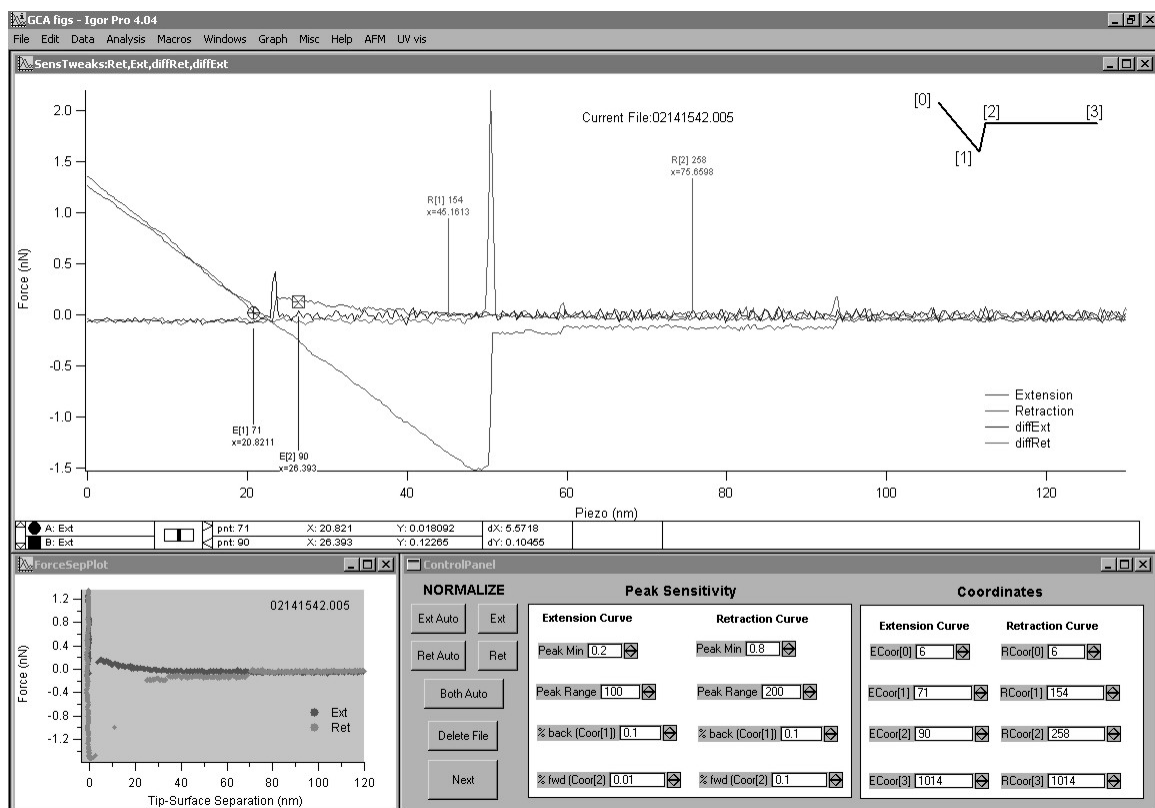


Figure A. 4 Screen shot of one module (Sensitivity Tweaks) in the force curve processing routine AFM 4.4 written in Igor Pro, 4.04, WaveMetrics, Inc. (Kendall and Hochella, 2003; some of the base code was provided by H. Skulason). It is designed primarily for handling force data produced Digital Instrument's Nanoscope IIIa MultiMode system. The Sensitivity Tweaks module is designed to rapidly review and assess how well the normalization routine automatically registers and normalizes force data to an origin. The normalization procedure includes the identification of a baseline in the region of no contact, calculating the detector sensitivity from the region of constant compliance and detecting when the tip and the sample are in contact. The latter is determined using peaks in the differentiated force wave that are selected based on threshold/sensitivity settings shown in the panel in the lower right. If initial normalization is unsatisfactory, these settings may be optimized and an auto-normalization may be run again; or features can be identified manually.

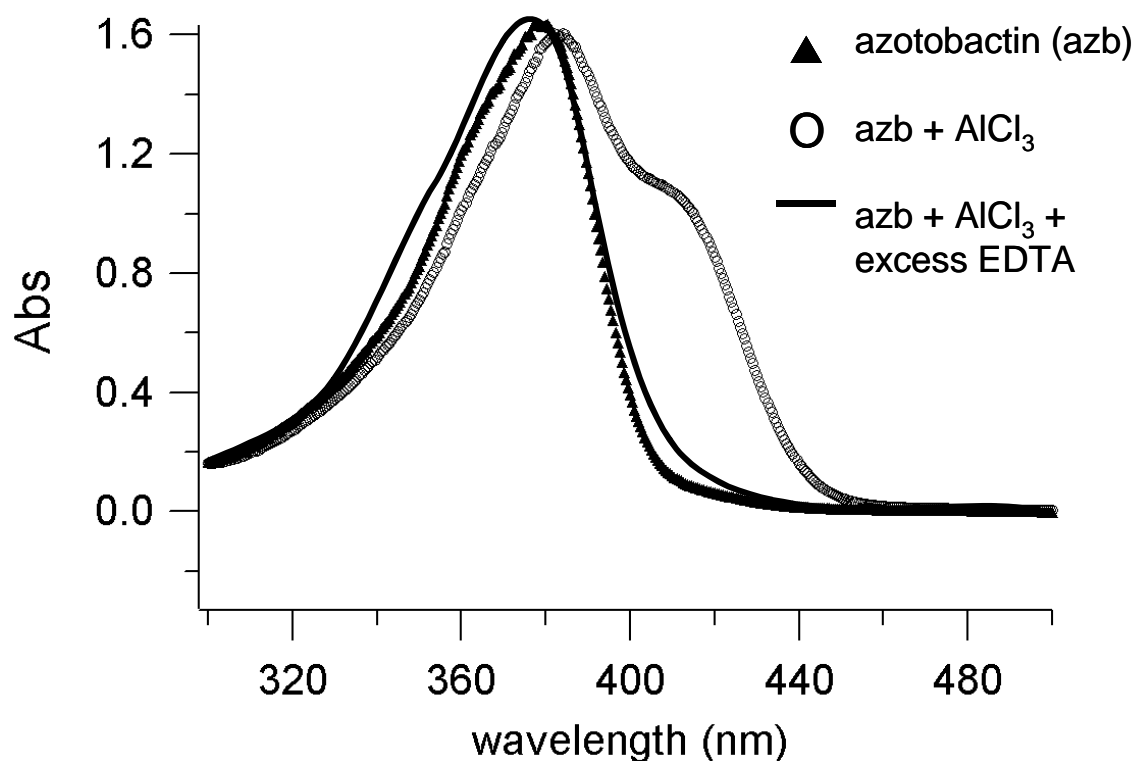


Figure A. 5 UV-vis spectra showing the transition of Al into and out of the azotobactin (Azb) structure; corrected for dilution. Upon the addition of Al to the system a characteristic shoulder appears in the spectra. This shoulder could be eliminated with high concentrations of EDTA. A similar process was employed to protect and then regenerate the azotobactin chelating groups during linkage of the siderophore to a hydrazide terminated AFM tip (see also Chapter 2; Tip Activation).

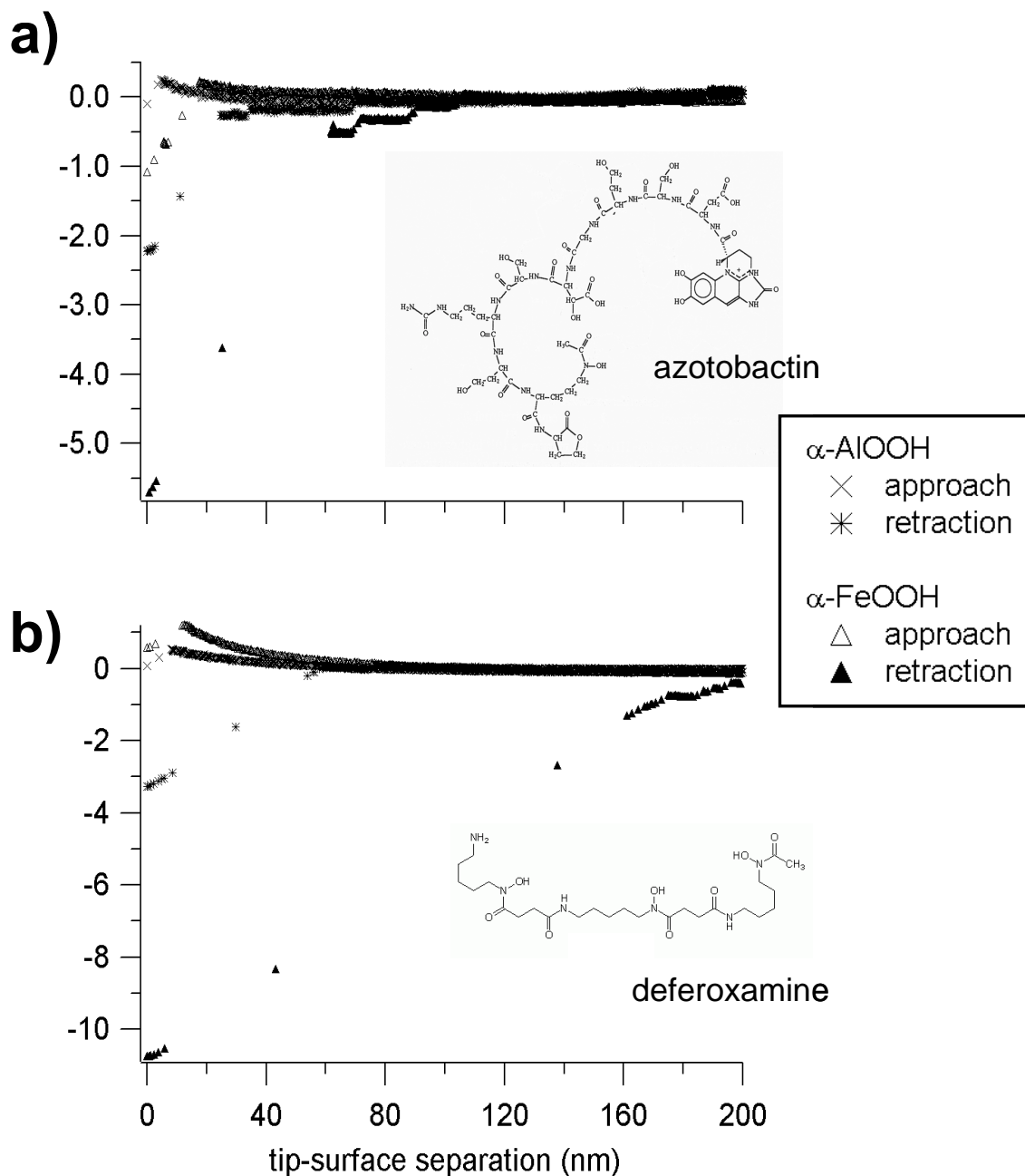


Figure A. 6 Force spectra showing the interaction of two siderophores a) azotobactin and b) deferoxamine (DFO) with goethite (FeOOH) and diaspore (AlOOH) surfaces. Note the large increase in the adhesion force between each siderophore and goethite and versus the adhesion value for diaspore.

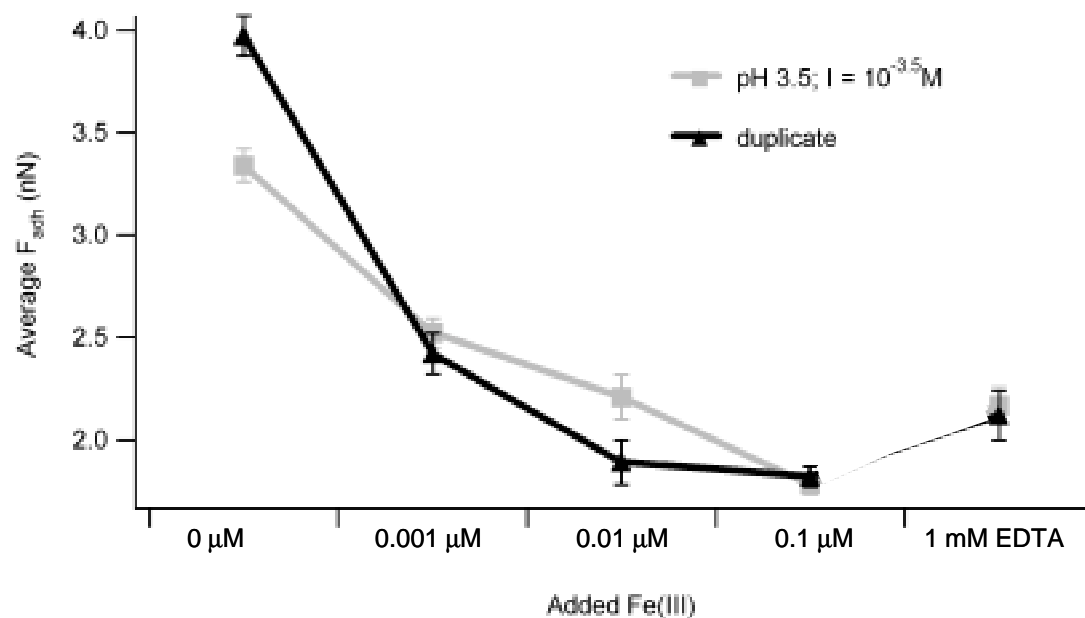


Figure A. 7 Plot showing decrease in azotobactin-goethite adhesion forces with increasing concentrations of added soluble iron ( $FeCl_3 \cdot 6H_2O$ ). Measurements were collected at pH 3.5 to minimize precipitation of solid iron phases upon the addition of the iron chloride. Taken from Kendall and Hochella (2003); Copyright Elsevier Science Ltd. 2003.

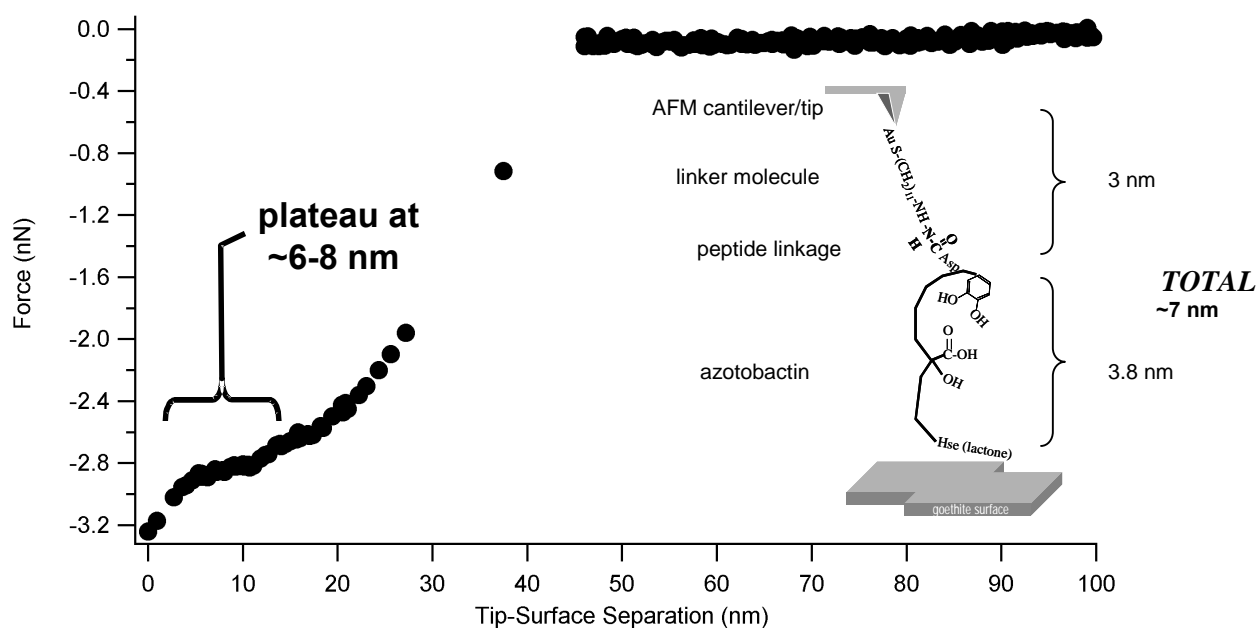


Figure A. 8 Plateau feature common in many retraction curves while probing oxide surfaces with an azotobactin activated AFM. It is suggested that this feature may represent the extension of the azotobactin and linker molecule during separation from the mineral surface as shown in the inset (not to scale). Also shown in the inset is the geometry of the linkage of the siderophore to the tip. Modified from Kendall and Hochella (2003) Copyright Elsevier Science Ltd. 2003.



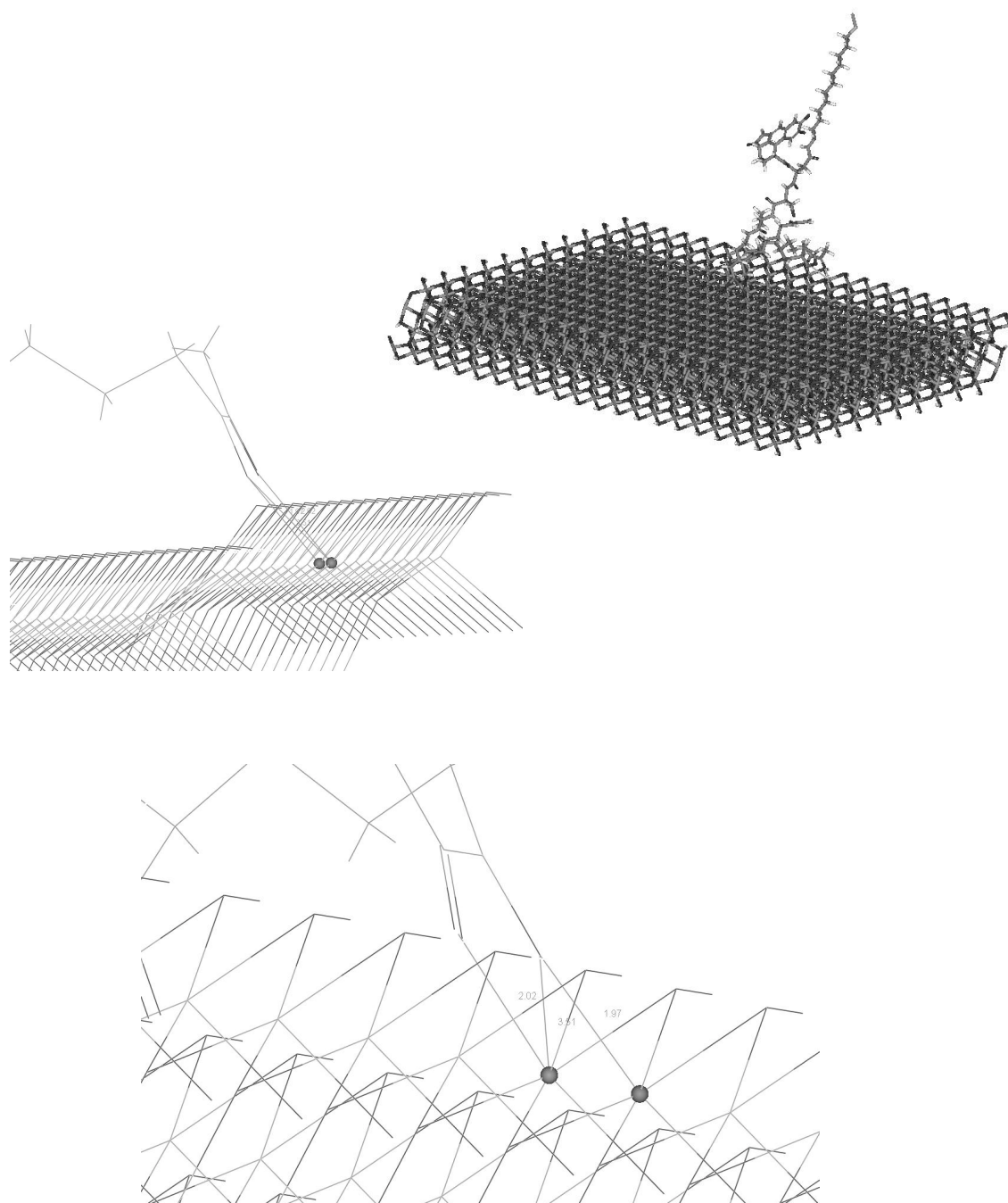


Figure A. 9 Molecular models of azotobactin (with linker molecule) interacting with a goethite surface. Simulations were completed using Cerius2, Accelrys, Inc. Arrows point to terminal hydroxamate group oxygens interacting and coordinating with irons (balls) in the lattice. Note the spacing of the siderophore oxygens allow for “bonds” (i.e., Fe-O distances <2.1 Angstroms) with neighboring irons. With this coordination, the cross-distance between a siderophore oxygen and an iron diagonally across is over 3 Angstroms.

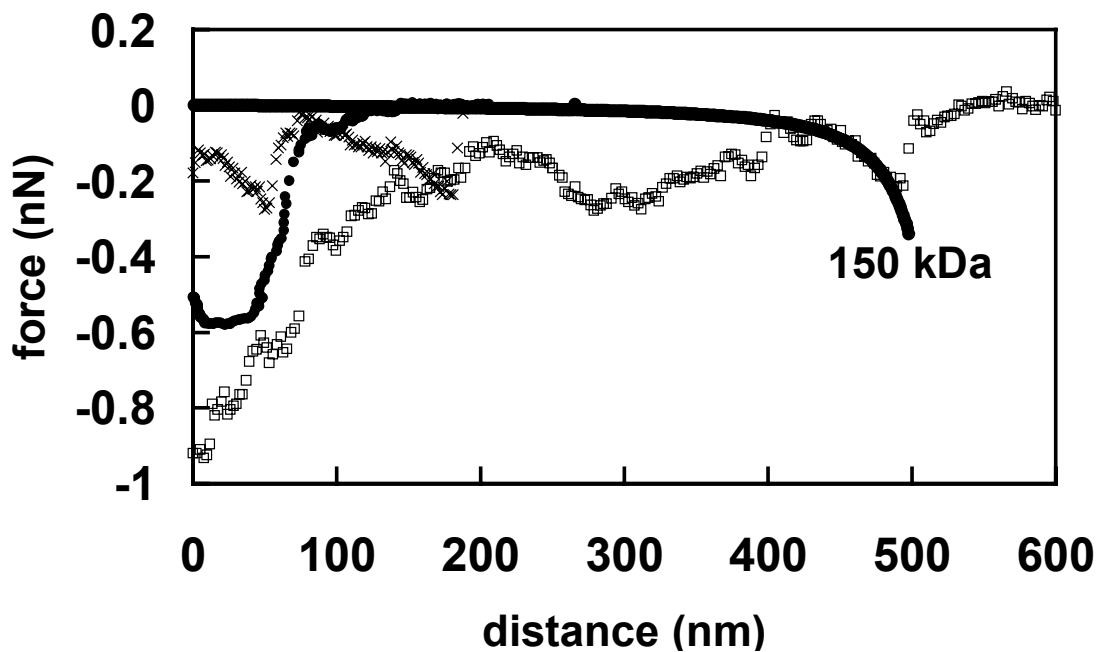


Figure A. 10 Force-distance relationship between the basal plane surface of muscovite and *E. coli* in solutions of high (open symbols across lower portion of figure) or low (closed symbols across upper portion of figure) ionic strength. Shown for each solution condition are five data curves that span the entire range of measurements for literally hundreds of force-distance curves. The lines correspond to the DLVO model prediction at high (dotted) or low (solid) ionic strength. Repulsive forces have a positive sign; whereas attractive forces have a negative sign. Only those forces measured upon approach of the mineral towards the bacteria are shown. See text for discussion.

## Curriculum Vitae

### *Curriculum Vitae of*

# TREAVOR A. KENDALL

---

*Department of Geological Sciences • Virginia Polytechnic Institute and State University  
Blacksburg, VA 24061-0420 • 540.231.8575 • tkendall@vt.edu*

## EDUCATION

### VIRGINIA TECH, PH.D.

*Department of Geological Sciences, Blacksburg, VA (8/99 to 5/03(expected))*

Doctoral Research: Molecular level forces of interaction between biomolecules and mineral surfaces.

Advisor: Dr. Michael F. Hochella, Jr.

### UNIVERSITY OF MONTANA - MISSOULA, M.S.

*Department of Geology, Missoula, MT (8/97 to 8/99)*

Thesis Research: Early diagenetic changes of microbially mediated textures in thermal spring deposits, Yellowstone National Park, WY.

Advisor: Dr. Nancy W. Hinman

### UNIVERSITY OF TEXAS AT AUSTIN, B.S.

*Department of Geological Sciences, Austin, TX (9/90 to 8/95)*

Course Emphasis: hydrogeology, geochemistry, chemistry, field geology (geology field camp), civil engineering (hydrology and hazardous waste management), structural geology.

## PROFESSIONAL EMPLOYMENT

POSTDOCTORAL FELLOW, *Dept. of Applied Sciences and Engineering, Harvard University*  
Begin June 2003

GRADUATE RESEARCH ASSISTANT, *Dept. of Geological Sciences, Virginia Tech*  
2000-May 2003

- Responsibilities include dissertation research, proposal writing, and laboratory and instrument maintenance. Designed computer routines in VBA and Igor to process AFM force and image data. Organized and conducted four-day nanoscience workshop and laboratory experience for five local high school science teachers.  
*Techniques Used:* atomic force microscopy (AFM), confocal laser scanning microscopy (CLSM), reverse-phase and high performance liquid chromatography (HPLC), field emission scanning electron microscopy (FE-SEM), UV-vis spectrophotometry, computer programming (Igor, C++, VBA), chemostat batch reactors

GRADUATE TEACHING ASSISTANT, *Dept. of Geological Sciences, Virginia Tech*  
1999-2000

- Head TA, Elements of Geology for Engineers. Designed laboratory exercises, lectures and examinations. Conducted separate one-on-one tutoring sessions. Managed and provided support for three additional teaching assistants.

GRADUATE RESEARCH ASSISTANT, *Dept. of Geology, Univ. of Montana, Missoula, MT*  
1998-1999

- Main focus was thesis research. Also responsible for laboratory maintenance and organization. Conducted chemical analyses, statistics, literature review and image processing in support of a study on ferricrete formation associated with mine drainage. Completed a two-week microprobe and SEM analysis of siliceous sinters at NASA's Johnson Space Center Astrobiology Institute.  
*Techniques Used:* scanning electron microscopy (SEM) with energy dispersive x-ray spectrometry (EDS), x-ray diffraction (XRD), petrographic image analysis (PIA), inductively coupled plasma spectrometry (ICP), ion chromatography (IC), atomic absorption spectrophotometry (AAS), geochemical modeling (MINTEQ, WATEQ4)

PROJECT HYDROGEOLOGIST/GEOCHEMIST, *ERM-Southwest, Inc., Houston, TX*  
1995-1997

- Geologic and hydrologic investigation of industrial facilities and Superfund sites, with additional experience in data management, flow modeling and GIS. Key achievements included the development of 3D steady state groundwater flow model for Montana refinery, creation of GIS system for Environmental Protection Dept. of chemical manufacturing facility, and ground water and soil quality assessment of iron forging facility where hydrocarbon plume was delineated with rapid optical screening technology (ROST).

UNDERGRADUATE RESEARCH ASSISTANT, *Bureau of Economic Geology, Univ. of Texas, Austin, TX*  
1993-1995

- Provided laboratory support for a project on the paleobiology, systematics and morphology of conodonts. Processed sediment cores for fossil extraction.

## **SELECTED HONORS AND ACTIVITIES**

- DOE Geosciences, Best University Research Award - 2003
- GAAN Fellowship, U.S. Department of Education and Virginia Tech – 2001-Present
- Invited speaker, Goldschmidt Conference, Davos, Switzerland – 2002
- Geological Sciences Student Research Symposium (GSSRS) Committee Chair – 2001-2002
- Committee Member – Dept. of Geological Sciences Seminar Series – 2001-2002
- Virginia Tech Travel Award – 2001, 2002
- GSSRS Committee Member – 2000-2001
- Delegate, Graduate Student Assembly, Virginia Tech – 1999
- Geology Faculty Scholarship Recipient, University of Montana – 1998
- Michael Lee Wilson Scholarship Recipient, University of Montana – 1998
- University of Montana Graduate School Travel Award – 1998
- Departmental Tutor, University of Montana – Hydrogeology – 1998
- President, AAPG, University of Texas Chapter – 1993
- Weeks Scholarship Recipient, University of Texas – 1993
- Delegate, Natural Sciences Council, University of Texas – 1993
- Bill Archer Congressional Internship, Washington D.C. - 1989

## PROFESSIONAL SOCIETY MEMBERSHIPS

Geochemical Society  
Mineralogical Society of America  
American Geophysical Union

## PUBLICATIONS AND ABSTRACTS

Kendall, T.A. and Hochella, M.F., Jr. (2003 in press). The measurement and interpretation of molecular level forces of interaction between the siderophore azotobactin and mineral surfaces. *Geochimica et Cosmochimica Acta*

Kendall, T.A. and Lower, S.K. (2003 Invited Paper; in review). Intermolecular forces at the interface of biological and mineralogical particles, *Advances in Agronomy*, 75 pp.

Kendall, T.A., Becker, U. and Hochella, M.F., Jr. (2003 in prep). Modeling siderophore-mineral interaction using molecular and quantum mechanical calculations. *Langmuir*

Kendall, T. A. and Hochella, M.F., Jr. (2002 Invited Presentation) “Probing siderophore-mineral interactions using force measurements”. 12th Annual Goldschmidt Conference in Davos, Switzerland.

Kendall, T.A. (2002). “New insights into organic ligand-mineral interactions via direct, molecular force measurements” (Talk). 2002 Geological Society of America (GSA) Annual Meeting in Denver, CO.

Cecil, K., Kendall, T.A. and Schreiber, M. (2002). “Nanobiogeochemistry of microbe/mineral interactions” (Poster). 2002 Geological Society of America (GSA) Annual Meeting in Denver, CO.

Kendall, T. A. (2001) “Investigating the mechanism of siderophore-driven Fe release from mineral surfaces using chemical force and confocal laser scanning microscopy” (Talk). 11th Annual Goldschmidt Conference in Hot Springs, VA.

Kendall, T. A. and Hinman, N.W., (1998) “Early diagenesis of thermal spring deposits” (Poster). American Geophysical Union Annual Fall Meeting Program With Abstracts, San Francisco, CA.

## RESEARCH FUNDING

As a graduate student at Virginia Tech, I significantly assisted in writing and generating experimental design for the following successfully funded proposals:

- Department of Energy OBES Geosciences, “Nanobiogeochemistry of microbe/mineral interactions: A Force Microscopy and Bioinformatics Approach”, (Hochella, PI) - \$400,000
- National Science Foundation, “Nanoscale Processes in the Environment”, (Hochella, PI) - \$1,000,000

## REFERENCES

Michael F. Hochella, Jr., Ph.D. (Ph.D. advisor)  
Professor  
Department of Geological Sciences  
Virginia Tech  
4044 Derring Hall  
Blacksburg, VA 24061-0420  
540.231.6277  
hochella@vt.edu

Steven K. Lower, Ph.D. (co-author, colleague)  
Assistant Professor  
Department of Geology  
University of Maryland  
Geology Bldg.  
College Park, MD 20742  
301.405.4094  
lower@geology.umd.edu

J. Don Rimstidt, Ph.D. (committee member)  
Professor  
Department of Geological Sciences  
Virginia Tech  
4044 Derring Hall  
Blacksburg, VA 24061-0420  
540.231.6589  
jdr02@vt.edu

Chris J. Tadanier, Ph.D. (committee member)  
Research Assistant Professor  
Department of Geological Sciences  
Virginia Tech  
4044 Derring Hall  
Blacksburg, VA 24061-0420  
540.231.4315  
ctadanie@vt.edu

Nancy W. Hinman, Ph.D. (M.S. advisor)  
Associate Professor  
Department of Geology  
University of Montana  
32 Campus Dr. #1296  
Missoula, MT 59812-1296  
406.243.5277  
hinman@selway.umt.edu

Johnnie N. Moore, Ph.D. (mentor,  
instructor)  
Professor  
Department of Geology  
University of Montana  
32 Campus Dr. #1296  
Missoula, MT 59812-1296  
406.243.2341  
gl\_jnm@selway.umt.edu

Susan C. Eriksson, Ph.D. (teaching mentor)  
Associate Dean, College of Arts and  
Sciences  
Associate Professor of Geology  
Virginia Tech  
203 Brodie Hall, Mail code: ASAB 0405  
Blacksburg, VA 24061-0405  
540.231.3703  
serikssn@vt.edu